A MATHEMATICAL MODEL OF TISSUE FACTOR-INDUCED BLOOD COAGULATION: DISCRETE SITES OF INITIATION AND REGULATION UNDER CONDITIONS OF FLOW

A Thesis
Presented to
The Academic Faculty

By

Sumanas W. Jordan

In Partial Fulfillment
of the Requirements for the Degree
Doctor of Philosophy in Biomedical Engineering

Emory University
Georgia Institute of Technology

May 2010

A MATHEMATICAL MODEL OF TISSUE FACTOR-INDUCED BLOOD COAGULATION: DISCRETE SITES OF INITIATION AND REGULATION UNDER CONDITIONS OF FLOW

Approved By

Dr. Elliot L. Chaikof, Advisor
Departments of Surgery and Biomedical
Engineering
Emory University
Georgia Institute of Technology

Dr. Larry V. McIntire
Department of Biomedical Engineering
Emory University
Georgia Institute of Technology

Dr. Eberhard O. Voit
Department of Biomedical Engineering
Emory University
Georgia Institute of Technology

Dr. Stephen R. Hanson
Department of Biomedical Engineering
Oregon Health & Science University

Dr. William J. Federspiel
Department of Bioengineering
University of Pittsburgh

Date Approved: March 31, 2010

TABLE OF CONTENTS

LIST OF TABLES

LIST OF FIGURES

CHAPTER 1

INTRODUCTION

Hemostasis is a highly dynamic, tightly regulated, process mediated by both cellular components and soluble coagulation factors, which ultimately results in rapid and localized clot formation at a site of injury. Physiologic clotting is essential for control of hemorrhage; however, deregulation of coagulation events can lead to thrombotic disease and significant clinical outcomes including deep vein thrombosis (DVT), pulmonary embolism (PE), myocardial infarction (MI), and stroke. It is estimated that over 200,000 new cases of venous thromboembolism (VTE), which includes both DVT and PE, occur each year with a 30-day mortality rate of 30%. An additional 30% of new VTE patients will experience a recurrent thromboembolic event within 10 years. Within the arterial circulation, myocardial infarction is associated with an estimated annual incidence of nearly 900,000 new and recurrent attacks and total-mention mortality of over 220,000 in 2002. The annual incidence of ischemic stroke is approximately 600,000 [1].

Furthermore, device thrombosis remains a considerable obstacle in the development of clinically durable small-diameter vascular prostheses as well as permanently implantable biosensors and blood-contacting artificial organs. Although 1-year patency rates of expanded polytetrafluoroethylene (ePTFE) prostheses and saphenous vein grafts for above knee infrainguinal bypass are similar, by 5 years, up to 60% of synthetic grafts will occlude or require revision compared with 20% to 30% of vein grafts. This disparity is even greater for bypass to the below knee popliteal artery or infrageniculate vessels or in the performance of synthetic arteriovenous dialysis grafts when compared with autologous fistulas. Growing appreciation of the processes

underlying coagulation and its regulation has driven the pursuit of bioinspired, antithrombogenic biomaterials functionalized with heparin, thrombomodulin, urokinase, as well as pharmacologic thrombin inhibitors [2].

The central hypothesis of this thesis is that a mathematical model of blood coagulation will contribute to the understanding of the hemostatic system and its disregulation and will therefore be useful as both a diagnostic tool and a design aid. The overall objective is to formulate a finite element model of coagulation that describes thrombin generation under defined flow conditions, initiated and modulated by spatially discrete regions of surface-bound tissue factor (TF) and thrombomodulin (TM), respectively. In Section I, we describe the model design and reproduce characteristic features of thrombin generation under simulated physiologic conditions. The behavior of the model system in response to perturbations in tissue factor and thrombomodulin surface densities, tissue factor site dimensions, and wall shear rate is explored. The classic time course characterized by initiation and amplification of thrombin generation is recreated, and the existence of threshold-like responses, which have been demonstrated *in vitro* as well as in computational studies [3-11], is illustrated. Secondly, a new parameter, the 'effective prothrombotic zone', is defined, and its dependence on model parameters is described. It was found that prothrombotic effects may extend significantly beyond the dimensions of the spatially discrete site of tissue factor expression in both axial and radial directions. Furthermore, we take advantage of the finite element modeling approach to explore the behavior of systems containing multiple spatially distinct sites of TF expression in a physiologic model. Additive prothrombotic interactions as well as TM-mediated suppressive interactions between TF sites are observed and discussed in the context of coronary artery disease. In Section II, the computational model is applied to assess individualized thrombotic risk from clinical data of plasma coagulation factor levels. We demonstrate a significant association of the

systems-based parameter with deep venous thrombosis and propose the use of

computational methods in combination with biochemical panels to predict

hypercoagulability for high risk populations.

1.1. REFERENCES

1. Rosamond, W., et al., *Heart Disease and Stroke Statistics - 2007 Update - a Report from the American Heart Association Statistics Committee and Stroke Statistics Subcommittee.* Circulation, 2007. **115**(5): p. E69-E171.
2. Jordan, S.W. and E.L. Chaikof, *Novel Thromboresistant Materials.* Journal of Vascular Surgery, 2007. **45**: p. 104A-115A.
3. vantVeer, C. and K.G. Mann, *Regulation of Tissue Factor Initiated Thrombin Generation by the Stoichiometric Inhibitors Tissue Factor Pathway Inhibitor, Antithrombin-III, and Heparin Cofactor-II.* Journal of Biological Chemistry, 1997. **272**(7): p. 4367-4377.
4. Mann, K.G., et al. *Models of Blood Coagulation.* 2006: Academic Press Inc Elsevier Science.
5. Shen, F., C.J. Kastrup, and R.F. Ismagilov, *Using Microfluidics to Understand the Effect of Spatial Distribution of Tissue Factor on Blood Coagulation.* Thrombosis Research, 2008. **122**: p. S27-S30.
6. Shen, F., et al., *Threshold Response of Initiation of Blood Coagulation by Tissue Factor in Patterned Microfluidic Capillaries Is Controlled by Shear Rate.* Arteriosclerosis Thrombosis and Vascular Biology, 2008. **28**(11): p. 2035-U226.
7. Kastrup, C.J., et al., *Modular Chemical Mechanism Predicts Spatiotemporal Dynamics of Initiation in the Complex Network of Hemostasis.* Proceedings of the National Academy of Sciences of the United States of America, 2006. **103**(43): p. 15747-15752.
8. Hockin, M.F., et al., *A Model for the Stoichiometric Regulation of Blood Coagulation.* Journal of Biological Chemistry, 2002. **277**(21): p. 18322-18333.
9. Willems, G.M., et al., *Simulation-Model for Thrombin Generation in Plasma.* Haemostasis, 1991. **21**(4): p. 197-207.
10. Beltrami, E. and J. Jesty, *The Role of Membrane Patch Size and Flow in Regulating a Proteolytic Feedback Threshold on a Membrane: Possible Application in Blood Coagulation.* Mathematical Biosciences, 2001. **172**(1): p. 1-13.
11. Kastrup, C.J., et al., *Characterization of the Threshold Response of Initiation of Blood Clotting to Stimulus Patch Size.* Biophysical Journal, 2007. **93**(8): p. 2969-2977.

CHAPTER 2

BACKGROUND

2.1.   Blood coagulation

Central to the hemostatic system is the formation of thrombin. The endpoint of a

cascade of reactions triggered by exposure of subendothelial tissue factor (TF), thrombin

converts fibrinogen to fibrin, activates platelets, and is involved in a number of other

mitogenic and inflammatory pathways [1]. The clotting 'cascade' involves a series of

serine protease reactions converting inactive zymogens to active enzymes. Coagulation

is traditionally divided into two parallel pathways, the intrinsic and extrinsic pathways,

which converge on a common pathway. The intrinsic pathway is defined by components

that reside entirely within the intravascular system. Specifically, factor XII is

autoactivated upon contact with negatively charged surfaces, including glass and many

biomaterials, in a reaction involving high molecular weight kininogen (HMWK) and

prekallikrein. Factor XIIa activates factor XI, and factor XIa, in turn, activates factor IX.

The complexation of factors IXa and VIIIa on a phospholipid surface, forming 'intrinsic

tenase', results in the generation of activated factor X. It is the extrinsic, or tissue factor

pathway, however, that is generally accepted as the principal initiating pathway of

coagulation *in vivo*. Exposure of subendothelial TF to the bloodstream and subsequent

formation of the TF/ VIIa complex leads to the activation of both factors IX and X. The

generation of factor Xa by either intrinsic (IXa/ VIIIa) or extrinsic (TF/ VIIa) tenase leads

to the assembly of prothrombinase (Xa/Va), which cleaves prothrombin (factor II) to

thrombin (IIa). Amplification of thrombin generation is achieved through positive

feedback of thrombin to activate factors V and VIII. Key themes relevant to the

coagulation cascade are the sequential reaction of zymogen-enzyme pairs, the requirement for cofactors, and the calcium-dependent, membrane-mediated coordination of enzyme complexes [2-4].

2.1.1. Regulation of thrombin generation

Physiologic regulators of thrombin include the protein C pathway, antithrombin III, and tissue factor pathway inhibitor (TFPI). The protein C pathway begins when thrombin binds to thrombomodulin, consequently redirecting the function of thrombin towards anticoagulant activity. Activated protein C inactivates the cofactors Va and VIIIa in a protein S-dependent manner [2-4]. Antithrombin III (ATIII) is a serine protease inhibitor that forms a 1:1 molar complex with factors IXa, Xa, and thrombin. The affinity of ATIII for its substrates is greatly enhanced in the presence of physiologic surface glcyosaminoglycans or pharmacologic heparin [5]. Finally, TFPI is a trivalent Kunitz-type serine protease inhibitor synthesized by endothelial cells, which inhibits factor Xa through binding with its second Kunitz domain and inactivates TF/ VIIa through binding with its first Kunitz domain [6, 7]. Thus, TFPI acts in a two-step process to form a quaternary complex with factor Xa and TF/ VIIa, neutralizing the tissue factor stimulus [8, 9]. The protein C pathway and TFPI pathway are classic examples of negative feedback, requiring the presence of thrombin and factor Xa, respectively, while ATIII acts primarily as a scavenger for activated enzymes. In the presence of TFPI, ATIII has been shown to play a critical role in regulating low-level basal activation of coagulation by TF [10-12].

2.1.2. Threshold response of thrombin formation

During the initiation phase of coagulation, very low levels of thrombin are produced. During this phase, inhibitors may dampen the thrombin response and prevent

6

amplification and full activation of the coagulation cascade; this is considered a 'sub-threshold' thrombin response. However, when the capacity of these inhibitors is overwhelmed by the magnitude of the thrombogenic stimulus, thrombin levels cross an activation threshold and rapid amplification of thrombin generation occurs. The combination of multiple long- and short-range positive feedback loops and complementary inhibitory mechanisms results in tight regulation of coagulation characterized by rapid, 'all-or-none' behavior [12, 13]. Ismagilov *et al.* have published a number of experimental studies characterizing coagulation thresholds with respect to TF patch size, wall shear rate, and spatial distribution of TF sites in both flow and non-flow environments [14-16]. Several computational groups have reported on the 'on/ off' response of coagulation to parameters such as TF and factor Xa stimulus [17, 18], TF patch size [19, 20], inhibitor concentrations and associated kinetic parameters [17], as well as blood flow [19, 20]. Threshold-like behavior was simulated in model systems as simple as two zymogen-enzyme pairs in a positive feedback loop with inhibition [21].

2.2. The Vascular surface

The surface of the blood vessel wall serves several functions in the regulation and promotion of blood coagulation. The 'resting' endothelium synthesizes and presents a number of antithrombogenic molecules including heparan sulfate proteoglycans, ecto-adenosine diphosphatase, prostacyclin, nitric oxide, and thrombomodulin [22-27]. In response to various stimuli, including inflammatory mediators, hypoxia, oxidative stress, and fluid shear stress, the cell surface becomes 'activated' and serves to organize membrane-associated enzyme complexes of coagulation. Additionally, the occupation of cell surface receptors for procoagulant products such as factor Xa and thrombin leads to a variety of cellular responses including mitogenic, chemoattractant, and yet uncharacterized effects [28-33].

2.2.1. Thrombomodulin

Thrombomodulin (TM) is a 60kD type I transmembrane protein expressed on the luminal surface of vascular endothelium and smooth muscle cells. TM switches off all known procoagulant functions of thrombin by occupying the functionally important exosite I on thrombin [34], and instead channels the catalytic power of the enzyme into anticoagulant activities, specifically enhancing the rate of thrombin inactivation by ATIII [35] and significantly accelerating the ability of thrombin to activate protein C (>1,000-fold). Once generated, activated protein C (APC) is one of the slowest of the serine proteases to be inactivated and cleared from the circulation with a half-life of 20 min . APC, together with protein S, inactivates factors Va and VIIIa, thereby preventing further amplification of factor Xa and thrombin [36-38]. It is well established that patients with protein C or protein S deficiency, as well as those with resistance to APC are prone to develop thromboembolic events [34].

Complete ablation of the TM gene causes embryonic lethality in mouse models [39]. However, mutations which severely reduce the capacity of TM to activate protein C cause increased fibrin deposition in selected organs [40], and endothelial cell-specific loss of TM leads to early onset thrombosis in mice [41]. In human studies, a heterozygous point mutation in the TM gene (G1456T) affecting the amino acid sequence located between the transmembrane domain and the sixth epidermal growth factor-like domain was identified in a 45-year-old man who presented with pulmonary embolism [42]. A heterozygous substitution of G127 to A was first detected in a 42-year-old woman who presented with sagittal sinus thrombosis [43] and has been associated with an increased risk of myocardial infarction before the age of 50 [44]. In a screen of 104 patients admitted for myocardial infarction, three distinct polymorphisms in the 5' promoter region of the TM gene were identified in five patients [45]. Finally, a mutation

consisting of both a silent base substitution (G1686C) and a base insertion (insT1689), which resulted in elongation of the intracellular domain and reduced trafficking to the cell surface, was associated with myocardial infarction in a thrombophilic family [46].

Thrombomodulin expression has been shown to be upregulated by a number of factors including cAMP [26, 27], retinoic acid [28-30], vitamin D [47], as well as 3-hydroxy-3-methylglutaryl coenzyme A reductase inhibitors, or statins [48-51], and autintricarboxylic acid [52]. Inflammatory mediators, specifically TNF-α [53-57], interleukin-1 [53, 58, 59], transforming growth factor (TGF-β) [60], and bacterial endotoxin [61], suppress TM expression in patients with severe bacterial sepsis, adult respiratory distress, and multiple organ system failure [62]. Additionally, hypoxia has been shown to downregulate TM expression [63].

2.2.2. Tissue factor

Tissue factor (TF) is a 47kD transmembrane protein whose primary role in blood coagulation is to bind factor VIIa and participate in the activation of factor X, thus initiating thrombin generation. Cell-associated TF is expressed in high levels within the vasculature of vital organs such as the skin, lungs, brain, heart, kidneys, testis, uterus, and placenta. In contrast, skeletal muscles and joints have relatively low levels of TF and appear to rely more heavily on the intrinsic pathway of coagulation for hemostasis [64, 65]. In healthy vessels, TF is found on adventitial fibroblasts and smooth muscle cells, allowing for rapid initiation of coagulation upon vascular injury [66]. In a mouse model of laser-induced vascular injury, Falati *et al.* [67] demonstrated using confocal intravital imaging that while TF was found throughout the growing thrombus, TF remained most concentrated at the interface between the vessel wall and the thrombus. Additionally, immunohistochemical staining of atherosclerotic lesions has shown significant levels of TF within the foam cells adjacent to the cholesterol clefts and within

the necrotic cores of plaque lesions. Upon rupture of the fibrous cap, large amounts of

TF are exposed to the bloodstream, precipitating thrombus formation. It is suggested

that the deposition of TF within the matrix of the atherosclerotic plaque is responsible for

the hyperthrombotic state of atherosclerotic vessels leading to serious clinical sequelae

including acute coronary syndrome and sudden cardiac death [66, 68, 69].

TF expression by endothelial cells and monocytes may be induced by a number

of inflammatory mediators including tissue necrosis factor (TNF-α), interleukin-1 (IL-1),

histamine, endotoxin, oxidized lipoproteins, and heme [68, 70-72]. C-reactive protein

enhances TF expression with concomitant decreases in tissue factor pathway inhibitor

(TFPI) expression in vascular smooth muscle cells [73]. In contrast, the anti-arrhythmia

drug amiodarone was found to inhibit TF protein translation and reduce carotid artery

thrombosis in a mouse photochemical injury model [74].

Circulating TF has gained recent attention although its role in physiology has yet

to be fully established. Alternatively spliced soluble tissue factor has been identified with

retained procoagulant activity. This isoform of TF is incorporated into growing thrombi

when exposed to phospholipids and has been induced from endothelial cells by

inflammatory mediators [75, 76]. Additionally, TF incorporated within the membrane of

circulating microparticles shed from a variety of cell types has been studied in relation to

coronary artery disease, inflammation, and cardiopulmonary bypass [77-80].

2.3.   Computational models of blood coagulation

Mathematical models of blood coagulation have been developed with varying

degrees of complexity for many different purposes. Several models restrict their

analysis to reaction kinetics of all or part of the intrinsic, extrinsic, and common

pathways, neglecting the role of blood flow. Those that have taken the effects of blood

flow into account have used a simple compartmental modeling approach, which relies

heavily on the assumption of spatial homogeneity in the direction of flow. Finite element models of surface-bound reactions under flow have so far have been limited in the number of reactions considered. Recently, spatially heterogeneous models, which describe the growth of clot formation in space or discrete 'patches' of surface expression, have been developed, though most do not include convective effects. In this section, we review models of blood coagulation that have been conceived for applications ranging from the study of coagulation dynamics and phenomena to the simulation of clinical diagnostic values.

2.3.1. Fluid phase models of coagulation

Nesheim *et al.* explored the properties of prothrombinase assembly and activity within an interface shell surrounding phospholipid vesicles in solution in a steady-state, two-phase model. The distribution of substrate and enzyme between the bulk and shell phases was used to rationalize the apparent inhibition by excess enzyme, substrate, and phospholipid [81]. Willems *et al.* studied a dynamic model of thrombin generation in plasma describing 14 pro- and anti-coagulant reactions, including inhibition of coagulation by activated protein C, antithrombin III, and exogenous hirudin. The stimulus was a transient pulse of factor Xa, and a threshold response to this stimulus was reported that was dependent on ATIII inactivation of thrombin and factor Xa [18]. Jones and Mann developed a more complex model of the dynamics of coagulation, which included the activation of factors IX, X, V, VIII, and thrombin, as well as the assembly of the phospholipid-associated enzyme complexes, intrinsic tenase (IXa/ VIIIa) and prothrombinase (Xa/Va). Thrombin generation was initiated by TF/VIIa in concentrations ranging from 5 pM to 5 nM [82]. The group later extended the model to include a number of additional substrate interactions and positive feedback mechanisms, and significantly, incorporated the coagulation inhibitors, tissue factor pathway inhibitor

(TFPI) and antithrombin III (ATIII), resulting in a model system describing the fates of 34 species. The major finding of the study was the threshold-like dependence of thrombin generation on the concentrations of TF, ATIII, and TFPI [17]. Furthermore, the numerical simulations were used to study the role of surface-localized versus circulating TF during the initiation, propagation, and termination phases of coagulation [83]. The Hockin model was also recently used to predict thrombin generation curves from clotting factor levels collected from the control population of the Leiden Thrombophilia Study (LETS) [84]. Jesty and colleagues considered, both analytically and numerically, the threshold behavior that resulted from representative systems ranging from an auto-activating zymogen-enzyme pair, to systems of two or four zymogen-enzyme pairs with multiple positive feedback mechanisms subject to irreversible, first-order inactivation. In the presence of inhibition, all systems exhibited threshold behavior, which was modulated by changes in initial concentrations of active enzymes, enzyme kinetics, the presence of multiple positive feedback loops, membrane patch size, and in later models, flow [19, 21, 85]. Similarly, Bungay *et al.* demonstrated the dependence of a threshold response on the availability of phospholipid surfaces [86, 87].

Several others have mathematically described the kinetics of the extrinsic and intrinsic pathways in solution to simulate the laboratory assays prothrombin time (PT) and activated partial thromboplastin time (aPTT), respectively, and to evaluate the sensitivities of the systems to clotting factor deficiencies [88-91]. Leipold *et al.* developed a model of the tissue factor pathway as a design aid for the development of exogenous serine protease inhibitors [92]. In contrast, Guo *et al.* focused on the reactions of the contact, or intrinsic pathway, to study parameters relevant to material-induced thrombosis, including procoagulant surface area [93].

Alternative approaches to modeling the coagulation cascade have been pursued including the use of stochastic activity networks to represent the intrinsic, extrinsic, and

common pathways through fibrin formation [94] and a kinetic Monte Carlo simulation of TF-initiated thrombin generation [95].

Generally, fluid phase models of the kinetics of coagulation are both computationally and experimentally less complex. As such, the computational models are able to incorporate a large number of species and their reactions, and empirical data is often available for regression analysis and model validation. The range of complexity and motivations for these models is wide, and the models have been used to describe various phenomena including the 'all-or-none' threshold behavior of thrombin generation. However, the role of blood flow in coagulation is well recognized in promoting the delivery of substrates to the vessel wall and in regulating the thrombin response by removing activated clotting factors.

2.3.2. Flow based models of coagulation

In 1990, Basmadjian presented a mathematical analysis of the effect of flow and mass transport on a single reactive event at the vessel wall and consequently laid the foundation for the first flow-based models of coagulation. It was proposed that for vessels greater than 0.1 mm in diameter, reactive events at the vessel wall could be adequately described by the assumption of a concentration boundary layer very close to the reactive surface, within which the majority of concentration changes took place. The height of the boundary layer and the mass transfer coefficient that described transport to and from the vessel wall were shown to stabilize on a time scale much shorter than the time scale over which concentration changes were empirically observed. Thus, the vascular space could be divided into two compartments, a boundary volume and a bulk volume, and furthermore, changes within the bulk phase could be considered negligible, thereby reducing the previously intractable problem to a pseudo-one compartment model described by a system of ordinary differential equations [96]. Baldwin and

Basmadjian subsequently published a limited model of six reactions, including two positive feedback reactions and two inhibitory reactions, of the common pathway of coagulation triggered by exogenous factor IXa under flow. As a consequence of the definition of the mass transfer coefficient, the kinetic parameters were dependent on the boundary layer height. Furthermore, the model did not explicitly account for intrinsic tenase or prothrombinase formation, but rather derived a rate expression for reaction in the presence of a cofactor. The major finding of the study was the predicted effect of increased mass transport to enhance thrombin generation by decreasing the induction time up to a critical mass transfer rate, beyond which transport significantly decreased peak thrombin levels thereby reducing overall thrombin production [97]. Kuharsky and Fogelson formulated a more comprehensive, pseudo-one compartment model of tissue factor-initiated coagulation under flow, which included the description of 59 distinct fluid- and surface-bound species. In contrast to the Baldwin-Basmadjian model, which defined a mass transfer coefficient as a rate of transport to the vessel surface, the Kuharsky-Fogelson model defined the mass transfer coefficient as a rate of transport into the boundary *volume*, thus eliminating the dependence of kinetic parameters on transport parameters. The computational study focused on the threshold response of thrombin generation to the availability of membrane binding sites. Additionally, the model suggested that adhered platelets may play a role in blocking the activity of the TF/ VIIa complex [98]. Fogelson and Tania later expanded the model to include the protein C and TFPI pathways [99]. One consequence of defining a boundary, or 'shell', volume is that surface-bound species, such as TF, are assumed to be uniformly distributed through the volume, and thus their effective concentrations, with units of moles per volume, become a function of flow rate. Furthermore, these pseudo-one compartment models, like the fluid phase models, assume spatially homogenous, or well mixed, compartments. The assumption breaks down as the dimensions of the boundary

volume increase, *e.g.* at low shear rates and for large reaction areas, due to the potential for substrate depletion and product accumulation at the surface or at upstream sites. Relevant to hemostasis, the surface of the vascular wall is highly non-uniform with respect to the protein expression and phosholipid composition, features which are important for the localization of thrombus formation to injury sites.

An alternative approach to modeling surface-associated reactions under flow uses finite element method (FEM), which is a technique for solving partial differential equations by dividing the vascular space into a finite number of discrete elements. Hall *et al.* used FEM to simulate factor X activation over a surface presenting TF in a parallel plate flow reactor. The steady state model was defined by the convection-diffusion equation and Michaelis-Menten reaction kinetics at the surface. The computational results were compared to experimental data for the generation of factor Xa by cultured rat vascular smooth muscle cells expressing TF. Based on discrepancies between numerical and experimental studies, the authors hypothesized the catalytic activity of the TF/ VIIa complex may be shear-dependent [100]. Towards the overall objective of developing an antithrombogenic biomaterial, Tummala and Hall studied the kinetics of factor Xa inhibition by surface-immobilized recombinant TFPI under unsteady flow conditions [101]. Similarly, Byun *et al.* investigated the association and dissociation kinetics of ATIII inactivation of thrombin accelerated by surface-immobilized heparin under steady flow conditions [102]. To date, finite element models that detail surface-bound reactions under flow have been restricted no more than a single reaction catalyzed by a single surface-immobilized species.

2.3.3. Models of coagulation incorporating spatial parameters

Ataullakhanov and colleagues developed mathematical models to describe the spatial dynamics of clot formation in the direction perpendicular to the vessel wall [103,

15

104]. In later reports, coagulation is initiated by a monolayer of TF-expressing cells and propagates into the bulk of plasma. Extrinsic, intrinsic, and protein C pathways were represented by 27 partial differential equations. Major findings include the roles of these specific coagulation pathways in the initiation, amplification, and termination phases of coagulation. It was observed that coagulation near the activating surface was determined by TF/VIIa catalyzed factor Xa production, which was rapidly inhibited close to the wall. In contrast, factor IXa diffused farther from the surface, and thus factor Xa generation and clot formation away from the reactive wall was dependent on intrinsic tenase (IXa/ VIIIa) activity. Additionally, the concentration wave of thrombin propagated away from the activation zone at a rate which was dependent on the efficiency of inhibitory mechanisms. Experimental and 'virtual' addition of plasma-phase thrombomodulin resulted in dose-dependent termination of thrombin generation and provided evidence of spatial localization of clot formation by TM with final clot lengths of 0.2-2 mm under diffusive conditions [105, 106]. These studies provide an interesting analysis of the roles of specific factors in relation to space due to diffusive effects, but neglect the essential role of blood flow in the transport analysis. Additionally, the spatial dynamics of clot localization by thrombomodulin would likely be affected by restricting the inhibitor to its physiologic site on the vessel surface.

Ismagilov *et al*. have studied the threshold response of coagulation to various spatial parameters, both *in vitro* and computationally, in microfluidic systems of TF-patterned phospholipid surfaces [14]. Numerically, initiation of a representative autocatalytic system by different sized and shaped patches was simulated using a finite element model, which defined three reactions and diffusion. The reaction 'modules' represented the kinetics of: 1) activation by the stimulus patch, corresponding to TF-mediated initiation of coagulation, 2) autocatalytic production of the activator in solution, representing the positive feedback mechanisms of coagulation, and 3) linear

16

consumption of the enzyme product in solution. A threshold response to the size of the TF patch was empirically and numerically shown to follow a simple scaling relationship based on the ratio of the rate of diffusion off of the patch to the rate of generation of the activating species [20]. Shape was also demonstrated to be a determinant of coagulation activation, with narrow rectangles and stars remaining below an activation threshold and circular, square, and wide rectangular patches resulting in significantly amplified product generation [107]. Furthermore, Kastrup *et al.* demonstrated that spatial distribution of TF patches, rather than total surface area, dictated the overall response of the system [16, 108]. Runyon *et al.* described the propagation of clotting from an initiating microchannel into a perpendicularly oriented channel with flowing plasma. In small microchannels, clotting was shown to be inhibited by surface-bound inhibitors, specifically TM, while in larger microchannels, the threshold response of clotting was regulated by the shear rate in the cross-flowing channel [109]. The simple numerical experiments served primarily to confirm experimental observations, and with the exception of the cross-flow channel, no convective effects were considered.

2.3.4. Models of fibrinolysis and platelet activation and aggregation

An important, yet still separate, area of modeling hemostasis and thrombosis involves the mechanical and rheological aspects of fibrinolysis and platelet activation and aggregation. Anand *et al.* have described some partial models of the formation and lysis of fibrin clots, including models of the extrinsic and fibrinolytic pathways in the absence of flow and continuum mechanical models of loose fibrin clots in a flow field [110, 111]. Fogelson and colleagues have modeled the adhesion and cohesion of activated platelets as elastic links which can influence the surrounding fluid motion. Simulations of platelet thrombus growth in small vessels demonstrated that shear stress exerted by the viscous fluid could modulate thrombus growth and cause remodeling of

thrombus shape [112]. Filipovic *et al.* described the motion, collision, adhesion, and cohesion of resting and activated platelets using dissipative particle dynamics (DPD) in which discretized blood components interact through conservative, dissipative, attractive, and random forces [113].

2.4.   Michaelis-Menten reaction kinetics

Michaelis-Menten kinetics are often used to describe the rate of biochemical reactions catalyzed by enzymes and are appropriate approximations in the absence of intermediate or product inhibition and in the absence of cooperativity. Leonor Michaelis and Maud Menten postulated that the enzyme (*E*) and substrate (*S*) were in fast equilibrium with the enzyme-substrate complex (*ES*), and that the enzyme-substrate complex dissociated irreversibly to yield free enzyme and product (*P*) (Eq. 2.1). Derivation of the Michaelis-Menten rate law (Eq. 2.2), which relates the initial reaction rate to the substrate concentration, relies on a quasi-steady state approximation for the enzyme-substrate intermediate [114].

Thus, reactions which are said to follow Michaelis-Menten kinetics are characterized by two parameters, k_{cat}, or the turnover number, and K_M, the Michaelis constant. The Michaelis constant is equal to the substrate concentration at which the reaction rate is half of its maximum value. K_M is related to, but does not fully describe, the affinity between enzyme and substrate.

$$E + S \underset{k_{-1}}{\overset{k_1}{\rightleftarrows}} ES \xrightarrow{k_{cat}} E + P$$
2.1

$$\frac{d[ES]}{dt} = k_1[E][S] - \left(k_{-1} + k_{cat}\right)[ES] = 0$$

$$\frac{d[P]}{dt} = k_{cat}[ES]$$

$$[E]_0 = [E] + [ES]$$

$$0 = k_1 \left([E]_0 - [ES]\right)[S] - \left(k_{-1} + k_{cat}\right)[ES]$$

$$0 = \left([E]_0 - [ES]\right)[S] - \underbrace{\frac{k_{-1} + k_{cat}}{k_1}}_{K_M}[ES] \qquad\qquad 2.2$$

$$\left(K_M + [S]\right)[ES] = [E]_0[S]$$

$$\frac{d[P]}{dt} = \frac{k_{cat}[E]_0[S]}{K_M + [S]}$$

2.5. Finite element modeling

Finite element method (FEM) is a numerical technique for solving partial differential equations. Originally proposed in the 1940s to approach structural analysis problems in civil engineering, FEM now finds application in a wide variety of disciplines. The computational method relies on mesh discretization of a continuous domain which subdivides the space into a finite number of 'elements'. The physics of each element are defined by its own set of physical properties and boundary conditions, and the simultaneous solution of the equations describing the individual elements approximate the behavior of the overall domain.

2.6. REFERENCES

1. Mann, K.G., K. Brummel, and S. Butenas. *What Is All That Thrombin For?* in *19th Congress of the International-Society-of-Thrombosis-and-Haemostasis.* 2003. Birmingham, England: Blackwell Publ Ltd.

2. Butenas, S., et al., *Mechanism of Factor VIIa-Dependent Coagulation in Hemophilia Blood.* Blood, 2002. **99**(3): p. 923-930.

3. Rock, G. and P. Wells, *New Concepts in Coagulation.* Critical Reviews in Clinical Laboratory Sciences, 1997. **34**(5): p. 475-501.

4. Mann, K.G., S. Butenas, and K. Brummel, *The Dynamics of Thrombin Formation.* Arteriosclerosis Thrombosis and Vascular Biology, 2003. **23**(1): p. 17-25.

5. Bourin, M.C. and U. Lindahl, *Glycosaminoglycans and the Regulation of Blood-Coagulation.* Biochemical Journal, 1993. **289**: p. 313-330.

6. Broze, G.J., *Tissue Factor Pathway Inhibitor.* Thrombosis and Haemostasis, 1995. **74**(1): p. 90-93.

7. Broze, G.J., *Tissue Factor Pathway Inhibitor and the Revised Theory of Coagulation.* Annual Review of Medicine, 1995. **46**: p. 103-112.

8. Jesty, J., T.C. Wun, and A. Lorenz, *Kinetics of the Inhibition of Factor XA and the Tissue Factor-Factor VIIA Complex by the Tissue Factor Pathway Inhibitor in the Presence and Absence of Heparin.* Biochemistry, 1994. **33**(42): p. 12686-12694.

9. Lu, G., G.J. Broze, and S. Krishnaswamy, *Formation of Factors IXa and Xa by the Extrinsic Pathway - Differential Regulation by Tissue Factor Pathway Inhibitor and Antithrombin III.* Journal of Biological Chemistry, 2004. **279**(17): p. 17241-17249.

10. Broze, G.J., K. Likert, and D. Higuchi, *Inhibition of Factor-VIIA Tissue Factor by Antithrombin-III and Tissue Factor Pathway Inhibitor.* Blood, 1993. **82**(5): p. 1679-1680.

11. Rao, L.V.M., S.I. Rapaport, and A.D. Hoang, *Binding of Factor-VIIA to Tissue Factor Permits Rapid Antithrombin-III Heparin Inhibition of Factor-VIIA.* Blood, 1993. **81**(10): p. 2600-2607.

12. vantVeer, C. and K.G. Mann, *Regulation of Tissue Factor Initiated Thrombin Generation by the Stoichiometric Inhibitors Tissue Factor Pathway Inhibitor, Antithrombin-III, and Heparin Cofactor-II.* Journal of Biological Chemistry, 1997. **272**(7): p. 4367-4377.

13. Mann, K.G., et al. *Models of Blood Coagulation.* 2006: Academic Press Inc Elsevier Science.

14. Shen, F., C.J. Kastrup, and R.F. Ismagilov, *Using Microfluidics to Understand the Effect of Spatial Distribution of Tissue Factor on Blood Coagulation.* Thrombosis Research, 2008. **122**: p. S27-S30.

15. Shen, F., et al., *Threshold Response of Initiation of Blood Coagulation by Tissue Factor in Patterned Microfluidic Capillaries Is Controlled by Shear Rate.* Arteriosclerosis Thrombosis and Vascular Biology, 2008. **28**(11): p. 2035-U226.

16. Kastrup, C.J., et al., *Modular Chemical Mechanism Predicts Spatiotemporal Dynamics of Initiation in the Complex Network of Hemostasis.* Proceedings of the National Academy of Sciences of the United States of America, 2006. **103**(43): p. 15747-15752.

17. Hockin, M.F., et al., *A Model for the Stoichiometric Regulation of Blood Coagulation.* Journal of Biological Chemistry, 2002. **277**(21): p. 18322-18333.

18. Willems, G.M., et al., *Simulation-Model for Thrombin Generation in Plasma.* Haemostasis, 1991. **21**(4): p. 197-207.

19. Beltrami, E. and J. Jesty, *The Role of Membrane Patch Size and Flow in Regulating a Proteolytic Feedback Threshold on a Membrane: Possible Application in Blood Coagulation.* Mathematical Biosciences, 2001. **172**(1): p. 1-13.

20. Kastrup, C.J., et al., *Characterization of the Threshold Response of Initiation of Blood Clotting to Stimulus Patch Size.* Biophysical Journal, 2007. **93**(8): p. 2969-2977.

21. Jesty, J., E. Beltrami, and G. Willems, *Mathematical-Analysis of a Proteolytic Positive-Feedback Loop - Dependence of Lag Time and Enzyme Yields on the Initial Conditions and Kinetic-Parameters.* Biochemistry, 1993. **32**(24): p. 6266-6274.

22. Marcum, J.A., et al., *Cloned Bovine Aortic Endothelial-Cells Synthesize Anticoagulantly Active Heparan-Sulfate Proteoglycan.* Journal of Biological Chemistry, 1986. **261**(16): p. 7507-7517.

23. Weksler, B.B., A.J. Marcus, and E.A. Jaffe, *Synthesis of Prostaglandin-I2 (Prostacyclin) by Cultured Human and Bovine Endothelial Cells - (Prostaglandin-X Inhibition of Platelet Aggregation Thrombogenesis).* Proceedings of the National Academy of Sciences of the United States of America, 1977. **74**(9): p. 3922-3926.

24. Marcus, A.J., et al., *Inhibition of Platelet-Function by an Aspirin-Insensitive Endothelial-Cell Adpase - Thromboregulation by Endothelial-Cells.* Journal of Clinical Investigation, 1991. **88**(5): p. 1690-1696.

25. Griffith, T.M., et al., *The Nature of Endothelium-Derived Vascular Relaxant Factor.* Nature, 1984. **308**(5960): p. 645-647.

26. Ignarro, L.J., et al., *Endothelium-Derived Relaxing Factor Produced and Released from Artery and Vein Is Nitric-Oxide.* Proceedings of the National Academy of Sciences of the United States of America, 1987. **84**(24): p. 9265-9269.

27. Radomski, M.W., R.M.J. Palmer, and S. Moncada, *Endogenous Nitric-Oxide Inhibits Human-Platelet Adhesion to Vascular Endothelium.* Lancet, 1987. **2**(8567): p. 1057-1058.

28. Nicholson, A.C., et al., *Effector Cell Protease Receptor-1 Is a Vascular Receptor for Coagulation Factor Xa.* Journal of Biological Chemistry, 1996. **271**(45): p. 28407-28413.

29. Cheung, W.F., et al., *Identification of the Endothelial Cell Binding Site for Factor IX.* Proceedings of the National Academy of Sciences of the United States of America, 1996. **93**(20): p. 11068-11073.

30. Rottingen, J.A., et al., *Binding of Human Factor Viia to Tissue Factor Induces Cytosolic Ca2+ Signals in J82 Cells, Transfected Cos-1 Cells, Madin-Darby Canine Kidney-Cells and in Human Endothelial-Cells Induced to Synthesize Tissue Factor.* Journal of Biological Chemistry, 1995. **270**(9): p. 4650-4660.

31. Ogawa, S., et al. *Modulation of Endothelial Function by Hypoxia - Perturbation of Barrier and Anticoagulant Function, and Induction of a Novel Factor-X Activator.* in *International Scientific Symp on Fibrinogen, Thrombosis, Coagulation, and Fibrinolysis*. 1989. Taipei, Taiwan: Plenum Press Div Plenum Publishing Corp.

32. Liu, L. and G.M. Rodgers, *Characterization of an Inducible Endothelial Cell Prothrombin Activator.* Blood, 1995. **86**(10): p. 300-300.

33. Vu, T.K.H., et al., *Molecular-Cloning of a Functional Thrombin Receptor Reveals a Novel Proteolytic Mechanism of Receptor Activation.* Cell, 1991. **64**(6): p. 1057-1068.

34. Dahlback, B. and B.O. Villoutreix, *Regulation of Blood Coagulation by the Protein C Anticoagulant Pathway - Novel Insights into Structure-Function Relationships and Molecular Recognition.* Arteriosclerosis Thrombosis and Vascular Biology, 2005. **25**(7): p. 1311-1320.

35. Bourin, M.C., et al., *Relationship between Anticoagulant Activities and Polyanionic Properties of Rabbit Thrombomodulin.* Journal of Biological Chemistry, 1988. **263**(17): p. 8044-8052.

36. Esmon, C.T. and W.G. Owen, *Identification of an Endothelial-Cell Cofactor for Thrombin-Catalyzed Activation of Protein-C.* Proceedings of the National Academy of Sciences of the United States of America-Biological Sciences, 1981. **78**(4): p. 2249-2252.

37. Esmon, N.L., W.G. Owen, and C.T. Esmon, *Isolation of a Membrane-Bound Cofactor for Thrombin-Catalyzed Activation of Protein-C.* Journal of Biological Chemistry, 1982. **257**(2): p. 859-864.

38. Owen, W.G. and C.T. Esmon, *Functional-Properties of an Endothelial-Cell Cofactor for Thrombin-Catalyzed Activation of Protein-C.* Journal of Biological Chemistry, 1981. **256**(11): p. 5532-5535.

39. Healy, A.M., et al., *Absence of the Blood-Clotting Regulator Thrombomodulin Causes Embryonic Lethality in Mice before Development of a Functional Cardiovascular-System.*

Proceedings of the National Academy of Sciences of the United States of America, 1995. **92**(3): p. 850-854.

40. Weiler-Guettler, H., et al., *A Targeted Point Mutation in Thrombomodulin Generates Viable Mice with a Prethrombotic State.* Journal of Clinical Investigation, 1998. **101**(9): p. 1983-1991.

41. Isermann, B., et al., *Endothelium-Specific Loss of Murine Thrombomodulin Disrupts the Protein C Anticoagulant Pathway and Causes Juvenile-Onset Thrombosis.* Journal of Clinical Investigation, 2001. **108**(4): p. 537-546.

42. Ohlin, A.K. and R.A. Marlar, *The First Mutation Identified in the Thrombomodulin Gene in a 45-Year-Old Man Presenting with Thromboembolic-Disease.* Blood, 1995. **85**(2): p. 330-336.

43. Norlund, L., B. Zoller, and A.K. Ohlin, *A Novel Thrombomodulin Gene Mutation in a Patient Suffering from Sagittal Sinus Thrombosis.* Thrombosis and Haemostasis, 1997. **78**(4): p. 1164-1166.

44. Doggen, C.J.M., et al., *A Mutation in the Thrombomodulin Gene, (127)G to a Coding for Ala25thr, and the Risk of Myocardial Infarction in Men.* Thrombosis and Haemostasis, 1998. **80**(5): p. 743-748.

45. Ireland, H., et al., *Thrombomodulin Gene Mutations Associated with Myocardial Infarction.* Circulation, 1997. **96**(1): p. 15-18.

46. Kunz, G., et al., *Identification and Characterization of a Thrombomodulin Gene Mutation Coding for an Elongated Protein with Reduced Expression in a Kindred with Myocardial Infarction.* Blood, 2000. **95**(2): p. 569-576.

47. Ohsawa, M., et al., *1 Alpha,25-Dihydroxyvitamin D-3 and Its Potent Synthetic Analogs Downregulate Tissue Factor and Upregulate Thrombomodulin Expression in Monocytic Cells, Counteracting the Effects of Tumor Necrosis Factor and Oxidized Ldl.* Circulation, 2000. **102**(23): p. 2867-2872.

48. Fu, Q., et al., *Involvement of Heat Shock Factor 1 in Statin-Induced Transcriptional Upregulation of Endothelial Thrombomodulin.* Circulation Research, 2008. **103**(4): p. 369-377.

49. Lin, S.J., et al., *Pravastatin Induces Thrombomodulin Expression in Tnf Alpha-Treated Human Aortic Endothelial Cells by Inhibiting Rac1 and Cdc42 Translocation and Activity.* Journal of Cellular Biochemistry, 2007. **101**(3): p. 642-653.

50. Masamura, K., et al., *Pitavastatin-Induced Thrombomodulin Expression by Endothelial Cells Acts Via Inhibition of Small G Proteins of the Rho Family.* Arteriosclerosis Thrombosis and Vascular Biology, 2003. **23**(3): p. 512-517.

51. Shi, J.M., et al., *Statins Increase Thrombomodulin Expression and Function in Human Endothelial Cells by a Nitric Oxide-Dependent Mechanism and Counteract Tumor Necrosis Factor Alpha-Induced Thrombomodulin Downregulation.* Blood Coagulation & Fibrinolysis, 2003. **14**(6): p. 575-585.

52. Kim, H.K., et al., *Aurintricarboxylic Acid Upregulates the Thrombomodulin Expression of Endothelial Cells and Peripheral Blood Monocytes.* Blood Coagulation & Fibrinolysis, 2008. **19**(6): p. 489-494.

53. Hirokawa, K. and N. Aoki, *Regulatory Mechanisms for Thrombomodulin Expression in Human Umbilical Vein Endothelial-Cells Invitro.* Journal of Cellular Physiology, 1991. **147**(1): p. 157-165.

54. Sohn, R.H., et al., *Regulation of Endothelial Thrombomodulin Expression by Inflammatory Cytokines Is Mediated by Activation of Nuclear Factor-Kappa B.* Blood, 2005. **105**(10): p. 3910-3917.

55. Conway, E.M. and R.D. Rosenberg, *Tumor Necrosis Factor Suppresses Transcription of the Thrombomodulin Gene in Endothelial-Cells.* Molecular and Cellular Biology, 1988. **8**(12): p. 5588-5592.

56. Lentz, S.R., M. Tsiang, and J.E. Sadler, *Regulation of Thrombomodulin by Tumor-Necrosis-Factor-Alpha - Comparison of Transcriptional and Posttranscriptional Mechanisms.* Blood, 1991. **77**(3): p. 542-550.

57. Moore, K.L., C.T. Esmon, and N.L. Esmon, *Tumor Necrosis Factor Leads to the Internalization and Degradation of Thrombomodulin from the Surface of Bovine Aortic Endothelial-Cells in Culture.* Blood, 1989. **73**(1): p. 159-165.

58. Maruyama, I., et al., *Increased Expression of Thrombomodulin on the Cultured Human Umbilical Vein Endothelial-Cells and Mouse Hemangioma Cells by Cyclic-Amp.* Thrombosis Research, 1991. **61**(3): p. 301-310.

59. Nawroth, P.P., et al., *Interleukin-1 Induces Endothelial-Cell Procoagulant While Suppressing Cell-Surface Anticoagulant Activity.* Proceedings of the National Academy of Sciences of the United States of America, 1986. **83**(10): p. 3460-3464.

60. Ohji, T., et al., *Transforming Growth-Factor Beta1 and Beta2 Induce Down-Modulation of Thrombomodulin in Human Umbilical Vein Endothelial-Cells.* Thrombosis and Haemostasis, 1995. **73**(5): p. 812-818.

61. Moore, K.L., et al., *Endotoxin Enhances Tissue Factor and Suppresses Thrombomodulin Expression of Human Vascular Endothelium Invitro.* Journal of Clinical Investigation, 1987. **79**(1): p. 124-130.

62. Faust, S.N., et al., *Dysfunction of Endothelial Protein C Activation in Severe Meningococcal Sepsis.* New England Journal of Medicine, 2001. **345**(6): p. 408-416.

63. Ogawa, S., et al., *Hypoxia Modulates the Barrier and Coagulant Function of Cultured Bovine Endothelium - Increased Monolayer Permeability and Induction of Procoagulant Properties.* Journal of Clinical Investigation, 1990. **85**(4): p. 1090-1098.

64. Drake, T.A., J.H. Morrissey, and T.S. Edgington, *Selective Cellular Expression of Tissue Factor in Human-Tissues - Implications for Disorders of Hemostasis and Thrombosis.* American Journal of Pathology, 1989. **134**(5): p. 1087-1097.

65. Fleck, R.A., et al., *Localization of Human Tissue Factor Antigen by Immunostaining with Monospecific, Polyclonal Anti-Human Tissue Factor Antibody.* Thrombosis Research, 1990. **57**(5): p. 765-781.

66. Wilcox, J.N., et al., *Localization of Tissue Factor in the Normal Vessel Wall and in the Atherosclerotic Plaque.* Proceedings of the National Academy of Sciences of the United States of America, 1989. **86**(8): p. 2839-2843.

67. Falati, S., et al., *Real-Time in Vivo Imaging of Platelets, Tissue Factor and Fibrin During Arterial Thrombus Formation in the Mouse.* Nature Medicine, 2002. **8**(10): p. 1175-1180.

68. Eilertsen, K.E. and B. Osterud, *Tissue Factor: (Patho)Physiology and Cellular Biology.* Blood Coagulation & Fibrinolysis, 2004. **15**(7): p. 521-538.

69. Badimon, L. *Atherosclerosis and Thrombosis: Lessons from Animal Models.* in *XVIIIth Congress of the International-Society-on-Thrombosis-and-Haemostasis.* 2001. Paris, France: F K Schattauer Verlag Gmbh.

70. Steffel, J., et al., *Histamine Induces Tissue Factor Expression - Implications for Acute Coronary Syndromes.* Circulation, 2005. **112**(3): p. 341-349.

71. Setty, B.N.Y., et al., *Heme Induces Endothelial Tissue Factor Expression: Potential Role in Hemostatic Activation in Patients with Hemolytic Anemia.* Journal of Thrombosis and Haemostasis, 2008. **6**(12): p. 2202-2209.

72. Bevilacqua, M.P., et al., *Recombinant Tumor-Necrosis-Factor Induces Procoagulant Activity in Cultured Human Vascular Endothelium - Characterization and Comparison with the Actions of Interleukin-1.* Proceedings of the National Academy of Sciences of the United States of America, 1986. **83**(12): p. 4533-4537.

73. Wu, J.B., et al., *C-Reactive Protein Enhances Tissue Factor Expression by Vascular Smooth Muscle Cells: Mechanisms and in Vivo Significance.* Arteriosclerosis Thrombosis and Vascular Biology, 2008. **28**(6): p. E40-E40.

74. Breitenstein, A., et al., *Amiodarone Inhibits Arterial Thrombus Formation and Tissue Factor Translation.* Arteriosclerosis Thrombosis and Vascular Biology, 2008. **28**(12): p. 2231-U177.

75. Bogdanov, V.Y., et al., *Alternatively Spliced Human Tissue Factor: A Circulating, Soluble, Thrombogenic Protein.* Nature Medicine, 2003. **9**(4): p. 458-462.

76. Szotowski, B., et al., *Procoagulant Soluble Tissue Factor Is Released from Endothelial Cells in Response to Inflammatory Cytokines.* Circulation Research, 2005. **96**(12): p. 1233-1239.

77.   Kushak, R.I., et al., *Detached Endothelial Cells and Microparticles as Sources of Tissue Factor Activity.* Thrombosis Research, 2005. **116**(5): p. 409-419.

78.   Mallat, Z., et al., *Shed Membrane Microparticles with Procoagulant Potential in Human Atherosclerotic Plaques - a Role for Apoptosis in Plaque Thrombogenicity.* Circulation, 1999. **99**(3): p. 348-353.

79.   Nieuwland, R., et al., *Cell-Derived Microparticles Generated in Patients During Cardiopulmonary Bypass Are Highly Procoagulant.* Circulation, 1997. **96**(10): p. 3534-3541.

80.   Satta, N., et al., *Monocyte Vesiculation Is a Possible Mechanism for Dissemination of Membrane-Associated Procoagulant Activities and Adhesion Molecules after Stimulation by Lipopolysaccharide.* Journal of Immunology, 1994. **153**(7): p. 3245-3255.

81.   Nesheim, M.E., R.P. Tracy, and K.G. Mann, *Clotspeed, a Mathematical Simulation of the Functional-Properties of Prothrombinase.* Journal of Biological Chemistry, 1984. **259**(3): p. 1447-1453.

82.   Jones, K.C. and K.G. Mann, *A Model for the Tissue Factor Pathway to Thrombin .2. A Mathematical Simulation.* Journal of Biological Chemistry, 1994. **269**(37): p. 23367-23373.

83.   Orfeo, T., et al., *The Tissue Factor Requirement in Blood Coagulation.* Journal of Biological Chemistry, 2005. **280**(52): p. 42887-42896.

84.   Brummel-Ziedins, K., et al., *The Plasma Hemostatic Proteome: Thrombin Generation in Healthy Individuals.* Journal of Thrombosis and Haemostasis, 2005. **3**(7): p. 1472-1481.

85.   Beltrami, E. and J. Jesty, *Mathematical-Analysis of Activation Thresholds in Enzyme-Catalyzed Positive Feedbacks - Application to the Feedbacks of Blood-Coagulation.* Proceedings of the National Academy of Sciences of the United States of America, 1995. **92**(19): p. 8744-8748.

86.   Bungay, S.D., P.A. Gentry, and R.D. Gentry, *A Mathematical Model of Lipid-Mediated Thrombin Generation.* Mathematical Medicine and Biology-a Journal of the Ima, 2003. **20**(1): p. 105-129.

87.   Bungay, S.D., *Modelling the Effect of Amplification Pathway Factors on Thrombin Generation: A Comparison of Hemophilias.* Transfusion and Apheresis Science, 2008. **38**(1): p. 41-47.

88.   Khanin, M.A., D.V. Rakov, and A.E. Kogan, *Mathematical Model for the Blood Coagulation Prothrombin Time Test.* Thrombosis Research, 1998. **89**(5): p. 227-232.

89.   Kogan, A.E., D.V. Kardakov, and M.A. Khanin, *Analysis of the Activated Partial Thromboplastin Time Test Using Mathematical Modeling.* Thrombosis Research, 2001. **101**(4): p. 299-310.

90.   Kramoroff, A. and J.M. Nigretto, *In Vitro Factor XI Activation Mechanism According to an Optimized Model of Activated Partial Thromboplastin Time Test.* Blood Coagulation & Fibrinolysis, 2001. **12**(4): p. 289-299.

91.   Zhu, D., *Mathematical Modeling of Blood Coagulation Cascade: Kinetics of Intrinsic and Extrinsic Pathways in Normal and Deficient Conditions.* Blood Coagulation & Fibrinolysis, 2007. **18**(7): p. 637-646.

92.   Leipold, R.J., et al., *Mathematical-Model of Serine-Protease Inhibition in the Tissue Factor Pathway to Thrombin.* Journal of Biological Chemistry, 1995. **270**(43): p. 25383-25387.

93.   Guo, Z., et al., *Mathematical Modeling of Material-Induced Blood Plasma Coagulation.* Biomaterials, 2006. **27**(5): p. 796-806.

94.   Mounts, W.M. and M.N. Liebman, *Qualitative Modeling of Normal Blood Coagulation and Its Pathological States Using Stochastic Activity Networks.* International Journal of Biological Macromolecules, 1997. **20**(4): p. 265-281.

95.   Lo, K., W.S. Denney, and S.L. Diamond, *Stochastic Modeling of Blood Coagulation Initiation.* Pathophysiology of Haemostasis and Thrombosis, 2005. **34**(2-3): p. 80-90.

96.   Basmadjian, D., *The Effect of Flow and Mass-Transport in Thrombogenesis.* Annals of Biomedical Engineering, 1990. **18**(6): p. 685-709.

97. Baldwin, S.A. and D. Basmadjian, *A Mathematical-Model of Thrombin Production in Blood-Coagulation .1. The Sparsely Covered Membrane Case.* Annals of Biomedical Engineering, 1994. **22**(4): p. 357-370.

98. Kuharsky, A.L. and A.L. Fogelson, *Surface-Mediated Control of Blood Coagulation: The Role of Binding Site Densities and Platelet Deposition.* Biophysical Journal, 2001. **80**(3): p. 1050-1074.

99. Fogelson, A.L. and N. Tania, *Coagulation under Flow: The Influence of Flow-Mediated Transport on the Initiation and Inhibition of Coagulation.* Pathophysiology of Haemostasis and Thrombosis, 2005. **34**(2-3): p. 91-108.

100. Hall, C.L., S.M. Slack, and V.T. Turitto, *A Computational Analysis of FXa Generation by TF : FVIIa on the Surface of Rat Vascular Smooth Muscle Cells.* Annals of Biomedical Engineering, 1998. **26**(1): p. 28-36.

101. Tummala, S.R. and C.L. Hall, *Computational Modeling of Factor Xa Inhibition by Immobilized Tissue Factor Pathway Inhibitor.* Annals of Biomedical Engineering, 2007. **35**(3): p. 408-418.

102. Byun, Y., H.A. Jacobs, and S.W. Kim, *Binding of Antithrombin III and Thrombin to Immobilized Heparin under Flow Conditions.* Biotechnology Progress, 1996. **12**(2): p. 217-225.

103. Zarnitsina, V.I., A.V. Pokhilko, and F.I. Ataullakhanov, *A Mathematical Model for the Spatio-Temporal Dynamics of Intrinsic Pathway of Blood Coagulation .1. The Model Description.* Thrombosis Research, 1996. **84**(4): p. 225-236.

104. Zarnitsina, V.I., A.V. Pokhilko, and F.I. Ataullakhanov, *A Mathematical Model for the Spatio-Temporal Dynamics of Intrinsic Pathway of Blood Coagulation .2. Results.* Thrombosis Research, 1996. **84**(5): p. 333-344.

105. Ataullakhanov, F.I., et al., *Spatio-Temporal Dynamics of Blood Coagulation and Pattern Formation. A Theoretical Approach.* International Journal of Bifurcation and Chaos, 2002. **12**(9): p. 1985-2002.

106. Panteleev, M.A., et al., *Spatial Propagation and Localization of Blood Coagulation Are Regulated by Intrinsic and Protein C Pathways, Respectively.* Biophysical Journal, 2006. **90**(5): p. 1489-1500.

107. Kastrup, C.J., F. Shen, and R.F. Ismagilov, *Response to Shape Emerges in a Complex Biochemical Network and Its Simple Chemical Analogue.* Angewandte Chemie-International Edition, 2007. **46**(20): p. 3660-3662.

108. Kastrup, C.J., et al., *Spatial Localization of Bacteria Controls Coagulation of Human Blood by 'Quorum Acting'.* Nature Chemical Biology, 2008. **4**(12): p. 742-750.

109. Runyon, M.K., et al., *Effects of Shear Rate on Propagation of Blood Clotting Determined Using Microfluidics and Numerical Simulations.* Journal of the American Chemical Society, 2008. **130**(11): p. 3458-3464.

110. Anand, M., K. Rajagopal, and K.R. Rajagopal, *A Viscoelastic Fluid Model for Describing the Mechanics of a Coarse Ligated Plasma Clot.* Theoretical and Computational Fluid Dynamics, 2006. **20**(4): p. 239-250.

111. Anand, M., K. Rajagopal, and K.R. Rajagopal, *A Model for the Formation, Growth, and Lysis of Clots in Quiescent Plasma. A Comparison between the Effects of Antithrombin III Deficiency and Protein C Deficiency.* Journal of Theoretical Biology, 2008. **253**(4): p. 725-738.

112. Fogelson, A.L. and R.D. Guy, *Platelet-Wall Interactions in Continuum Models of Platelet Thrombosis: Formulation and Numerical Solution.* Mathematical Medicine and Biology-a Journal of the Ima, 2004. **21**(4): p. 293-334.

113. Filipovic, N., M. Kojic, and A. Tsuda, *Modelling Thrombosis Using Dissipative Particle Dynamics Method.* Philosophical Transactions of the Royal Society a-Mathematical Physical and Engineering Sciences, 2008. **366**(1879): p. 3265-3279.

114. Briggs, G.E. and J.B.S. Haldane, *A Note on the Kinetics of Enzyme Action.* Biochemical Journal, 1925. **19**(2): p. 338-339.

CHAPTER 3

SIMULATED SURFACE-INDUCED THROMBIN GENERATION IN A FLOW FIELD

Abstract

A computational model of blood coagulation is presented with particular emphasis on the regulatory effects of blood flow, spatial distribution of tissue factor (TF), and the importance of the thrombomodulin (TM)-APC inhibitory pathway. Significantly, we demonstrate that an 'effective prothrombotic zone' (EPZ) may be defined that extends well beyond the dimensions of injury. The size of this zone is dependent not only on the concentrations of all reactive species, but also on the dimensions of TF expression, the densities of surface molecules, and the characteristics of the flow field. In the case of tandem sites of TF, the relationship between the magnitude of the EPZ and the interval distance between TF sites dictated the net response of the system. Multiple TF sites, which individually failed to activate the coagulation pathway, were shown to interact in an additive manner to yield a prothrombotic system. Furthermore, activation of the TM-APC pathway in the regions between sites of TF downregulated the thrombin response at subsequent TF sites. The implications of prothrombotic effects which extend downstream beyond the discrete site of injury to interact with subsequent lesions are critical given the systemic nature of atherosclerotic disease.

3.1.   Introduction

Blood coagulation is a highly dynamic, nonlinear reaction network that is characterized by the activation and amplification of circulating zymogens, several surface-associated enzyme complexes, and positive and negative feedback loops. The

26

clotting 'cascade' involves a series of serine protease reactions converting inactive

zymogens to active enzymes. Coagulation is traditionally divided into two parallel

pathways, the intrinsic and extrinsic pathways, which converge on a common pathway.

However, it is widely accepted that the extrinsic pathway is principal initiating pathway of

coagulation *in vivo*. Exposure of subendothelial tissue factor (TF) to the bloodstream

and subsequent formation of the TF/VIIa complex leads to the activation of both factors

IX and X. The generation of factor Xa by either intrinsic (IXa/VIIIa) or extrinsic (TF/VIIa)

tenase leads to the assembly of prothrombinase (Xa/Va), which cleaves prothrombin

(factor II) to thrombin (IIa). Amplification of the cascade is achieved through positive

feedback of thrombin to activate factors V and VIII [1-3]. Regulators of thrombin

generation include the thrombin- and thrombomodulin (TM)-dependent protein C

pathway, factor Xa-dependent tissue factor pathway inhibitor (TFPI), and the multi-

substrate serine protease inhibitor, antithrombin III (ATIII) [1-6]. Additionally, blood flow

serves as a critical regulator of thrombosis by removing activated enzymes from the site

of reactivity [7]. The temporal and spatial dynamics of coagulation under flow are

complex and mathematical modeling provides a means for the systematic study of

individual components and their roles in promoting or regulating clot formation.

3.2.   Rationale for model approach

Mathematical models of blood coagulation have been developed with varying

degrees of complexity and for applications including, but not limited to, the study of

coagulation dynamics and phenomena, pharmacologic and biomaterial development,

and the simulation of clinical diagnostic values. Generally, fluid phase models of the

kinetics of coagulation are both computationally and experimentally less complex. As

such, computational models are able to incorporate a large number of species and their

reactions, and empirical data is often available for regression analysis and model

validation. However, the essential role of blood flow in promoting the delivery of substrates to the vessel wall and in regulating the thrombin response by removing activated clotting factors is well recognized. The major limitation of existing pseudo-one compartment models of coagulation under flow [8, 9], in which the vascular space is divided into bulk and a boundary volumes, is the assumption of spatially homogenous, or well mixed, plasma compartments. This assumption breaks down as the dimensions of the boundary volume increase, such as that which would occur at low shear rates and for large reaction areas, due to the potential for substrate depletion and product accumulation at the surface or at upstream sites. In contrast, while models incorporating spatial effects have recently been reported [10-12], most describe only reaction and diffusion and do not include convective effects.

A finite element model does not require the assumption of spatial homogeneity and permits the definition of a flow model of thrombin generation that accounts for distinct sites of tissue factor (TF) and thrombomodulin (TM) surface expression. Uniquely, spatial parameters quantifying the localization or propagation of thrombin formation, in both vertical and longitudinal directions, may be defined. To date, finite element models that detail surface-bound reactions under flow have been restricted to no more than a single reaction catalyzed by a single surface-immobilized species bound to a cofactor [13-15]. We present the first comprehensive model of thrombin generation under flow conditions characterized by distinct sites of coagulation initiation and regulation.

3.3. Methods

3.3.1. Model description

Herein, we describe a finite element model of thrombin generation under defined flow conditions, initiated and modulated by spatially discrete regions of surface bound

tissue factor and thrombomodulin, respectively. The model incorporates fluid phase and surface-associated reactions of the extrinsic, intrinsic, and common pathways, as well as three inhibitory pathways (Figure 3.1). The spatially heterogeneous model describes coagulation events that occur following tissue factor exposure at a discrete upstream site, as well as related mechanisms that regulate thrombin generation, including those mediated by an intact endothelium, represented as a thrombomodulin-containing surface (Figure 3.2A). Specifically, we assume that the coagulation cascade is initiated by binding of factor VIIa to tissue factor, leading to the formation of extrinsic tenase. Generation of factor Xa leads to activation of factors V and VII. The resultant surface-associated complex, Xa/Va, or prothrombinase, cleaves prothrombin to thrombin, which by activating factors V and VIII serves as a positive feedback mediator. Generation of factor VIIIa, in association with IXa, affords intrinsic tenase, or IXa/VIIIa. We assume that factor IXa is generated solely by TF/VIIa without participation of intrinsic pathway factors XI and XII.

Three major reaction pathways that serve to inhibit thrombin generation are included in the model system - antithrombin III (ATIII), tissue factor pathway inhibitor (TFPI), and the protein C pathway. ATIII serves to inactivate factors IXa, Xa, and thrombin. Tissue factor pathway inhibitor is incorporated as an inhibitor of TF/VIIa through a two-step process, whereby TFPI binds to Xa followed by its reversible association with TF/VIIa. Finally, we account for the production of activated protein C, which inactivates factors Va and VIIIa. Table 3.1 summarizes all model reactions and the kinetic parameters and distinguishes between surface-bound reactions and those that occur both in the fluid phase and at the blood-vessel wall interface.

Table 3.1. Michaelis-Menten kinetic parameters for coagulation and inhibitory reactions

No.	Description of reaction	(F)luid-phase or (S)urface-bound	k_{cat} (s^{-1})	K_m (μM)	Ref.
1	Activation of factor X by TF/VIIa	S	1.2	0.45	[22]
2	Conversion of prothrombin by Va-Xa	S	33	0.21	[23]
3	Activation of protein C by thrombin-TM	S	5.58	0.7	[24]
4	Inactivation of factors Va and VIIIa by APC	S	0.58	0.025	[25]
5	Activation of factor IX by TF-VIIa	S	0.34	0.17	[26]
6	Activation of factor VIII by thrombin	F	0.9	0.20	[27, 28]
7	Activation of factor X by VIIIa-IXa	S	20	0.16	[29]
8	Activation of factor V by thrombin	F	0.23	0.072	[30]
9	Activation of factor VII by factor Xa	F	5.0	1.2	[29]
10	Activation of factor V by factor Xa	S	0.046	0.01	[30]
11	Activation of factor VII by thrombin	F	0.061	2.7	[31]

The reaction area of interest is modeled as a two-dimensional flow field of length, *L*, and half-height, *B*, with upper and lower inert and reactive surfaces, respectively. Steady, one-dimensional, parabolic flow, which is algebraically defined, is assumed (Eq. 3.1). In contrast to previous models of surface-induced coagulation, mass transfer approximations are not used to describe transport of reactants to the surface. Equation 3.2 describes convective-diffusive transport of species, *i*, with accumulation and convective terms on the left-hand side and diffusive and reaction terms on the right-hand side.

$$u(y) = \frac{B}{2} \dot{\gamma} \left[1 - \left(\frac{y - B}{B} \right)^2 \right]$$

3.1

$$\frac{\partial c_i}{\partial t} + u \frac{\partial c_i}{\partial x} = D_i \left(\frac{\partial^2 c_i}{\partial x^2} + \frac{\partial^2 c_i}{\partial y^2} \right) + R$$

3.2

where x and y are parallel and perpendicular to the reactive wall, respectively, $y=0$ is defined at the reactive surface, $u(y)$ is the fluid velocity in the x-direction as a function of y, B is the half-height of the chamber, γ is wall shear rate, c_i is the concentration of species, i, t is time, D_i is the diffusion coefficient of species, i, and R is the rate of production in the solution phase.

All fluid-phase zymogen and enzyme concentrations are initially set to zero. The surface density of tissue factor and thrombomodulin remain constant and, at the outset, both are free of bound cofactors. Convective flux transports zymogens into the flow field at constant inlet concentrations equal to mean physiologic values. Initial conditions assumes that 1% of factor VII circulates as VIIa [16]. Diffusion transports coagulation factors to the lower reactive surface, where reaction kinetics define flux boundary conditions. Table 3.2 summarizes inlet concentrations, molecular weights, and diffusivities for all coagulation factors [1, 16-18]. Moderate hemophilias A and B were defined at 5% of the normal plasma concentration of factors VIII and IX, respectively. Diffusion coefficients were calculated from molecular weights according to Young *et al.* [19].

The reactive boundary is divided into localized upstream TF and downstream TM regions. The primary analysis was performed assuming a 10 mm entrance region, 2 mm TF region, and a 34 mm TM region. The length of the TF region is similar in dimension to that of a ruptured coronary plaque or the interface between a vascular graft and host vessel at an anastomotic site [20].

31

Table 3.2. Plasma concentrations of coagulation factors, inhibitors, and related diffusion coefficients

Coagulation factor	Plasma levels (nM)	Molecular weight (kD)	Diffusivity [†] (x 10^{-7} cm^2/s)	Ref.
Prothrombin	1400	72	6.21	[1]
Thrombin	--	36.7	7.78	--
Factor V	20	330	3.74	[1]
Factor Va	--	168	4.69	--
Factor VII	10	50	7.02	[1]
Factor VIIa	0.1	50	7.02	[16]
Factor VIII	0.7	170	4.67	[1]
Factor VIIIa	--	166	4.70	--
Factor IX	90	55	6.80	[1]
Factor IXa	--	45	7.27	--
Factor X	170	58.9	6.64	[1]
Factor Xa	--	46	7.22	--
Protein C	60	62	6.53	[1]
Activated protein C	--	56.2	6.75	--
Antithrombin III	2400	58	6.68	[17]
TFPI	2.5	34	7.98	[18]
TFPI-Xa	0	80	6.00	--

[†] Calculated from molecular weight according to Young *et al.* [19].

3.3.2. Model assumptions

Reactive surface. A number of simplifying assumptions were made with respect to surface-bound species and reactions. The model defines discrete regions of TF or TM expression, but otherwise does not discriminate between subendothelium, resting endothelium, activated endothelium, or platelet membrane surfaces. TF and TM surface expression is assumed constant over all time points. TF only binds factor VIIa and not factor VII. Activation of factor VII is assumed to occur in the fluid phase only for computational simplicity. The model assumes that phospholipid conditions promote surface-associated enzyme complex assembly, or in other words, that membrane-binding sites are in excess. Surface complexes, such as prothrombinase (Xa/Va), are assumed to be generated through a bimolecular reaction between two solution phase species spatially localized at $y=0$. For simplicity, the assembly of these complexes is assumed to occur in one step. Lateral diffusion along the reactive surface is considered negligible compared to transport by flow along the direction parallel to the surface.

Kinetic parameters. Serine protease activation involves one or more cleavage events and is therefore considered irreversible. All reactions are assumed to follow Michaelis-Menten kinetics. Furthermore, the capacity of enzymes, in the absence of respective cofactors, to convert primary substrates is considered negligible. For example, conversion of prothrombin to thrombin by Xa/Va is 10^5-fold faster than Xa alone [21]. Only the former reaction is considered. Kinetic parameters were obtained from the experimental literature of isolated reaction systems (Tables 3.1 and 3.3) with preference given to studies deemed most relevant with respect to substrate and enzyme concentrations within the physiologic range, the presence of appropriate cofactors such as phospholipid surfaces and calcium, where applicable, and method of measurement [5, 22-34]. In the cases where only equilibrium binding constants, K_d, were reported, k_a

was set to the diffusional limit, 10^8 M^{-1} s^{-1}, and k_d was calculated ($k_d = K_d \times k_a$).

Association and dissociation reactions are reversible except where noted.

Table 3.3. Equilibrium association and dissociation parameters for coagulation and inhibitory reactions

No.	Enzyme	Cofactor or Inhibitor	k_a (μM^{-1} s^{-1})	k_d (s^{-1})	Ref.
Enzymatic complexes [†]					
1	Factor VIIa	TF	100	0.06	[32]
2	Factor Xa	Factor Va	100	0.01	[33]
3	Thrombin	TM	100	0.01	[24]
4	Factor IXa	Factor VIIIa	100	0.01	[33]
Inhibitory reactions					
5	Thrombin	ATIII	6.8e-3	-- [‡]	[34]
6	Factor IXa	ATIII	2.6e-3	-- [‡]	[34]
7	Factor Xa	TFPI	16	3.3e-4	[5]
8	TF-VIIa	TFPI-Xa	10	1.1e-3	[5]

[†] k_a assumed to be at the diffusional limit; k_d calculated from equilibrium constant, K_d.

[‡] Irreversible binding reaction.

Inhibitory reactions. Thrombin activates protein C when bound to TM, and the thrombin-TM complex is considered the only source for protein C activation. Factor Xa-mediated activation of protein C has not been confirmed and, therefore, is not considered [35, 36]. Thrombin's ability to participate in procoagulant reactions is eliminated once bound to TM. Irreversible inactivation of factors Va and VIIIa by APC follows Michaelis-Menten kinetics. The cofactor activity of protein S was indirectly accounted for through the choice of kinetic parameters for APC-mediated inactivation of

factor Va and VIIIa which were measured in the presence of physiologic concentrations

of protein S [25]. Inactivation of factors Va and VIIIa is assumed to occur at equal rates,

though factor Va inactivation has been reported to be up to 6x faster than VIIIa

inactivation [30]. Factors IXa and Xa protect their respective cofactors VIIIa and Va from

inactivation by APC when associated [25, 37]. PC and APC are assumed to have

similar diffusion coefficients for computational simplicity. Antithrombin III irreversibly

removes factors IXa, Xa, and thrombin by a bimolecular binding reaction. Acceleration

of ATIII activity by surface glycosaminoglycans is not considered. Tissue factor pathway

inhibitor acts in a two-step process. TFPI binds reversibly to factor Xa in the fluid phase,

followed by reversible TFPI/Xa association with surface bound TF/VIIa [5]. Only plasma

TFPI is considered. Inducible TFPI from cellular sources, specifically platelets and

endothelial cells, are not included.

    Flow Regime. Simulations were conducted assuming a steady, non-pulsatile,

fully developed parabolic flow profile. In select instances, analyses were performed for a

range of shear rates between 100 and 1500 s^{-1}. However, in most cases, comparisons

were conducted at simulated arterial (500 s^{-1}) and venous (50 s^{-1}) flow regimes.

3.3.3. Model implementation

    Notation. Model reactions and corresponding rate constants are summarized in

Table 3.1. Postscripts of model parameters correspond to the reaction number (*e.g.,*

k_{cat2} is the turnover number for the second reaction, conversion of prothrombin to

thrombin by Va/Xa). Fluid phase concentrations are denoted by the letter *c* followed by

the numerical species (*e.g., c_2* refers to the concentration of prothrombin; c_{5a} refers to

the concentration of Va). Surface-bound species, defined only at *y*=0, are additionally

denoted by the addition of a postscript *s* (*e.g., c_{TF7as}* refers to the surface concentration

of TF/VIIa).

Equations. The full set of partial differential equations and boundary conditions can be found in Supplementary Material. Model equations were non-dimensionalized and geometrically scaled to moderate the range of parameter values and to reduce mesh size. All fluid phase species are defined by a conservation equation (Eq. 3.3), which contains the rate of accumulation and convective term on the left hand side and the diffusive term and fluid-phase reaction rate on the right hand side. Concentration is a function of time and two-dimensional space. Surface-phase reaction rates appear as a flux condition in the boundary conditions. As an example, the governing equations for thrombin (IIa) are presented as follows:

$$\delta_{ts} \frac{\partial c_{2a}}{\partial t} + \frac{Pe}{\alpha} \frac{\partial c_{2a}}{\partial x} = D_{2a} \left(\frac{1}{\alpha^2} \frac{\partial^2 c_{2a}}{\partial x^2} + \frac{\partial^2 c_{2a}}{\partial y^2} \right) + \delta_{ts} R_{2a} \tag{3.3}$$

$$-D_{2a} \frac{\partial c_{2a}}{\partial y}(y=0)\Big|_{TF} = \frac{k_{cat2} \times c_{5a10as} \times c_2}{K_{m2} + c_2} \tag{3.4}$$

$$-D_{2a} \frac{\partial c_{2a}}{\partial y}(y=0)\Big|_{TM} = \frac{k_{cat2} \times c_{5a10as} \times c_2}{K_{m2} + c_2} - (k_{a3} \times c_{2a} \times (TM_{total} - c_{TTMs}) - k_{d3} \times c_{TTMs}) \tag{3.5}$$

$$R_{2a} = -k_{a5} \times c_{2a} \times c_{AT3} \tag{3.6}$$

where δ_{ts} is a time-scaling coefficient, Pe is a modified Peclet number, α is an anisotropic scaling coefficient; c_2, c_{2a}, and c_{AT3} are the concentrations of prothrombin, thrombin, and antithrombin III, respectively, c_{5a10as} and c_{TTMs} are the surface concentrations of prothrombinase and thrombin-TM, respectively, (TM_{total} - c_{TTMs}) is the concentration of free TM; R_{2a} is the rate of production of thrombin in the solution phase, D_{2a} is the diffusivity of thrombin; k_{cat2} and K_{m2} are the turnover number and Michaelis constant, respectively, for the conversion of prothrombin to thrombin by prothrombinase (Va/Xa), k_{a3} and k_{d3} are the association and dissociation constants, respectively for thrombin-TM, and k_{a5} is the irreversible association constant for thrombin-ATIII.

The normal flux of factor IIa (c_{2a}) from surface-bound TF is equal to the rate of prothrombinase (c_{5a10as})-catalyzed conversion from factor II (c_2) (Eq. 3.4). The reaction is expressed as a Michaelis-Menten rate law governed by the turnover number, k_{cat2}, and the Michaelis constant, K_{m2}. In the vicinity of surface-bound TM, an additional term on the right hand side of the flux condition describes the removal of thrombin upon bimolecular association with free TM (term beginning with k_{a3}) and the release of thrombin back upon dissociation (term beginning with k_{d3}) (Eq. 3.5). Association and dissociation reaction rates are described by second- and first-order rate laws, respectively. The fluid phase reaction rate, R_{2a}, reflects the depletion of thrombin upon irreversible binding to ATIII, again defined by a second-order rate law (Eq. 3.6).

Computer implementation. The finite element model was implemented in COMSOL Multiphysics 3.4 (COMSOL, Inc., Burlington, MA) on a 64-bit Windows workstation. The automatically generated mesh contained approximately 2100 triangular elements, with finer resolution over the reactive boundaries and intersection points. Soluble species were defined by a convection-diffusion application mode. Surface-bound enzymatic complex formation was specified by a weak form (boundary) application mode. Time dependent simulations were solved using a direct parallel solver. Simulations were run to 60 min. Post-processing was performed in both COMSOL and MATLAB (MathWorks, Inc., Natick, MA).

3.3.4. System parameters describing surface-induced thrombin generation over spatially discrete regions of TF and TM

Simulations provide transient concentration profiles in two dimensions for each of the 21 computationally-defined species (16 fluid-phase, 5 surface-bound). System parameters were defined to describe the behavior of the initiating TF region and to quantify the effectiveness of the TM-expressing downstream region to modulate the

thrombin response. **Peak thrombin concentration** and **flow simulated thrombin generation (FSTG)** were chosen to evaluate the threshold-like response of the model system. Peak thrombin concentration was defined as the maximum level of thrombin attained at any point in the computational space. FSTG is derived from a consideration of the total thrombin generated over the downstream region at $y=0$ during the course of a 60-min simulation, thus acting as a global variable incorporating both spatial and temporal information. The downstream average was chosen as an indication of the effectiveness of downstream TM to modulate thrombin production initiated by the upstream TF region. One-hour was chosen as the default simulation time to ensure that all phases of coagulation, *e.g.* initiation and propagation, were included in the analysis for all runs. In other words, the simulation time exceeded the timecourse of the least thrombogenic simulation conditions. A cutoff >10nM FSTG was defined as the 'above-threshold' criteria. **Lag time** characterizes the initiation phase of the coagulation cascade and was defined as the time-intercept of the linear slope that defined the onset of the maximum rate of thrombin generation. Finally, unique to our spatial model, an **effective prothrombotic zone** (EPZ) defined the extent to which thrombin propagated away from the site of surface-bound TF, in both axial and radial directions, by delineating a region wherein at any point within the space the thrombin concentration was within 95% of the peak level. The dimensions of this effective prothrombotic zone, the **effective prothrombotic length** (EPL) and the **effective prothrombotic height** (EPH) were determined as the *x*-intercept and maximum *y*-coordinate of the delineating contour line, respectively. It should be noted, therefore, that the effective prothrombotic length includes the entire length of the site of expressed TF.

3.3.5. Modeling tandem lesions

Additionally, we explored the behavior of systems containing multiple spatially distinct sites of surface-bound TF. The reactive boundary is divided into three spatially distinct sites of TF with intervening regions that present surface-bound TM (Figure 3.2B). TF length and density were 200 μm and 9 fmol/cm^2, respectively. These TF conditions represent lengths and concentrations previously found to be just below the activation threshold when adjacent to transport-limited levels of TM (1000 fmol/cm^2). TF lengths shorter than the previous section were chosen in order to achieve a wider range of effective prothrombotic lengths that would fit within a manageable total chamber length. The total length of the system of interest was 3 cm, unless otherwise noted. A **TF interval** was defined as the distance between the upstream ends of two adjacent sites of TF. **Regional flow-simulated thrombin generation (rFSTG)** was derived from a consideration of the total thrombin generated over the downstream interval regions during the course of a 60-min simulation. An rFSTG>10nM was similarly defined as the threshold criteria for characterizing a segment as 'above-threshold'. Model equations governing flow and reaction kinetics remained unchanged. Similar mesh and solver algorithms were employed.
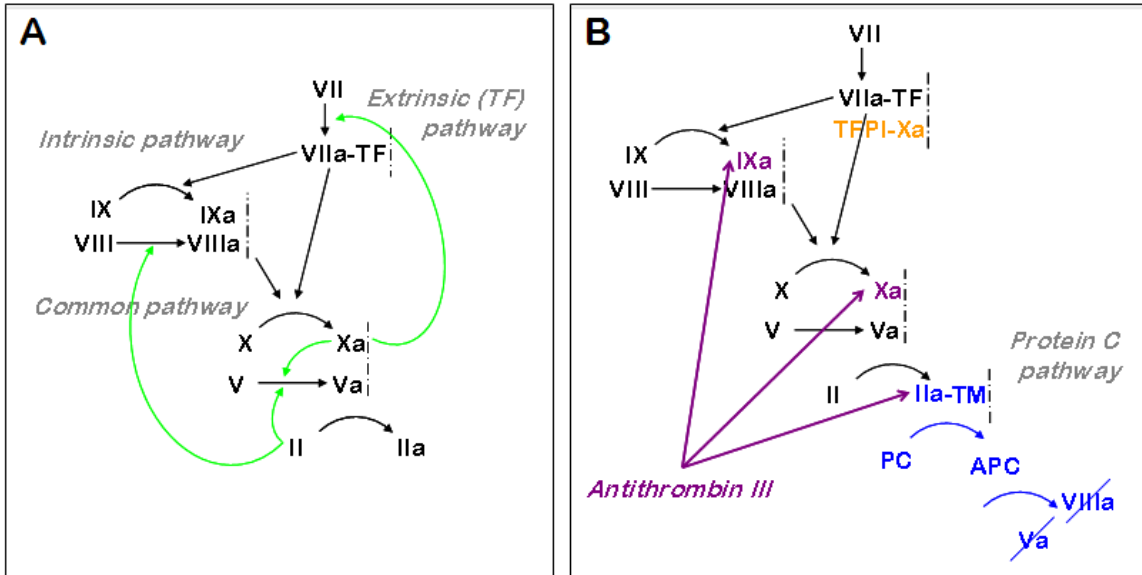
Figure 3.1. Coagulation reaction network described in the computational model.
Dotted lines indicate surface-associated complexes. (**A**) Procoagulant reactions with short- and long-range positive feedback loops (green arrows). Coagulation is initiated by extrinsic pathway (TF-VIIa) activation of FX. Formation of intrinsic tenase (IXa-VIIa) amplifies thrombin generation. Note that fibrinogen cleavage is not included in the model, but is shown for illustrative purposes only. (**B**) Anticoagulant mechanisms. ATIII binds irreversibly to FIXa, FXa, and thrombin. TFPI acts in a two-step mechanism, first binding to FXa, followed by formation of the quaternary TFPI-Xa-TF-VIIa complex. The PC pathway is triggered upon thrombin binding to TM.
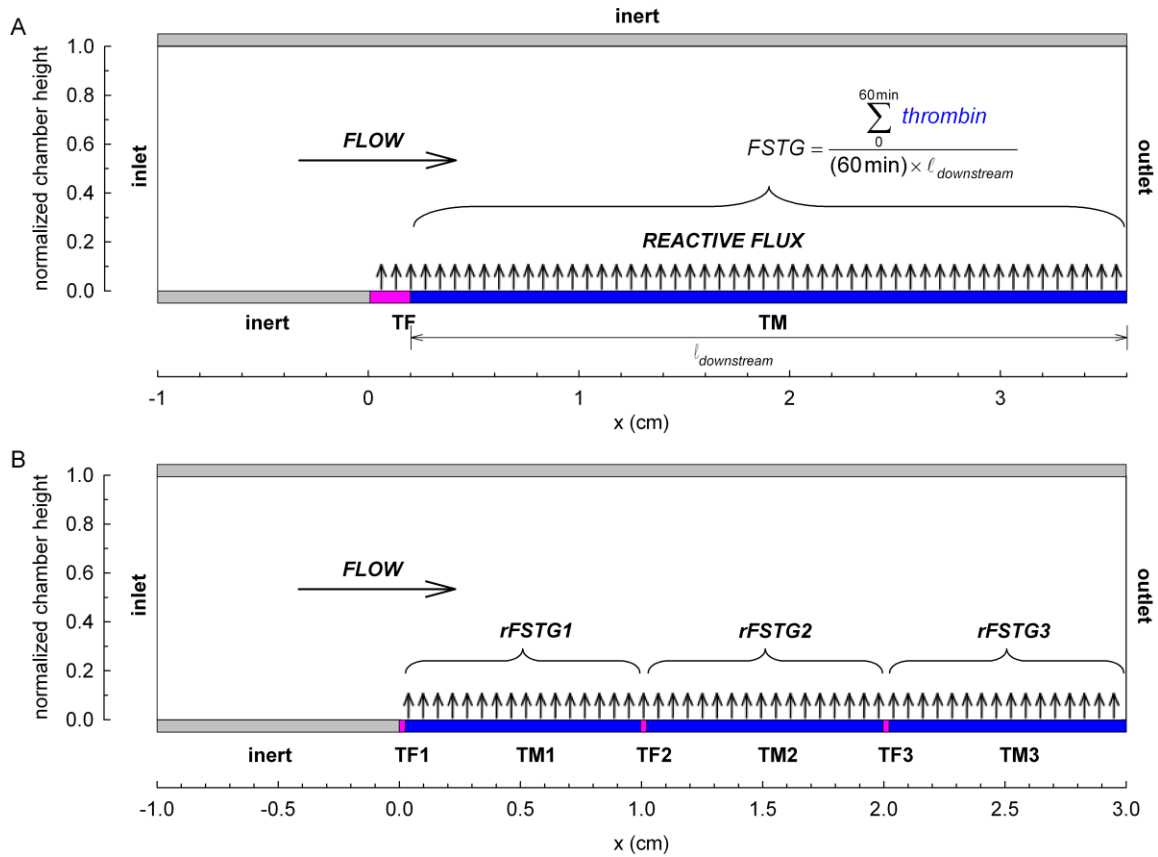
Figure 3.2. Formulation of a spatially heterogeneous model of surface-induced thrombin generation in a flow field. Blood flow carries proteins into the flow field at constant inlet concentrations. Diffusion transports coagulation factors to the lower reactive surface, where reaction kinetics define flux boundary conditions. Convective flux removes soluble species at the outlet. The upper boundary is inert. (**A**) Initial geometric conditions include a 10 mm entrance region, 2 mm TF region, and a 34 mm TM region. FSTG is defined as the integral of the downstream thrombin surface concentration over the 60-min simulation time, normalized by time and length. (**B**) In the tandem model, overall chamber length is fixed at 3 cm. Three TF regions of length 200 μm each are spaced at fixed intervals (10 mm in this illustration) with intervening TM regions. rFSTG is defined as the integral of the thrombin surface concentration over the intervening TM surface over the 60-min simulation time, normalized by time and length.

41

3.4.   Results

The degree to which the computational model recapitulated established experimental observations was determined for both normal and pathologic systems of hemostasis. The relationship of thrombin generation to increasing surface concentrations of TF was initially benchmarked in the absence of TM. This was followed by analysis of APC generation in response to increasing concentrations of surface bound TM. Subsequently, the existence of an 'all-or-none' threshold effect in a regulated coagulation system was defined with respect to the dimensions of the TF region, surface densities of TF and TM, and wall shear rate. The capacity of hemophilia A (factor VIII deficiency) and B (factor IX deficiency) to modulate the density of surface bound TF needed to exceed the threshold for thrombin generation was examined.   Appropriate model behavior was further confirmed by examining the time course of a prothrombotic system, which is characteristically defined by initiation and amplification phases. The prothrombotic response was compared to a thrombin response, which remained suppressed by inhibitory mechanisms. Significantly, we demonstrate that an effective prothrombotic zone may be defined that extends well beyond the dimensions of surface-bound TF. The size of this zone is dependent not only on concentrations of all reactive species, but also the site of TF expression, the surface densities of TF and TM, as well as the characteristics of the flow field. Furthermore, in the case of multiple sites of TF, the relationship between the magnitude of the effective prothrombotic zones and the interval distance between TF sites dictated the net thrombotic response of the system. Notably, multiple TF sites, which individually failed to activate the coagulation pathway, were shown to interact in an additive manner to yield a prothrombotic system. Furthermore, the expression of TM in the regions between sites of TF downregulated the thrombin response to subsequent TF sites.

3.4.1. Thrombin generation increases with increasing TF surface density up to a transport limit

In response to an upstream site of TF expression, surface-associated enzymatic complexes assemble on the non-functionalized downstream surface. Under conditions of arterial ($500s^{-1}$) flow, increasing TF expression in the absence of TM lead to a linear increase in the maximum rate of thrombin generation, a reduction in the lag time to achieve a maximum rate of thrombin production, and a concomitant increase in FSTG (Figure 3.3A). Both the lag time and FSTG approached a transport limit at a TF density of ~1 fmol/cm^2. Above this surface concentration of TF, full activation of the coagulation cascade resulted in approximately 86% peak substrate conversion (~1200 nM thrombin generated / 1400 nM inlet prothrombin). At or below a TF concentration of 0.2 fmol/cm^2, full activation of the coagulation cascade was not observed, which reflects the capacity of flow to suppress thrombin production by active removal of reactive species, unless, as detailed below, the dimension of the TF region are increased. Similar effects were observed at $50s^{-1}$, although the transport limit was defined by a significantly lower TF surface concentration (data not shown).

3.4.2. APC generation increases with increasing TM surface density up to a transport limit

Activated protein C (APC) concentrations as a function of TM surface density were determined in response to a fixed TF stimulus ([TF] 0.8 fmol/cm^2). Under arterial ($500 s^{-1}$) conditions, APC concentration increased with increasing TM concentration up to ~500 fmol/cm^2. At higher levels of TM, the reaction became substrate-limited with 94.8 and 97.1% peak substrate conversion within the local environment of the TM surface at TM concentrations of 500 and 1000 fmol/cm^2, respectively (Figure 3.3B). Under transport-limited conditions, the reaction rate for APC production exceeded the

rate of substrate delivery and product removal. The transport-limited TM concentration is in general agreement with experimental studies previously conducted in our laboratory [38].

3.4.3. The model system exhibits threshold responses to tissue factor, thrombomodulin, and wall shear rate

Characteristically, during the initiation phase of coagulation, very low levels of thrombin are produced. During this phase, inhibitors may dampen the thrombin response and prevent amplification and full activation of the coagulation cascade; this is considered a 'sub-threshold' thrombin response. However, when the capacity of these inhibitors is overwhelmed by the magnitude of the thrombogenic stimulus, thrombin levels cross an activation threshold and rapid amplification of thrombin generation occurs. This threshold effect may be defined with respect to a number of variables (*e.g.* blood flow, fluid- and surface-phase levels of procoagulant factors and inhibitors, kinetic variables), and thus an infinite set of threshold-defining permutations exist beyond which thrombin is produced in an almost instantaneous manner. Using our computational model, we conducted parametric studies which would not have been experimentally efficient. With respect to our system parameters, peak thrombin concentration reflected the 'all-or-none' behavior of thrombin generation and easily differentiated between sub-threshold and fully activated systems. Likewise, by setting a cutoff of 10nM for FSTG, notably the concentration reported to induce platelet activation [39], systems were reliably categorized into sub- and above-threshold groups. By incorporating both spatial and temporal information, FSTG was additionally a sensitive parameter that further enabled stratification of prothrombotic states.

We examined the relationship between the length of the TF region and thrombin production while maintaining TF and TM surface densities at or near transport-limited

44

levels of 1 and 1000 fmol/cm^2, respectively. At a shear rate of 500 s^{-1}, peak thrombin

concentration and FSTG fell below the activation threshold of 10 nM, if the TF site was

less than 1.6 mm in length (Figure 3.4A and B). With further lengthening of the TF

region, peak thrombin concentration and FSTG increased sharply and peak thrombin

approached 1200 nM, consistent with full activation of the coagulation cascade.

A similar threshold effect was observed in relation to TF surface concentration.

At venous (50 s^{-1}) and arterial (500 s^{-1}) shear rates, TM (1000 fmol/cm^2) inhibited

thrombin production at TF concentrations below 0.03 and 0.8 fmol/cm^2, respectively.

However, at TF densities that exceeded these concentrations, peak thrombin

concentration reached substrate-limited levels (~1200 nM) and FSTG exceeded the 10

nM activation definition (Figure 3.4C and D, venous data not shown).   Threshold-type

behavior was also observed in relation to TM surface concentration (Figure 3.4E and F).

Minimum TM surface densities required to limit thrombin propagation were 1.4 and 60

fmol/cm^2 for TF concentrations of 0.03 and 0.8 fmol/cm^2 under venous and arterial shear

rates, respectively. As would be anticipated, the magnitude of flow had a pronounced

effect on the threshold for thrombin production, as well. Assuming a TF site of 2 mm in

length and TF and TM concentrations of 1 and 1000 fmol/cm^2, respectively, threshold

activation was suppressed at shear rates above 750 s^{-1} (Figure 3.4G and H).

3.4.4. Hemophilia A & B increase required levels of tissue factor and reduce the
rate of thrombin formation

Model simulations confirm that threshold requirements for activation of the

coagulation cascade are increased for moderate hemophilia A and B when compared to

a normal hemostatic system. Specifically, the concentration of surface-bound TF

required to surpass the threshold for thrombin production were approximately two-fold

higher under arterial and venous conditions. Moreover, the more gradual transition to

full amplification of the coagulation cascade, as evident by the slower rise of peak

thrombin production in response to the concentration of surface-bound TF, is consistent

with a dampened positive feedback system (Figure 3.5A and B). Similarly, the

hemophilias were associated with a decrease in the rate of thrombin generation and a

lower FSTG (Figure 3.5C and D). Notably, despite increasing the concentration of TF to

compensate for the hemophilic state, such that the peak thrombin concentration is

similar to that attained under normal hemostatic conditions, a normalized rate of

thrombin production was not achieved. Under arterial (500 s^{-1}) flow, the maximum rate

of thrombin generation was 48.8 nM/min under normal hemostatic conditions ([TF] 1

fmol/cm^2), while half that (14.2 nM/min) for hemophilia A, despite doubling the surface

density of TF to 2 fmol/cm^2 to afford similar peak thrombin responses. Likewise at low

shear (50 s^{-1}), the maximum rate of thrombin generation was 26.3 nM/min under normal

hemostatic conditions ([TF] 0.04 fmol/cm^2), but less than one-half of that (10.9 nM/min)

for hemophilia A conditions even when expressed tissue factor was increased to 0.08

fmol/cm^2 to yield similar maximum levels of thrombin. Indeed, experimental studies have

noted that hemophilia A and B are associated with decreased rates of thrombin

generation [40].

3.4.5. The effectiveness of APC to inhibit the onset of the amplification phase of coagulation is determined within the first 3-5 min of the initiation phase

The time course of thrombin, factor Va, and APC production was examined for

systems residing at an activation interface. Under conditions in which an activation

threshold was exceeded (*e.g.*, TF 0.9 fmol/cm^2, TM 1000 fmol/cm^2, 500 s^{-1}), modulation

of Va and thrombin production by APC occurred within the first 3-5 min, but after an

initiation period of 37 min, thrombin concentration rose rapidly and plateaued at a

substrate-limited level of 1180 nM (Figure 3.6A). In contrast, below an activation

threshold, (*e.g.*, TF 0.8 fmol/cm^2, TM 1000 fmol/cm^2, 500 s^{-1}), Va decreased in response

to increases in APC, restricting thrombin to very low levels. The effectiveness of factor

Va suppression by APC is determined within the first few minutes, with Va

concentrations reaching steady state by approximately 20 min for the sub-threshold case

(Figure 3.6B). These results are similar to pseudo-one compartment models run by

Kuharsky *et al*. under conditions of high and low TF density [9].

3.4.6. Extrinsic tenase governs initiation of coagulation, while intrinsic tenase governs amplification

The intrinsic and extrinsic pathways converge on the common pathway to

generate factor X and thrombin. The time courses of intrinsic tenase (IXa/ VIIIa),

extrinsic tenase (TF/VIIa), and prothrombinase (Xa/Va) was evaluated under arterial flow

conditions (Figure 3.6C and D). Extrinsic tenase is produced rapidly as flow and

diffusion transport circulating VIIa to surface-bound TF. As factors IX and VIII are

activated by TF/VIIa and thrombin, respectively, subsequent formation of intrinsic tenase

is observed. Overall prothrombinase assembly, and subsequent thrombin production,

follows the time course established by intrinsic tenase. These computational results are

consistent with the role of the extrinsic pathway in initiation and the importance of the

intrinsic pathway in amplification of coagulation [3, 41, 42].

3.4.7. Tissue factor, thrombomodulin, and shear rate dictate the dimensions of an effective prothrombotic zone that extends beyond the initiating site of thrombin generation

These studies emphasize the existence of a spatially defined zone of thrombin

that may extend well beyond the site of TF expression. Under arterial flow conditions

(500 s^{-1}), the threshold length for surface bound TF at 1 fmol/cm^2, above which explosive thrombin production is observed, was previously determined to be 1.6 mm. Although activation of coagulation at this dimension is relatively limited, this case conveniently illustrates the presence of an effective prothrombotic length (EPL) that is characterized by thrombin propagation in space. This phenomenon holds true whether or not a system exceed an activation threshold. As shown in Figure 3.7A, the relationship between a spatially discrete site of TF expression and the effective prothrombotic length is non-linear. For example, increasing the size of the TF region by 60% (from 1 mm to 1.6 mm) leads to a 640% increase in the EPL (3.06 versus 19.6 mm).

The influence of the flow regime on the dimensions of the effective prothrombotic zone was investigated at shear rates ranging from 500 to 2000 s^{-1}. It might be anticipated that higher flow rates would promote downstream propagation of thrombin. However, increasing shear rate decreased the effective prothrombotic zone, due to enhanced removal of activated clotting factors and greater APC generation attributed to increased transport of thrombin and protein C to TM. Propagation of the effective prothrombotic zone in both parallel and perpendicular to the direction of flow was reduced at higher shear rates (Figure 3.7B). In particular, at the chamber outlet (x=3.6 cm), the height of the effective prothrombotic zone increased linearly from 11.3% to 15.3% of the total chamber height, and the length increased non-linearly from 0.49 to 0.95 cm for shear rates of 2000 and 750s^{-1}, respectively.

Increasing TF and TM surface concentration lead to a respective increase or decrease in the dimensions of the prothrombotic zone. Specifically, the length of the effective prothrombotic zone increased exponentially with TF density (Figure 3.7C), while decreasing in response to TM (Figure 3.7D). The effective prothrombotic length was linearly related to peak APC concentration. It is noteworthy that similar EPZ dimensions may arise from widely varying sized sites of TF expression, TF and TM

concentrations, and shear rate. Steady state surface plots of thrombin concentration for decreasing concentrations of surface TM are shown in Figure 3.8. Under conditions that did not exceed the activation threshold (Panel B), the effective prothrombotic zone remained near the site of TF expression. For conditions in which an activation threshold was exceeded (Panels C and D), the effective prothrombotic zone encompassed and extended beyond the entire downstream region.

3.4.8. Thrombomodulin expression within the intervening regions dictates the suppressive interactions that occur between sequential TF sites

Multiple TF sites acted cooperatively to promote or suppress thrombin generation, dependent, in part, on the concentration of surface-bound TM within intervening regions. In Figure 3.9, mean thrombin concentrations generated in three regions located between sequential sites of TF were compared as a function of TM surface densities ranging from 40 to 1000 fmol/cm^2. TF length and concentration were fixed at 200 μm and 9 fmol/cm^2, respectively. The interval distance between TF sites was 1 cm. At low levels of TM, thrombin generated from the first TF region enhanced thrombin production at downstream TF sites by driving positive feedback loops of the coagulation cascade. At intermediate levels of TM expression, thrombin generated by the upstream site additionally served to activate protein C, thus counteracting thrombin propagation to some degree. Significantly, at high surface densities of TM, the extent of thrombin-mediated APC generation was great enough to suppress thrombin production by downstream sites of TF. The degree of suppression between TF sites was proportional to TM surface concentration and was more pronounced between the first and second regions than between the second and third TF sites (56 and 8% decrease in mean thrombin, respectively for [TM] 500 fmol/cm^2 and 83 and 28% decrease,

49

respectively for [TM] 1000 fmol/cm^2). Because thrombin regulates its own generation

through the activation of protein C, the dampened suppressive effects between the

second and third TF sites can be accounted for by the reduced levels of thrombin

generated by the second TF site. Representative surface plots of thrombin

concentration for additive, intermediate, and suppressive interactions that occur between

sequential sites of TF are shown in Figure 3.9. We observed that extent to which

sequential regions of TF and TM acted to inhibit or promote thrombin generation was

dictated by the degree to which tandem effective prothrombotic zones overlapped.

3.4.9. The sequential interaction of effective prothrombotic zones produced by tandem sites results in enhancement of the overall thrombotic response

Figure 3.10 depicts mean thrombin concentration in three regions located

downstream to each TF site (TF$_{length}$ 200 µm, [TF] 9 fmol/cm^2) for interval distances of

0.5, 1, and 2 cm. The overlap of the effective prothrombotic zones of high density TF

sites spaced 1 cm apart is illustrated in Figure 3.10. Encroachment of the effective

prothrombotic zones of upstream TF sites over downstream sites promotes thrombin

generation over the downstream sites by contributing to positive feedback loops of the

coagulation cascade. In Figure 3.10A, the length of the effective prothrombotic zone (>3

cm) was much greater than the interval distance, resulting in considerable overlap of

effective prothrombotic zones and cumulative thrombin levels in downstream regions

which greatly exceeded the 10 nM activation threshold. The intensity of the additive

effects increased as the interval distance was decreased. Moderate overlap of the EPZs

(length ~1.3 cm) resulted in some additive propagation of thrombin generation to

downstream sites (Figure 3.10B). However, in the presence of higher TM surface

concentrations, thrombin also functioned to activate protein C, leading to suppression of

thrombin generation. The net effect was an apparent lack of, or minimal, interaction between TF sites. Prothrombotic interactions played a larger role when the TF sites were more closely positioned. Conversely, when the interval distance was increased such that the EPZ no longer overlapped, suppressive effects begin to dominate. These suppressive effects were particularly pronounced at a TM surface concentration of 1000 fmol/cm^2 with limited overlap of effective prothrombotic zones. The capacity of tandem sites to inhibit thrombin generation is attenuated by prothrombotic interactions as the distance between sites approach the boundaries of the effective prothrombotic zone (Figure 3.10C). For example, at interval distances of 2, 1, and 0.5 cm, mean thrombin concentration between the first and second sites of TF expression decreased by 86, 83, and 58%, respectively.
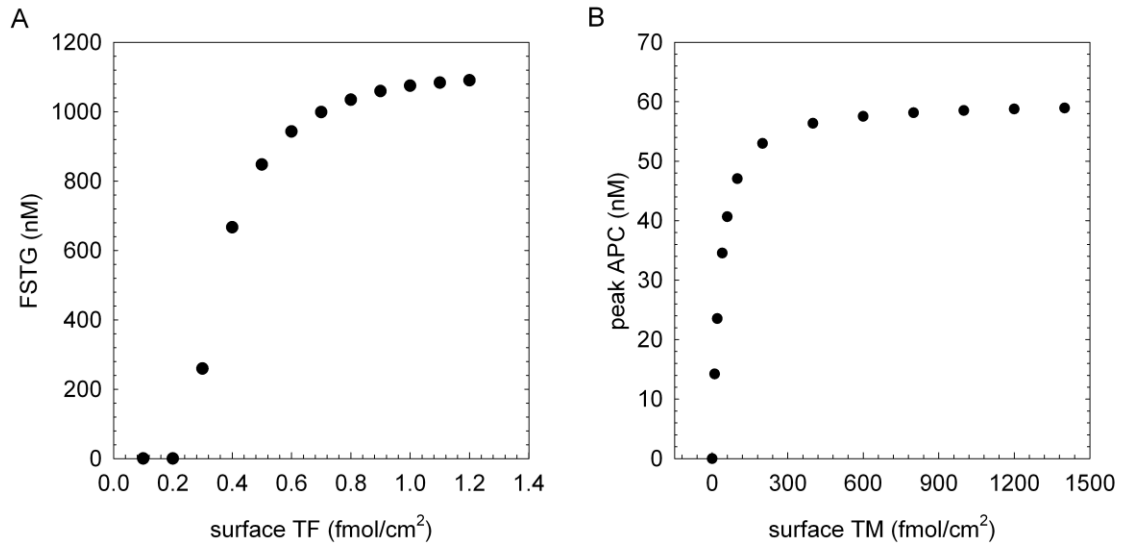
Figure 3.3. Characterization of transport-limited regimes under arterial flow (500s^{-1}) (A) Mean downstream thrombin generated by a localized TF region of length 2 mm in the absence of TM expression in the downstream region. **(B)** Simulated peak APC generation as a function of TM surface density in response to a fixed TF stimulus located in the upstream region ([TF] 1.0 fmol/cm^2).
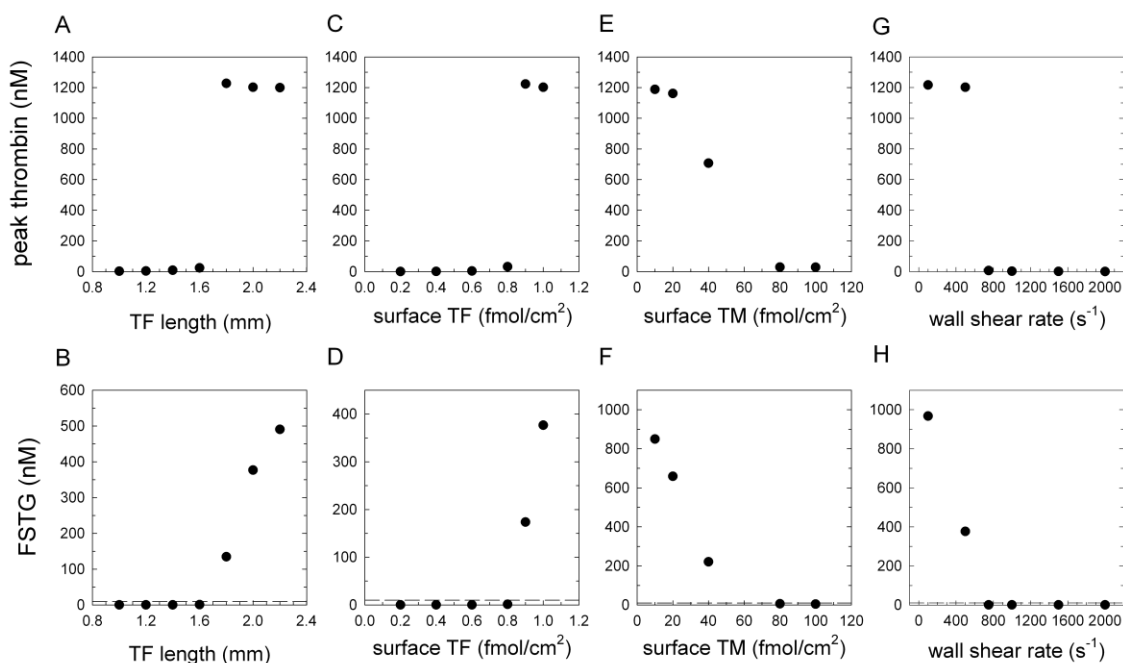
Figure 3.4. Threshold response of thrombin to TF site length, TF surface density, and TM surface density under simulated arterial flow (500 s^{-1}). (A, B) Peak thrombin concentration and FSTG as functions of the length of the site of TF expression at a wall shear rate of 500 s^{-1}. TF and TM surface densities were 1 and 1000 fmol/cm^2, respectively. (C, D) Peak thrombin concentration and FSTG as functions of TF surface density. TF and TM lengths were 2 and 34 mm, respectively. TM surface concentration was fixed at 1000 fmol/cm^2. (E, F) Peak thrombin concentration and FSTG as functions of TM surface density. TF surface concentration was fixed at 0.8 fmol/cm^2. (G, H) Peak thrombin concentration and FSTG as functions of wall shear rate. TF and TM lengths were 2 and 34 mm, respectively. TF and TM surface densities were 1 and 1000 fmol/cm^2, respectively. Simulations were run to 60-min. Activation of clotting is defined at FSTG of 10 nM (dotted line).
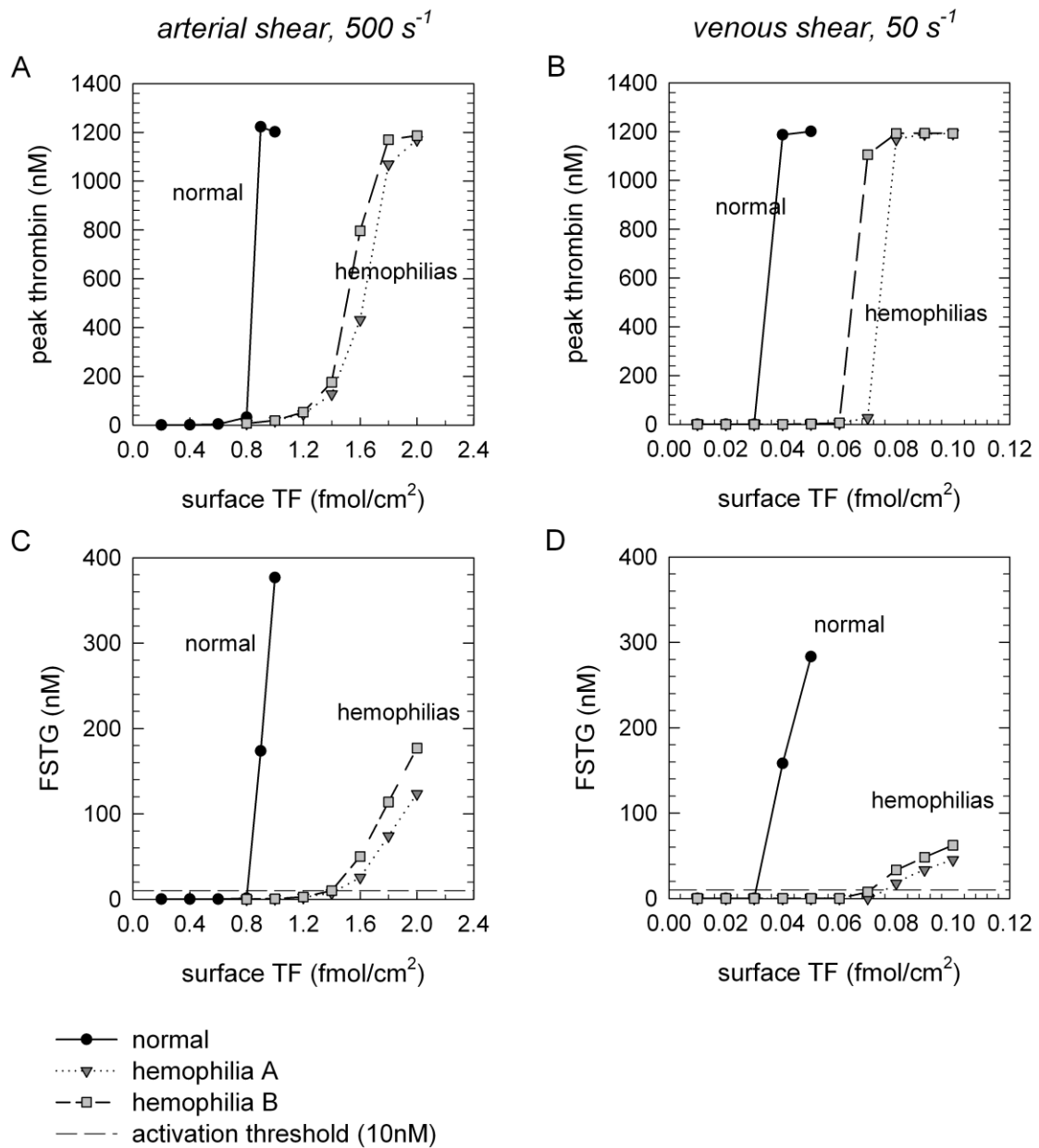
Figure 3.5. Threshold response of thrombin generation to TF surface density for normal physiologic and hemophiliac conditions. Peak thrombin (**A, B**) and FSTG (**C, D**), during the course of a 60-min flow period at wall shear rates of (**A, C**) 500 s^{-1} and (**B, D**) 50 s^{-1}. [TM] 1000 fmol/cm^{2}. Moderate hemophilias A and B (5% normal FVIII & FIX, respectively) increase the TF concentration required to exceed the activation threshold, defined at FSTG of 10 nM (dotted line).
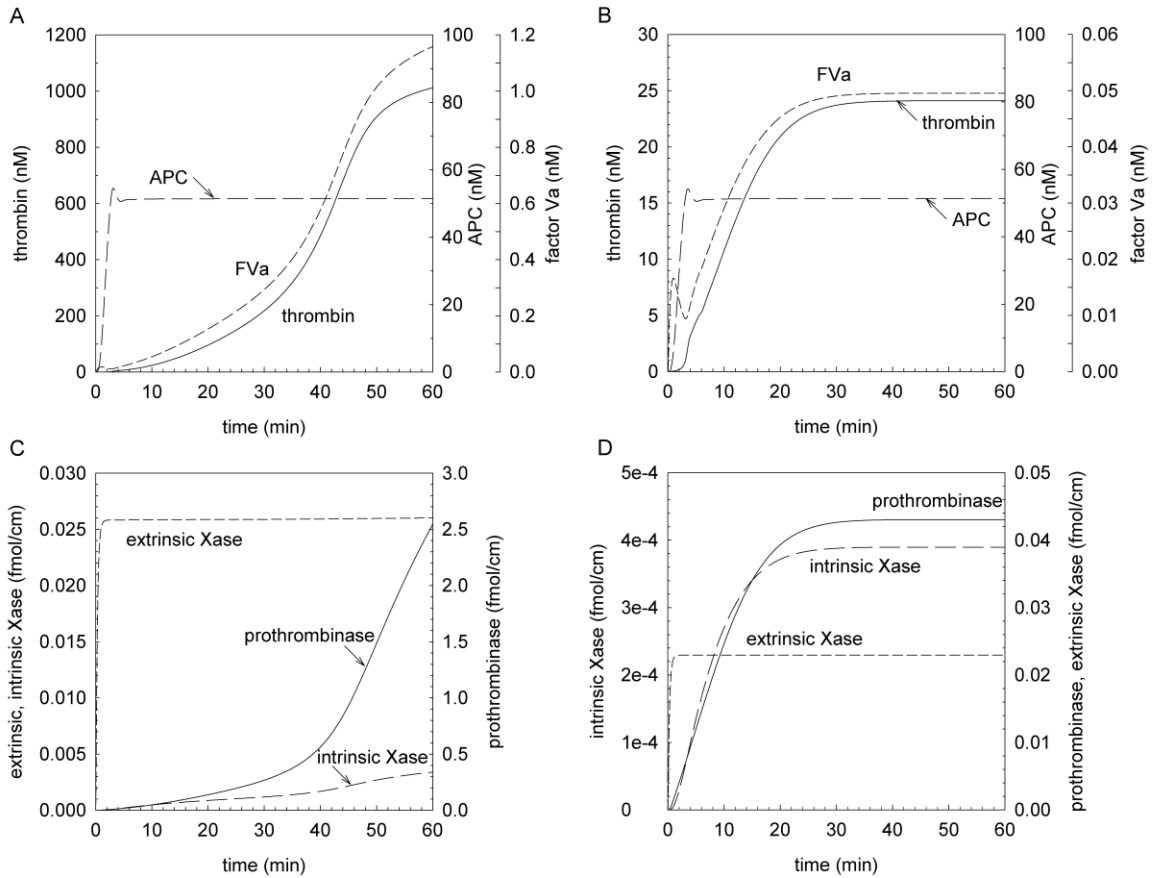
Figure 3.6. Time course for coagulation systems that lie above or below a prothrombotic activation threshold. Throbmin, APC, and factor Va concentrations at the TF-TM intersection (x=0.2 cm) at 500 s^{-1} for systems that exceeded (TF 0.9 fmol/cm^{2}, TM 1000 fmol/cm^{2}) (A) or resided below (TF 0.8 fmol/cm^{2}, TM 1000 fmol/cm^{2}) (B) an activation threshold. Total upstream extrinsic and intrinsic tenase and prothrombinase concentrations at 500 s^{-1} for systems that exceeded (TF 0.9 fmol/cm^{2}, TM 1000 fmol/cm^{2}) (C) or resided below (TF 0.8 fmol/cm^{2}, TM 1000 fmol/cm^{2}) (D) an activation threshold. Note different scales.
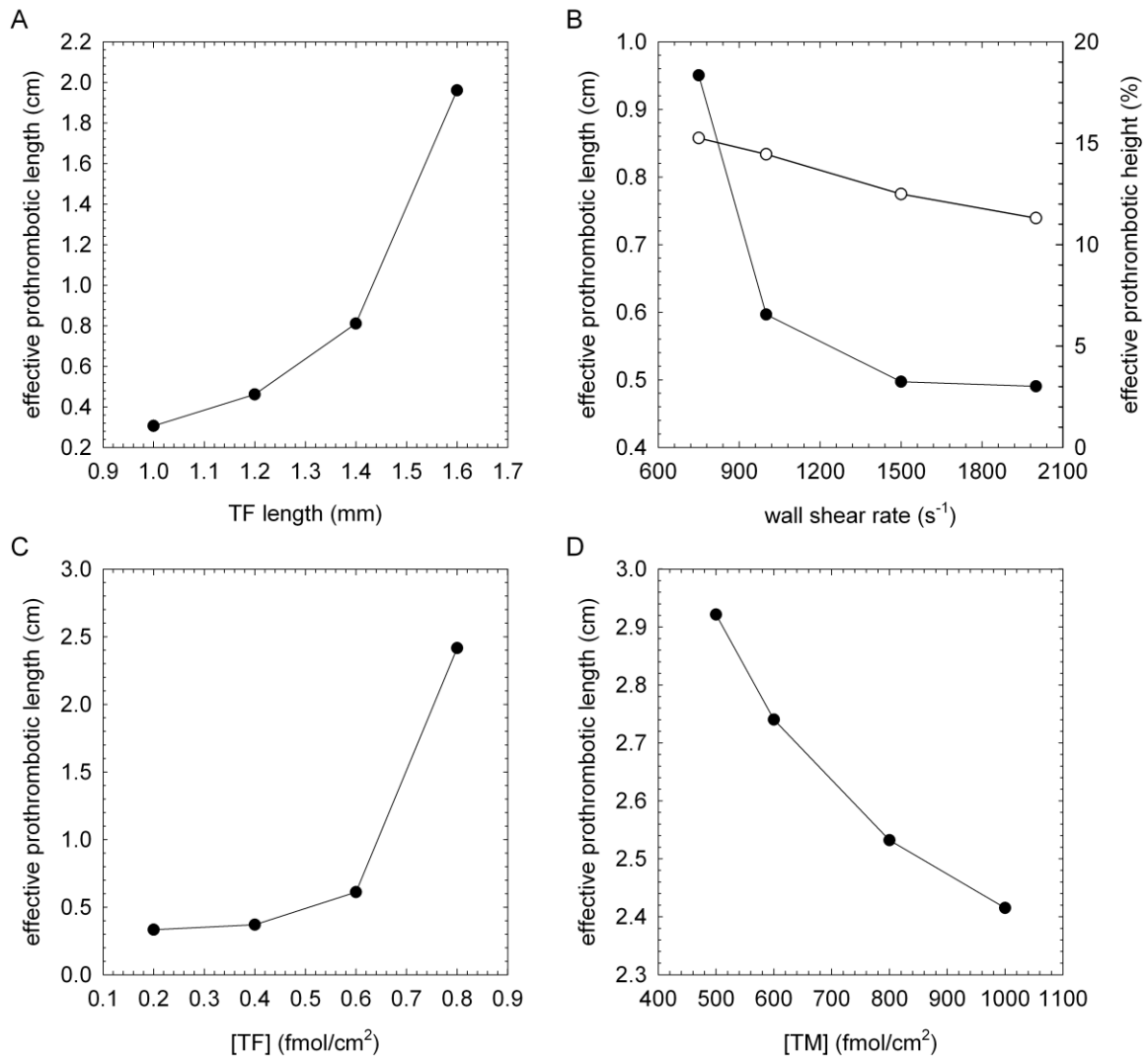
Figure 3.7. Factors influencing the length of the EPZ. Relationship of effective prothrombotic length to (**A**) TF length, (**B**) wall shear rate, (**C**) TF density, and (**D**) TM density. Effective prothrombotic height, as a percentage of total chamber height, is plotted in panel (**B**). For panels (**A-C**), TF length was 2 mm, wall shear rate was 500 s^{-1}, [TF] 1 fmol/cm^2, and [TM] was 1000 fmol/cm^2 when fixed. (**D**), [TF] 0.8 fmol/cm^2 expressed over a 2 mm length, wall shear rate 500 s^{-1}.
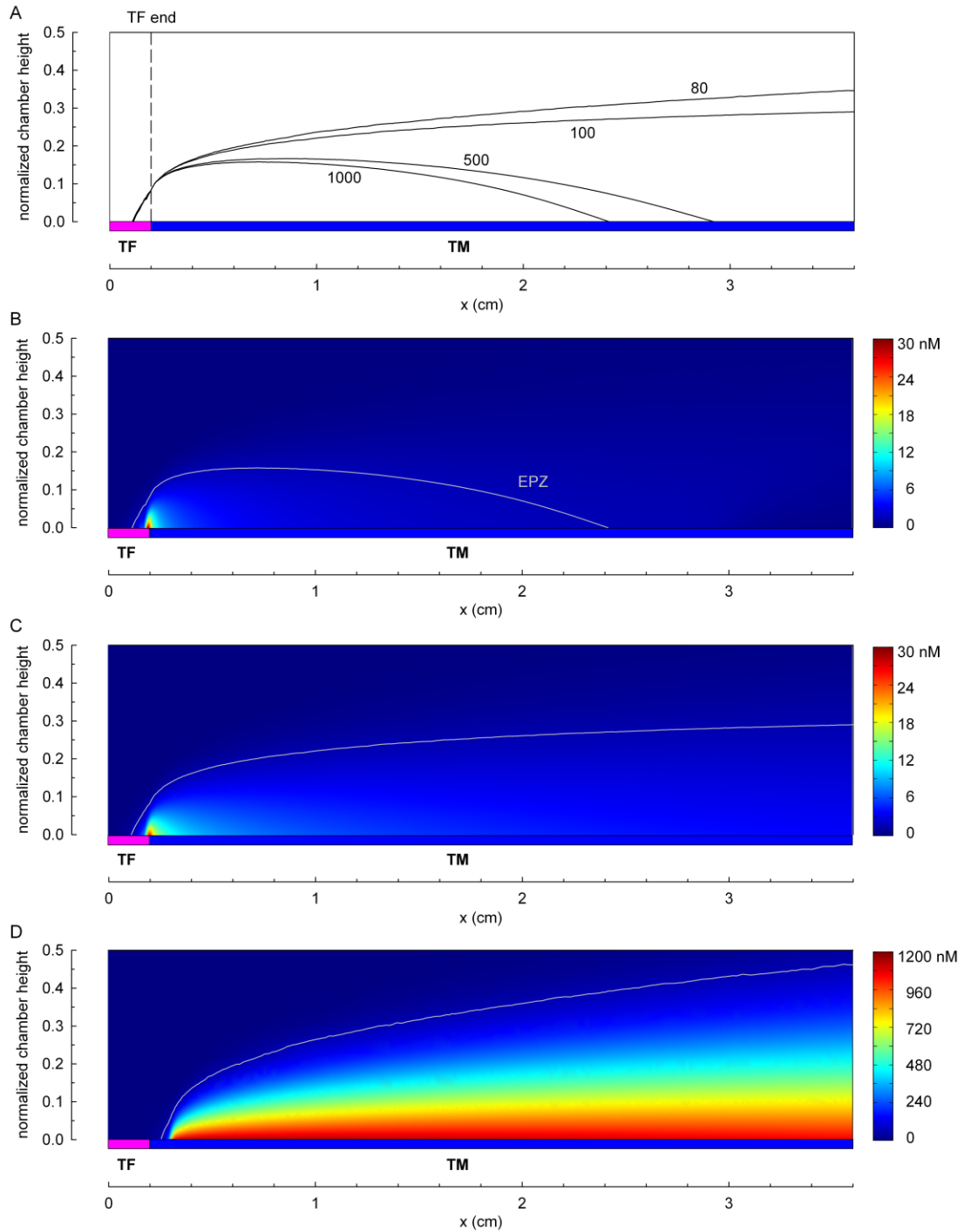
Figure 3.8. Effective prothrombotic zone and its dependence on TM surface concentration. Thrombin generation is initiated at a wall shear rate 500 s^{-1} in response to a region 2 mm in length expressing TF at a density of 0.8 fmol/cm^{2}. Simulations are run to 60-minutes. (**A**) EPZ as a function of TM surface density (1000, 500, 100, and 80 fmol/cm^{2}). Steady state thrombin concentration profiles for downstream TM densities of (**B**) 1000, (**C**) 100, and (**D**) 10 fmol/cm^{2}. The EPZ is delineated by a contour line wherein at any point within the space the thrombin concentration was within 95% of the peak level.

57
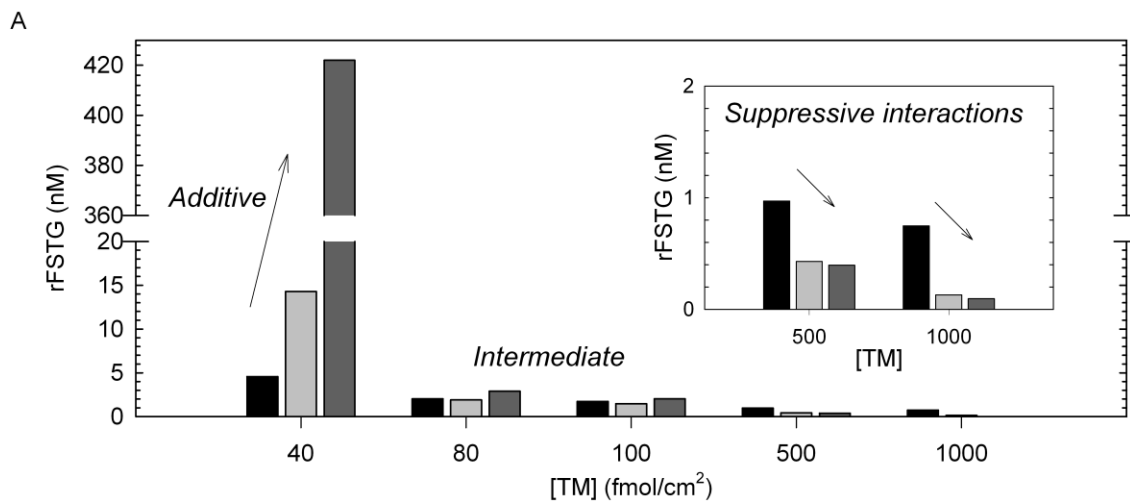
Figure 3.9. Additive, intermediate, and suppressive interactions between tandem prothrombotic sites. (**A**) rFSTG as a function of intervening TM surface density (40-1000 fmol/cm^2) under simulated arterial conditions (500 s^{-1}) over three sequential sites of TF (TF$_{length}$ 200 µm, [TF] 9 fmol/cm^2). From left to right, each bar represents rFSTG for the regions downstream of each site of surface-bound TF. (**B-D**) EPZ, previously calculated from a simulation of a single site of TF, is overlaid on the surface plot to illustrate the overlap of EPZ between sequential TF sites. Panel (**B**) is representative of additive effects at low surface densities of TM (40 fmol/cm^2). Panel (**C**) is representative of the net effect of both additive and suppressive interactions between TF sites at intermediate surface concentrations of TM (100 fmol/cm^2). Panel (**D**) is representative of suppressive interactions between TF sites at high surface concentrations of TM (1000 fmol/cm^2). Simulations were run to 60 min. However, concentration profiles shown here are at *t*=18 min to avoid scaling artifacts. Note different scale bars.
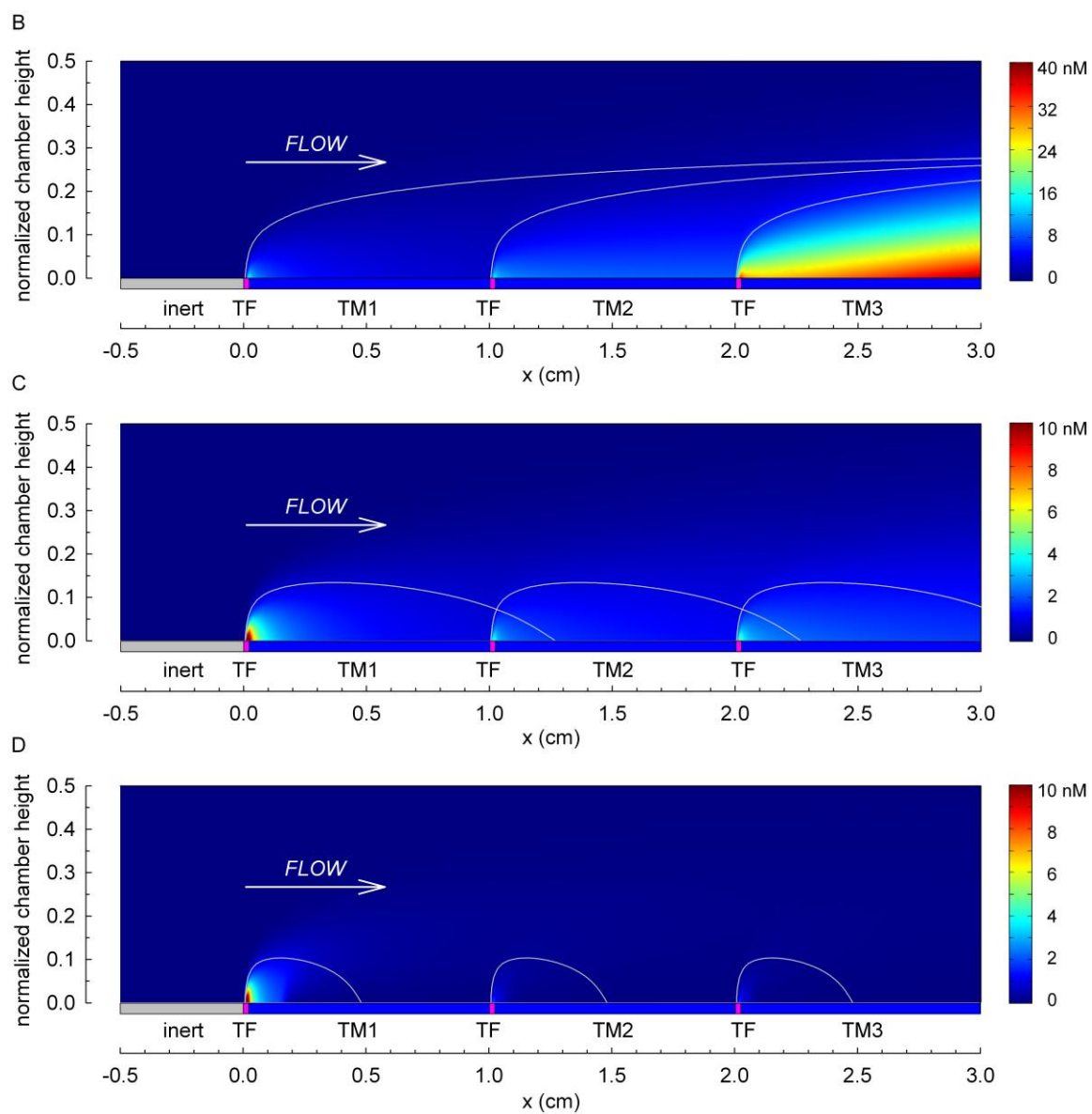
Figure 3.9. (continued)
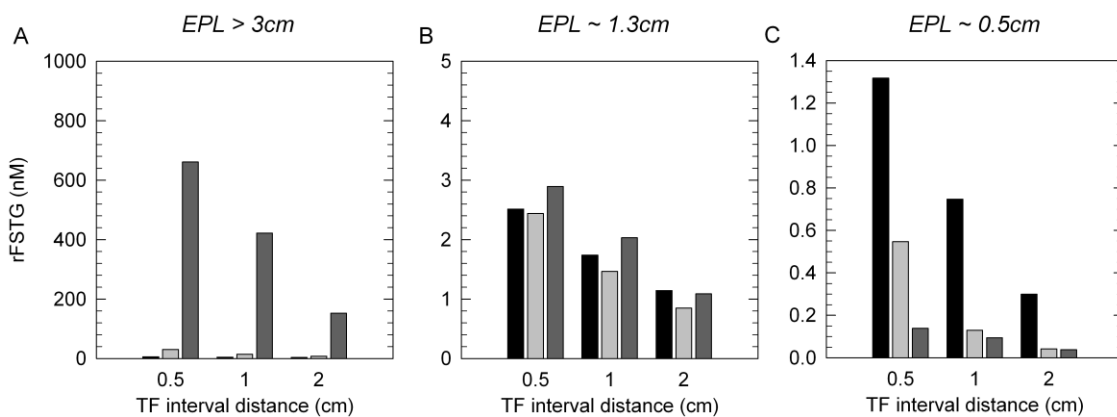
Figure 3.10. **Effect of TF interval on additive and suppressive interactions between tandem TF sites.** From left to right, each bar represents rFSTG for the regions downstream of each site of surface-bound TF during the course of a 60-min flow period at a wall shear rate of 500 s^{-1}. TF$_{length}$ 200 µm, [TF] 9 fmol/cm^2. Varied EPL achieved by varying TM surface density: (**A**) 40 fmol/cm^2, (**B**) 100 fmol/cm^2, (**C**) 1000 fmol/cm^2.

3.5. Discussion

3.5.1. Computational modeling of blood coagulation

Several models restrict their analysis to reaction kinetics of all or part of the intrinsic, extrinsic, and common pathways, neglecting the role of blood flow. Nesheim *et al.* [43] explored the properties of prothrombinase assembly and activity within an interface shell surrounding phospholipid vesicles in solution in a steady-state, two-phase model. Willems *et al.* [44] studied a dynamic model of thrombin generation in plasma describing 14 pro- and anti-coagulant reactions, including inhibition of coagulation by activated protein C, antithrombin III, and exogenous hirudin. The stimulus was a transient pulse of factor Xa, and a threshold response to this stimulus was reported that was dependent on ATIII inactivation of thrombin and factor Xa. Jones and Mann [45] developed a more complex model of the dynamics of coagulation, which included the activation of factors IX, X, V, VIII, and thrombin, assembly of the phospholipid-associated enzyme complexes, intrinsic tenase (IXa/VIIIa) and prothrombinase (Xa/Va), and initiation of thrombin generation by TF/VIIa. This model was subsequently extended to include a number of additional substrate interactions and positive feedback mechanisms, and significantly, incorporated the coagulation inhibitors, tissue factor pathway inhibitor (TFPI) and antithrombin III (ATIII), resulting in a model system describing the fate of 34 species [41]. Jesty and colleagues [46-48] considered, both analytically and numerically, the threshold behavior that resulted from representative systems ranging from an auto-activating zymogen-enzyme pair, to systems of two or four zymogen-enzyme pairs with multiple positive feedback mechanisms subject to irreversible, first-order inactivation. In the presence of coagulation inhibitors, all systems exhibited threshold behavior, which was modulated by changes in initial concentrations of active enzymes, enzyme kinetics, the presence of multiple positive feedback loops, membrane patch size, and in later models, flow [46-48]. Similarly, Bungay *et al*. [49, 50]

demonstrated the dependence of a threshold response on the availability of phospholipid surfaces.

Computational models that have incorporated the effects of blood flow have commonly used a simple compartmental modeling approach, which divides the vascular space into two compartments, a boundary volume and a bulk volume. Additionally, pseudo-one compartment models assume that changes within the bulk phase are negligible, thereby reducing the problem to a system of ordinary differential equations [51]. Baldwin and Basmadjian [8] published a limited model of six reactions, including two positive feedback reactions and two inhibitory reactions, of the common pathway of coagulation triggered by exogenous factor IXa under flow. The major finding of the study was the predicted effect of increased mass transport to enhance thrombin generation by decreasing the induction time up to a critical mass transfer rate, beyond which transport significantly decreased peak thrombin levels, thereby reducing overall thrombin production. Kuharsky and Fogelson [9] formulated a more comprehensive, pseudo-one compartment model of tissue factor-initiated coagulation under flow, which included the description of 59 distinct fluid- and surface-bound species. In the process, the threshold response of thrombin generation was related to the availability of membrane binding sites. In contrast to the Baldwin-Basmadjian model, which defined the mass transfer coefficient in terms of the rate of transport to the vessel surface, the Kuharsky-Fogelson model defined the mass transfer coefficient as a rate of transport into the boundary *volume*, thus eliminating the dependence of kinetic parameters on transport parameters. This model was subsequently extended by Fogelson and Tania [52] to include protein C and TFPI pathways. While the Fogelson models incorporated the essential phenomena of flow and surface reactivity, their indirect method relied heavily on the assumption of well-mixed compartments and therefore is limited at low

shear rates, for large surfaces, and physiologic relevance of a homogeneous surface presentation.

Ataullakhanov and colleagues [10, 11] developed mathematical models to describe the spatial dynamics of clot formation initiated by a monolayer of TF-expressing cells in the direction perpendicular to the vessel wall. Extrinsic, intrinsic, and protein C pathways were represented by 27 partial differential equations. Major findings include the roles of these specific coagulation pathways in the initiation, amplification, and termination phases of coagulation. It was observed that coagulation near the activating surface was determined by TF/VIIa catalyzed factor Xa production, while clot formation away from the reactive wall was dependent on intrinsic tenase (IXa/VIIIa) activity. These studies provide an interesting analysis of the roles of specific factors in relation to space due to diffusive effects, but neglect the essential role of blood flow in the transport analysis. Additionally, the spatial dynamics of clot localization by thrombomodulin would likely be affected by restricting the inhibitor to its physiologic site on the vessel surface. Ismagilov *et al.* studied the threshold response of coagulation to various spatial parameters in microfluidic systems of TF-patterned phospholipid surfaces [12]. Numerically, initiation of a representative autocatalytic system by different sized and shaped patches was simulated using a finite element model, which defined three reactions and diffusion. The reaction 'modules' represented the kinetics of: 1) activation by the stimulus patch, corresponding to TF-mediated initiation of coagulation, 2) autocatalytic production of the activator in solution, representing the positive feedback mechanisms of coagulation, and 3) linear consumption of the enzyme product in solution. A threshold response to the size and shape of the TF patch was empirically and numerically shown to follow a simple scaling relationship based on the ratio of the rate of diffusion off the patch to the rate of generation of the activating species [53, 54]. Runyon *et al.* [55] described the propagation of clotting from an initiating microchannel

63

into a perpendicularly oriented channel with flowing plasma. In small microchannels, clotting was shown to be inhibited by surface-bound inhibitors, specifically TM, while in larger microchannels, the threshold response of clotting was regulated by the shear rate in the cross-flowing channel. The simple numerical experiments served primarily to confirm experimental observations, and with the exception of the cross-flow channel, convective effects were not considered.

We have characterized a computational model of coagulation, which integrates the effects of reaction kinetics, a simple, yet computationally expandable, flow regime, and uniquely heterogeneous surface expression. Our model simulated threshold effects with respect to the length of the TF site, TF and TM surface densities, and wall shear rate, and reproduced the classic time course characterized by initiation and amplification of thrombin generation. Furthermore, our TF length threshold was consistent with experimental work by Shen and colleagues who measured a TF threshold size of approximately 400 μm in a capillary perfusion system under low shear rates (40 s^{-1}) in the absence of TM regulation [56]. Interestingly, the threshold TF length in this study at transport-limited levels of TF and TM was found to be within the length range of ruptured plaques associated with acute thrombotic occlusion [20]. With respect to TF density, we computed thresholds of 0.03 and 0.8 fmol/cm^2 for wall shear rates of 50 and 500 s^{-1}, respectively. Using patterned microarrays, Okorie et al. determined critical TF concentrations of 0.6, 1.4, and 1.7 fmol/cm^2 for wall shear rates of 100, 500, and 1000 s^{-1}, respectively [57]. Computationally, Kuharsky and Fogelson predicted a TF density threshold of approximately 3 fmol/cm^2 at 500 s^{-1} [9]. It has been estimated using ex vivo carotid plaque scraping that the average phospholipid membrane-associated TF underlying atherosclerotic plaques is 33 pg TF/cm^2, or 1 fmol/cm^2 [58]. The principle of a TF threshold is significant since it is unlikely that the vasculature is completely without defect. An understanding of the regulation of blood coagulation requires consideration

not only of antithrombotic biochemical pathways, but also consideration of coagulation thresholds. As we have demonstrated, these variables may not be studied in isolation; for example, wall shear rate has profound effect on TF density threshold.

In addition to generating complete concentration profiles for each coagulation factor and inhibitor, we have defined a global parameter, FSTG, which reflects three key qualities of the thrombin response: 1) intensity of response, 2) relative onset of amplification, and 3) localization of the thrombin foci near to the upstream injury area. Sub-threshold systems are characterized by FSTG <10nM, while those systems that cause full activation of the coagulation cascade fall along a continuous scale >10nM FSTG. The choice of a consistent one-hour simulation time ensured inclusion of early and late phases of coagulation. While there is some post-processing loss of information due to averaging, it is notable that the results of spatially homogeneous models are intrinsically averaged.

Perhaps the most intriguing result of this study was the identification of an effective prothrombotic zone (EPZ) that may be significantly larger than the dimensions of the spatially discrete site of tissue factor expression in both radial (EPH) and axial (EPL) directions, with implications for clot growth leading to arterial or venous thrombosis, as well as systemic procoagulant effects leading to further hypercoagulability. The geometric parameters EPL and EPH are therefore measures of the vital function of hemostasis to confine thrombus formation to an injury site. Shen et al. reported that spatial propagation of thrombin was limited to a 100-µm distance from a discrete patch of TF, under conditions which did not lead to exceeding a threshold for thrombin propagation [56]. Significantly, a remarkable increase in the effective prothrombotic zone may occur under conditions that lead to a reduction in the surface concentration of thrombomodulin. This effect is further enhanced in a low flow regime. These results are consistent with those reported by Ataullakhanov and colleagues for

experimental and computational studies for a diffusion limited system, in which thrombin generation and clot formation were inhibited by solution-phase TM with final clot lengths of 0.2-2 mm under diffusive conditions [10, 11].

3.5.2. Simulated hemophilias

Hemophilias A and B are X-linked genetic deficiencies of factor VIII and IX with annual worldwide incidence of 1:5,000 and 1:30,000 male births, respectively. Both "severe" (<1% of normal, 50-60% of pts) and "moderate" (<5% of normal, 25-30%) hemophilia patients experience spontaneous bleeding into joints and soft tissues and excessive bleeding with surgery or trauma. Recurrent episodes of intra-articular hemorrhage and inflammation cause progressive damage to cartilage and bone, leading to disabling arthropathy [59]. Factors VIII and IX are components of the enzyme complex, intrinsic tenase, which is essential for the rapid rate of thrombin formation during the propagation phase of coagulation. It has been shown that the rapid thrombin burst, not simply high concentrations of thrombin, contributes to the formation of a stable fibrin plug that is resistant to premature fibrinolysis. Thus, although initial clot formation is often normal in hemophilia patients, the loose fibrin networks formed are easily dissolved leading to prolonged bleeding [60, 61]. Consistent with these experimental reports, lower maximum rates of thrombin generation were observed in our simulation for both hemophilia A and B. Additionally, we determined that both hemophilic states required an increase in TF density for activation of coagulation as compared to a normal hemostatic system without these deficiencies. Of note, the parameter FSTG reflected changes in both the peak thrombin concentration and the maximum rate of thrombin generation.

3.5.3. Atherosclerosis and the importance of interactions between multiple lesions

Despite advances in prevention, patient education, and pharmaceutical therapies, atherosclerosis remains a significant source of morbidity and is estimated to be responsible for nearly 75% of all cardiovascular-related mortality [62]. Atherosclerosis is a diffuse disease affecting all vessels and long range communication between sites cannot be excluded, particularly in the presence of flow. Furthermore, tandem lesions, or more than one stenosis in series within a single coronary or carotid artery, are common occurrences and pose unique hemodynamic challenges [63, 64]. It may be concluded from these computational observations, that measurement of lesion morphology [65] is not sufficient for determining the vulnerability of coronary atherosclerotic plaques and the likelihood of acute coronary syndromes or sudden cardiac death. The number and distance between lesions may be of equal or greater importance. Indeed, it has been suggested that smaller, non-obstructive plaques, could be most dangerous simply because they by far outnumber the larger, obstructive plaques [66]. Accurate assessment of plaque vulnerability and subsequent management of high-risk plaques or 'systems of plaques' through pharmaceutical or interventional therapies could greatly diminish morbidity associated with ischemic cardiac injury and decrease the incidence of sudden cardiac death [67]. We have explored blood coagulation in the setting of multiple spatially discrete regions of tissue factor expression. The existence of an effective prothrombotic length that extends significantly beyond the anatomical dimensions of an injury site establishes a foundation for procoagulant interactions between the injury sites. The effective prothrombotic length is governed not only by the dimension and concentration of the TF-expressing site, but also by flow effects and surrounding TM-protein C pathway regulation. As a consequence, the additive effects of more than one sub-clinical atherosclerotic plaque

lesion may result in a clinically relevant thrombotic response. The major determinant of

a system's overall pro- or anti-thrombotic behavior is the relationship between the

effective prothrombotic length and the interval distance between lesions. More

precisely, the relationship between the effective prothrombotic length and the interval

distance governs the intensity of additive, prothrombotic interactions. In contrast,

suppressive interactions are governed by the surface density of TM within the

intervening regions. In our analysis of the effect of the EPL to interval distance ratio, the

effective prothrombotic length was shortened by increasing TM surface concentration.

This had the confounding effect of also causing downregulation of thrombin generation

over downstream TF sites. The effective prothrombotic length may also be shortened by

decreasing the surface concentration of TF.

Acute clinical events including stroke and myocardial infarction (MI) occur upon

rupture of atherosclerotic plaques. Exposure of large amounts of tissue factor (TF) to

the bloodstream from within the necrotic core of plaque lesions is thought to be

responsible for the hyperthrombotic state of atherosclerotic vessels [68-70]. Campo et

al. measured factor VII and TF antigen levels for 256 patients admitted for acute MI and

correlated these levels with increased incidence of death and reinfarction within a

median follow-up period of 397 days (hazard ratio 2.1 for FVII and 4.1 for TF) [71]. The

investigators of the Athero*Gene* study, which included 1669 patients with coronary artery

disease (CAD) with a median follow-up of 2.3 years, reported a hazard ratio of 2.06 for

soluble plasma TF levels and cardiovascular death in individuals with acute coronary

syndrome [72]. Similarly, a 30-year review of the Northwick Park Heart Study (NPHS-1)

observed a significant association of factor VII with fatal coronary heart disease (RR

1.58 in men, 1.78 in women); no correlation was found with non-fatal heart disease [73].

Amiodarone, an anti-arrhythmic agent known to decrease mortality in patients with CAD

and decreased ejection fraction, has been shown to interfere with tumor necrosis factor

(TNFα)- and thrombin-induced TF expression in culture human vascular cells as well as in a mouse photochemical carotid injury model [74].

Interestingly, upstream TF regions promote TM and thrombin-mediated generation of the anticoagulant APC that acts to dampen the thrombin response at distal sites. In a study of 335 patients admitted to the emergency department for ST-elevation myocardial infarction, decreased APC levels were found to be a prognostic parameter for high risk of death with an adjusted odds ratio of 9.4 for an APC cutoff at 65% [75]. In a retrospective study comparing patients with severe atherosclerosis and ischemic cardiomyopathy to matched controls, Laszik *et al.* [76] determined a 2.4-fold decrease in thrombomodulin staining of endothelial cells of the coronary arteries. In concordance with our findings, it may be inferred that management strategies which support TM expression and upregulation should be encouraged in patients found to have more than a few coronary plaques, despite the apparent sub-clinical size of individual lesions. The effects of TM surface concentration may also have implications for early autologous vein graft failure due to thrombosis. Immunohistochemical staining and Western blot analysis revealed a transient reduction in TM expression of over 95% during the first 2 weeks following implantation of autologous vein graft sections in a rabbit model [77].

3.5.4. Model limitations and extensions

Certainly, any theoretical model is limited in the absence of direct experimental validation. However, experimental studies in a parallel plate flow reactor of TF- and TM-functionalized membrane-mimetic assemblies yielded predictions of surface densities for mass transfer limited regimes which were within reasonable agreement with numerical studies. Direct experimental vaildation is challenging given the obstacles of obtaining species concentrations at specific spatial points within the flow field with sufficient temporal resolution. Moreover, the measurement of outlet concentrations becomes

irrelevant for systems in which thrombin generation is effectively localized to the upstream environment, as extremely minute concentrations, diluted additionally by the bulk stream and the collection volume required for assay, would need to be detected. Given the available indirect validation and the relatively well-defined nature of the coagulation cascade, it is likely that the model provides a close approximation of surface-induced thrombin generation under flow conditions.

Our computational model is not without value in its ability to simulate features of the coagulation cascade, namely the rapid 'all-or-none' response of thrombin activation, characteristic initiation and amplification phases, and quantitative values within the appropriate range of concentrations. While it may be suggested that any phenomena may be mathematically reproduced given 16 diffusion coefficients, 10 inlet concentrations, and 36 kinetic parameters, it bears emphasis that the reaction pathways and related kinetic parameters are largely well-defined for the coagulation cascade, and furthermore, that no parameter fitting was performed for our model system. Given a different set of physiologically relevant parameters, the qualitative trends observed in our studies would have remained the same, though quantitative values may have changed to some degree.

A number of simplifying assumptions were made for reasons of computational simplicity and feasibility. First, steady, one-dimensional laminar flow in a two-dimensional, rectangular flow field was assumed. This simple, algebraically-defined flow profile enabled the effect of wall shear rate to be directly studied, but did not reflect the pulsatile flow of the arterial system or turbulent flow patterns often observed at bifurcation, or branching points. It should be noted, however, that the FEM approach taken in these studies allows for the possibility of incorporating more complex flow geometries and non-steady flows by the addition of the Navier-Stokes equation to solve for x- and y- components of flow velocity, or by coupling to other existing computational

fluid dynamics (CFD) models. Future work may model atherosclerotic lesions, which not only represent areas of increased TF, but are often areas of stenosis and consequently locally increased wall shear rates. Our initial modeling studies would suggest a protective effect; however, the decreased shear immediately downstream of the plaque may decrease the ability of unaffected vasculature to abrogate the thrombin load.

Tissue factor surface presentation was assumed constant over the 60-min simulation period. In other words, the TF stimulus responsible for initiating the reaction cascade is never 'turned off', and its catalytic activity is inhibited only by TFPI. In addition to being challenging to define computationally, the dynamics of TF trafficking are complex and dependent on factor VIIa. Upon binding, factor VIIa induces clathrin-mediated cellular reuptake of the TF/VIIa complex in a time-dependent manner, with maximum internalization measured at 60 min [78]. Additionally, factor VIIa-dependent internalization of cell surface TF is promoted by TFPI [79]. While internalized TF is not recycled back to the cell surface, factor VIIa also causes the release of stored TF from the Golgi apparatus to the cell surface, resulting in a net increase of surface TF by 20-30% [78]. It is unclear whether this mechanism is responsible for the dynamic increase in TF surface expression in endothelial cells and monocytes when exposed to inflammatory mediators including tissue necrosis factor (TNF-α), interleukin-1 (IL-1), histamine, endotoxin, oxidized lipoproteins, and heme [68, 80-83]. Recently, the phenomena of 'TF decryption' has been described in response to cellular activation [68, 84]. Though the mechanism and kinetics of decryption have not been well-defined, it has been suggested that post-translational reduction of an allosteric disulfide bond between two extracellular immunoglobulin-like domains may be required for enhanced binding affinity for factor VIIa. In a murine model of endothelial cell injury, TF-initiated fibrin formation was directly correlated to the activity of the oxidoreductase protein disulfide isomerase (PDI) released from adherent platelets and vascular wall cells at the

71

injury site [85]. Finally, surface-bound TF may be physically inhibited by fibrin and

platelet deposition [9]. The time-dependent profile of active tissue factor presentation on

the cell surface is complex and warrants further consideration in our computational

model. Additionally, circulating TF, both soluble and lipid-bound, was excluded from the

model as its role in thrombosis continues to be elucidated [86]. Alternatively spliced

soluble tissue factor has been identified with retained procoagulant activity. This isoform

of TF is incorporated into growing thrombi when exposed to phospholipids and has been

induced from endothelial cells by inflammatory mediators [87, 88]. Additionally, TF

incorporated within the membrane of circulating microparticles shed from a variety of cell

types has been studied in relation to coronary artery disease, inflammation, and

cardiopulmonary bypass [89-92].

Thrombomodulin expression was also assumed to remain constant over the 60-

min flow period. Although a number of agents are known to affect TM expression,

including cyclic adenosine monophosphate (cAMP), retinoic acid, and numerous

inflammatory mediators, several of these factors affect expression on a transcriptional

level [93-96], and thus do not affect our assumption of constant TM density over the 60-

min time period. In contrast, internalization, degradation, and recycling of TM are

temporally relevant events that may be mediated by thrombin [97]. Following a 5-min

exposure to thrombin, radiolabeled cell surface TM on cultured endothelial cells

decreased linearly to less than 50% of its original concentration within 30 min,

accompanied by cessation of cofactor activity. TM surface concentration returned to

baseline by 90 min. However, in the presence of physiologic concentrations of protein

C, thrombin-mediated endocytosis was inhibited [98]. Additionally, homocysteine, a

sulfur-containing amino acid formed during the metabolism of methionine, can

irreversibly eliminate TM cofactor activity in cultured endothelial cells by reducing the

disulfide-bond rich EGF-like domains [99]. However, concentrations of homocysteine

used in this study were 10^3-times higher than normal the normal physiologic range as well as levels observed in inherited hyperhomocysteinemia, and thus the relevance of TM inactivation by homocysteine remains unclear. TM activity may also be inactivated by neutrophil-mediated oxidative damage to a susceptible methionine residue on the sixth EGF-like domain of TM [100]. While surface TM activity may be affected by a number of factors, the assumption of steady TM over the course of our simulation period is a reasonable one.

Only a limited portion of the intrinsic pathway is included in the model. Factor IXa is assumed to be generated solely by TF/ VIIa without participation of factors XI and XII (Hageman factor). The role of the intrinsic, or contact pathway in the activation of coagulation *in vivo* remains undefined. *In vitro*, factor XII is autoactivated to XIIa when exposed to negatively charged surfaces in a reaction involving high molecular weight kininogen (HMWK) and prekallikrein. Factor XIIa, in turn, catalyzes the activation of factor XI, and factor XIa activates factor IX in the classic 'cascade' or 'waterfall' model of coagulation [101]. *In vivo,* however, the role of factor XII in coagulation is unclear, with reports of increased risk of thrombosis associated with both deficiency and elevation of factor XII [102-105]. Furthermore, it has been shown that thrombin is in fact 10-times more effective than factor XIIa in activating factor XI, and that factor XIIa-independent activation of XI may be further enhanced in the presence of glycosaminoglycans [101, 106]. Alternate physiologic roles for factor XII, HMWK, and prekallikrein have been proposed in processes including vasodilation, inflammation, fibrinolysis, cell adhesion, and angiogenesis [107]. In contrast, factor XI deficiency, or hemophilia C, is associated with a mild to moderate bleeding diathesis, specifically in the settings of trauma and surgery [108], and high levels of factor XI are associated with increased risk of venous and arterial thrombosis [109-111]. In contrast, it has been suggested that factor XI may be important in sustaining coagulation once tissue factor has been blocked by either

TFPI or growing thrombus formation [42, 112]. Notably, even in the absence of factor

XI, our model reflects the role of intrinsic tenase in amplifying thrombin generation after

the initiation phase. While the dominant mechanism for factor IX activation seems to be

TF/VIIa mediated, the physiologic role of factor XIa continues to evolve and may be

considered in future model iterations.

Additional biochemical constituents related to coagulation that were not

described by our model include, but are not limited to, protein C inhibitor (PCI), protein

S, heparin cofactor II (HcII), von Willebrand factor (vWF), and endothelial protein C

receptor (EPCR). Protein C inhibitor, as well as α_1-antiproteinase inhibitor and α_2-

macroglobulin, inactivates activated protein C [113, 114]. Heparin cofactor II is a serine

protease inhibitor homologous to ATIII that binds thrombin, but not factors IXa or Xa, in

the presence of dermatan sulfate [115]. Von Willebrand factor protects factor VIIIa from

APC-mediated inactivation [116]. EPCR is a transmembrane protein that promotes

thrombin-TM catalyzed protein C activation by facilitating the association of protein C

with the cell surface and promoting the assembly of the substrate-enzyme complex

[117]. Although these pathways are relatively well characterized, the impact of these

mediators on the overall system was believed to be outweighed by the computational

effort required to define the additional species and kinetic parameters. Protein S is a

vitamin K-dependent plasma protein that acts as a necessary cofactor for the

anticoagulant functions of activated protein C [118]. The cofactor activity of protein S

was accounted for in the model through the choice of kinetic parameters for APC-

mediated inactivation of factor Va and VIIIa which were measured in the presence of

physiologic concentrations of protein S [25]. However, heterozygous protein S

deficiency is associated with thrombotic risk similar to that cased by heterozygous

protein C deficiency, and APC resistance caused by acquired protein S deficiency is

thought to be a contributory factor in hypercoagulability associated with pregnancy and

oral contraceptive use [119, 120]. Thus mechanistic inclusion of protein S may be useful

for the representation and study of pathologic states.

The computational model considered only free TFPI, not associated with

circulating lipoproteins nor inducible from cellular sources, specifically endothelial cells

and platelets [42]. Lipoprotein-bound TFPI does not retain its anticoagulant activity and

is thought to play a role in atherosclerosis [121]. In culture, the majority of TFPI

synthesized by endothelial cells remains sequestered within granules near the cell

surface [122]. The rapid release of TFPI may be induced in a dose-dependent manner

by heparin infusion [123, 124] and thrombin exposure in culture [125]. The rates of

release in response to stimulation *in vivo* are not well-defined.

Likewise, while the fibrinolytic pathway and platelet activation, adhesion, and

aggregation are essential components of overall hemostasis, mathematical description

of these pathways are beyond the scope of the current investigation. Such undertakings

require the consideration of rheological and mechanical phenomena as well as

biochemical pathways. Anand *et al.* have described some partial models of the

formation and lysis of fibrin clots, including models of the extrinsic and fibrinolytic

pathways in the absence of flow and continuum mechanical models of loose fibrin clots

in a flow field [126, 127]. Others have developed methods to computationally describe

the mechanical aspects of the motion, collision, adhesion, and cohesion of platelets

within a viscous fluid [128, 129].

3.5.5. Summary

With the advances in computational methods, theoretical models of coagulation

may consider many phenomenological aspects efficiently and more completely.

Compared to previous models of blood coagulation, we have presented the most

comprehensive finite element model of coagulation reactions under flow to date with particular attention to spatial regulation. In addition to the procoagulant reactions of the intrinsic, extrinsic, and common pathways, three physiologically relevant inhibitory pathways were mechanistically considered. By eliminating the assumption of spatial homogeneity and describing discrete sites of TF and TM surface reactivity, localization of thrombin formation by downstream TM was not only demonstrated, but quantified by the definition of an effective prothrombotic zone in two dimensions. While extension of thrombin generation away from the wall towards the center of the vascular space may contribute to vessel occlusion and stasis of flow, prothrombotic effects which extend downstream beyond the discrete site of injury to interact with subsequent lesions are critical given the systemic nature of atherosclerotic disease. The TM-APC pathway is a key determinant of the overall thrombin response in the setting of multiple TF-laden lesions.

3.6. REFERENCES

1. Butenas, S., C. van't Veer, and K.G. Mann, *"Normal" Thrombin Generation.* Blood, 1999. **94**(7): p. 2169-2178.
2. Rock, G. and P. Wells, *New Concepts in Coagulation.* Critical Reviews in Clinical Laboratory Sciences, 1997. **34**(5): p. 475-501.
3. Mann, K.G., S. Butenas, and K. Brummel, *The Dynamics of Thrombin Formation.* Arteriosclerosis Thrombosis and Vascular Biology, 2003. **23**(1): p. 17-25.
4. Bourin, M.C. and U. Lindahl, *Glycosaminoglycans and the Regulation of Blood-Coagulation.* Biochemical Journal, 1993. **289**: p. 313-330.
5. Jesty, J., T.C. Wun, and A. Lorenz, *Kinetics of the Inhibition of Factor XA and the Tissue Factor-Factor VIIA Complex by the Tissue Factor Pathway Inhibitor in the Presence and Absence of Heparin.* Biochemistry, 1994. **33**(42): p. 12686-12694.
6. Lu, G., G.J. Broze, and S. Krishnaswamy, *Formation of Factors IXa and Xa by the Extrinsic Pathway - Differential Regulation by Tissue Factor Pathway Inhibitor and Antithrombin III.* Journal of Biological Chemistry, 2004. **279**(17): p. 17241-17249.
7. Nemerson, Y. and V.T. Turitto, *The Effect of Flow on Hemostasis and Thrombosis.* Thrombosis and Haemostasis, 1991. **66**(3): p. 272-276.
8. Baldwin, S.A. and D. Basmadjian, *A Mathematical-Model of Thrombin Production in Blood-Coagulation .1. The Sparsely Covered Membrane Case.* Annals of Biomedical Engineering, 1994. **22**(4): p. 357-370.
9. Kuharsky, A.L. and A.L. Fogelson, *Surface-Mediated Control of Blood Coagulation: The Role of Binding Site Densities and Platelet Deposition.* Biophysical Journal, 2001. **80**(3): p. 1050-1074.
10. Ataullakhanov, F.I., et al., *Spatio-Temporal Dynamics of Blood Coagulation and Pattern Formation. A Theoretical Approach.* International Journal of Bifurcation and Chaos, 2002. **12**(9): p. 1985-2002.
11. Panteleev, M.A., et al., *Spatial Propagation and Localization of Blood Coagulation Are Regulated by Intrinsic and Protein C Pathways, Respectively.* Biophysical Journal, 2006. **90**(5): p. 1489-1500.
12. Shen, F., C.J. Kastrup, and R.F. Ismagilov, *Using Microfluidics to Understand the Effect of Spatial Distribution of Tissue Factor on Blood Coagulation.* Thrombosis Research, 2008. **122**: p. S27-S30.
13. Byun, Y., H.A. Jacobs, and S.W. Kim, *Binding of Antithrombin III and Thrombin to Immobilized Heparin under Flow Conditions.* Biotechnology Progress, 1996. **12**(2): p. 217-225.
14. Hall, C.L., S.M. Slack, and V.T. Turitto, *A Computational Analysis of FXa Generation by TF : FVIIa on the Surface of Rat Vascular Smooth Muscle Cells.* Annals of Biomedical Engineering, 1998. **26**(1): p. 28-36.
15. Tummala, S.R. and C.L. Hall, *Computational Modeling of Factor Xa Inhibition by Immobilized Tissue Factor Pathway Inhibitor.* Annals of Biomedical Engineering, 2007. **35**(3): p. 408-418.
16. Morrissey, J.H., *Tissue Factor Modulation of Factor Viia Activity - Use in Measuring Trace Levels of Factor Viia in Plasma.* Thrombosis and Haemostasis, 1995. **74**(1): p. 185-188.
17. Murano, G., et al., *Some Properties of Antithrombin-III and Its Concentration in Human Plasma.* Thromb Res, 1980. **18**(1-2): p. 259-62.
18. Novotny, W.F., et al., *Plasma Antigen Levels of the Lipoprotein-Associated Coagulation Inhibitor in Patient Samples.* Blood, 1991. **78**(2): p. 387-93.
19. Young, M.E., P.A. Carroad, and R.L. Bell, *Estimation of Diffusion-Coefficients of Proteins.* Biotechnology and Bioengineering, 1980. **22**(5): p. 947-955.
20. Nakazawa, G., et al., *Delayed Arterial Healing and Increased Late Stent Thrombosis at Culprit Sites after Drug-Eluting Stent Placement for Acute Myocardial Infarction Patients - an Autopsy Study.* Circulation, 2008. **118**(11): p. 1138-1145.
21. Nesheim, M.E., J.B. Taswell, and K.G. Mann, *Contribution of Bovine Factor-V and Factor-Va to the Activity of Prothrombinase.* Journal of Biological Chemistry, 1979. **254**(21): p. 952-962.

22. Mann, K.G., et al., *Surface-Dependent Reactions of the Vitamin-K-Dependent Enzyme Complexes.* Blood, 1990. **76**(1): p. 1-16.

23. Rosing, J., et al., *Role of Phospholipids and Factor‑Va in the Prothrombinase Complex.* Journal of Biological Chemistry, 1980. **255**(1): p. 274-283.

24. Galvin, J.B., et al., *Reconstitution of Rabbit Thrombomodulin into Phospholipid‑Vesicles.* Journal of Biological Chemistry, 1987. **262**(5): p. 2199-2205.

25. Solymoss, S., M.M. Tucker, and P.B. Tracy, *Kinetics of Inactivation of Membrane-Bound Factor‑Va by Activated Protein‑C - Protein‑S Modulates Factor‑XA Protection.* Journal of Biological Chemistry, 1988. **263**(29): p. 14884-14890.

26. Zur, M. and Y. Nemerson, *Kinetics of Factor-IX Activation Via the Extrinsic Pathway - Dependence of Km on Tissue Factor.* Journal of Biological Chemistry, 1980. **255**(12): p. 5703-5707.

27. Lollar, P., G.J. Knutson, and D.N. Fass, *Activation of Porcine Factor-VIII-C by Thrombin and Factor XA.* Biochemistry, 1985. **24**(27): p. 8056-8064.

28. Lollar, P., E.T. Parker, and P.J. Fay, *Coagulant Properties of Hybrid Human Porcine Factor‑VIII Molecules.* Journal of Biological Chemistry, 1992. **267**(33): p. 23652-23657.

29. Rawala-Sheikh, R., et al., *Kinetics of Coagulation Factor-X Activation by Platelet-Bound Factor‑1xa.* Biochemistry, 1990. **29**(10): p. 2606-2611.

30. Monkovic, D.D. and P.B. Tracy, *Activation of Human Factor-V by Factor-XA and Thrombin.* Biochemistry, 1990. **29**(5): p. 1118-1128.

31. Butenas, S. and K.G. Mann, *Kinetics of Human Factor VII Activation.* Biochemistry, 1996. **35**(6): p. 1904-1910.

32. Nemerson, Y., *The Tissue Factor Pathway of Blood-Coagulation.* Seminars in Hematology, 1992. **29**(3): p. 170-188.

33. Mann, K.G., *The Assembly of Blood-Clotting Complexes on Membranes.* Trends in Biochemical Sciences, 1987. **12**(6): p. 229-233.

34. Rezaie, A.R. and S.T. Olson, *Calcium Enhances Heparin Catalysis of the Antithrombin-Factor Xa Reaction by Promoting the Assembly of an Intermediate Heparin-Antithrombin-Factor Xa Bridging Complex. Demonstration by Rapid Kinetics Studies.* Biochemistry, 2000. **39**(39): p. 12083-12090.

35. Haley, P.E., M.F. Doyle, and K.G. Mann, *The Activation of Bovine Protein-C by Factor-Xa.* Journal of Biological Chemistry, 1989. **264**(27): p. 16303-16310.

36. Thompson, E.A. and H.H. Salem, *Factor-Ixa, Factor-Xa, Factor-Xia and Activated Protein-C Do Not Have Protein-C Activating Ability in the Presence of Thrombomodulin.* Thrombosis and Haemostasis, 1988. **59**(2): p. 339-339.

37. Regan, L.M., et al., *Factor-Ixa Protects Factor‑Viiia from Activated Protein-C - Factor-Ixa Inhibits Activated Protein-C-Catalyzed Cleavage of Factor-Viiia at Arg(562).* Journal of Biological Chemistry, 1994. **269**(13): p. 9445-9452.

38. Tseng, P.Y., et al., *Catalytic Efficiency of a Thrombomodulin-Functionalized Membrane-Mimetic Film in a Flow Model.* Biomaterials, 2006. **27**(13): p. 2768-2775.

39. Brummel, K.E., et al., *Thrombin Functions During Tissue Factor-Induced Blood Coagulation.* Blood, 2002. **100**(1): p. 148-152.

40. Allen, G.A., et al., *Impact of Procoagulant Concentration on Rate, Peak and Total Thrombin Generation in a Model System.* Journal of Thrombosis and Haemostasis, 2004. **2**(3): p. 402-413.

41. Hockin, M.F., et al., *A Model for the Stoichiometric Regulation of Blood Coagulation.* Journal of Biological Chemistry, 2002. **277**(21): p. 18322-18333.

42. Broze, G.J., *Tissue Factor Pathway Inhibitor and the Revised Theory of Coagulation.* Annual Review of Medicine, 1995. **46**: p. 103-112.

43. Nesheim, M.E., R.P. Tracy, and K.G. Mann, *Clotspeed, a Mathematical Simulation of the Functional-Properties of Prothrombinase.* Journal of Biological Chemistry, 1984. **259**(3): p. 1447-1453.

44. Willems, G.M., et al., *Simulation-Model for Thrombin Generation in Plasma.* Haemostasis, 1991. **21**(4): p. 197-207.

45.   Jones, K.C. and K.G. Mann, *A Model for the Tissue Factor Pathway to Thrombin .2. A Mathematical Simulation.* Journal of Biological Chemistry, 1994. **269**(37): p. 23367-23373.

46.   Jesty, J., E. Beltrami, and G. Willems, *Mathematical-Analysis of a Proteolytic Positive-Feedback Loop - Dependence of Lag Time and Enzyme Yields on the Initial Conditions and Kinetic-Parameters.* Biochemistry, 1993. **32**(24): p. 6266-6274.

47.   Beltrami, E. and J. Jesty, *Mathematical-Analysis of Activation Thresholds in Enzyme-Catalyzed Positive Feedbacks - Application to the Feedbacks of Blood-Coagulation.* Proceedings of the National Academy of Sciences of the United States of America, 1995. **92**(19): p. 8744-8748.

48.   Beltrami, E. and J. Jesty, *The Role of Membrane Patch Size and Flow in Regulating a Proteolytic Feedback Threshold on a Membrane: Possible Application in Blood Coagulation.* Mathematical Biosciences, 2001. **172**(1): p. 1-13.

49.   Bungay, S.D., P.A. Gentry, and R.D. Gentry, *A Mathematical Model of Lipid-Mediated Thrombin Generation.* Mathematical Medicine and Biology-a Journal of the Ima, 2003. **20**(1): p. 105-129.

50.   Bungay, S.D., *Modelling the Effect of Amplification Pathway Factors on Thrombin Generation: A Comparison of Hemophilias.* Transfusion and Apheresis Science, 2008. **38**(1): p. 41-47.

51.   Basmadjian, D., *The Effect of Flow and Mass-Transport in Thrombogenesis.* Annals of Biomedical Engineering, 1990. **18**(6): p. 685-709.

52.   Fogelson, A.L. and N. Tania, *Coagulation under Flow: The Influence of Flow-Mediated Transport on the Initiation and Inhibition of Coagulation.* Pathophysiology of Haemostasis and Thrombosis, 2005. **34**(2-3): p. 91-108.

53.   Kastrup, C.J., et al., *Characterization of the Threshold Response of Initiation of Blood Clotting to Stimulus Patch Size.* Biophysical Journal, 2007. **93**(8): p. 2969-2977.

54.   Kastrup, C.J., F. Shen, and R.F. Ismagilov, *Response to Shape Emerges in a Complex Biochemical Network and Its Simple Chemical Analogue.* Angewandte Chemie-International Edition, 2007. **46**(20): p. 3660-3662.

55.   Runyon, M.K., et al., *Effects of Shear Rate on Propagation of Blood Clotting Determined Using Microfluidics and Numerical Simulations.* Journal of the American Chemical Society, 2008. **130**(11): p. 3458-3464.

56.   Shen, F., et al., *Threshold Response of Initiation of Blood Coagulation by Tissue Factor in Patterned Microfluidic Capillaries Is Controlled by Shear Rate.* Arteriosclerosis Thrombosis and Vascular Biology, 2008. **28**(11): p. 2035-U226.

57.   Okorie, U.M., et al., *Determination of Surface Tissue Factor Thresholds That Trigger Coagulation at Venous and Arterial Shear Rates: Amplification of 100 Fm Circulating Tissue Factor Requires Flow.* Blood, 2008. **111**(7): p. 3507-3513.

58.   Bonderman, D., et al., *Coronary No-Reflow Is Caused by Shedding of Active Tissue Factor from Dissected Atherosclerotic Plaque.* Blood, 2002. **99**(8): p. 2794-800.

59.   Kaufman, R.J., S.E. Antonarakis, and P.J. Fay, *Factor VIII and Hemophilia A*, in *Hemostasis and Thrombosis: Basic Principles and Clinical Practice.* 2001, Lippincott Williams and Wilkins: Philadelphia.

60.   Blomback, B., et al., *Fibrin in Human Plasma - Gel Architectures Governed by Rate and Nature of Fibrinogen Activation.* Thrombosis Research, 1994. **75**(5): p. 521-538.

61.   Wolberg, A.S., et al., *High Dose Factor VIIa Enhances Clot Stability in a Model of Hemophilia.* Blood, 2001. **98**(11): p. 826a-827a.

62.   Rosamond, W., et al., *Heart Disease and Stroke Statistics - 2007 Update - a Report from the American Heart Association Statistics Committee and Stroke Statistics Subcommittee.* Circulation, 2007. **115**(5): p. E69-E171.

63.   Hirota, M., et al., *Coronary Pressure Measurement to Identify the Lesion Requiring Percutaneous Coronary Intervention in Equivocal Tandem Lesions.* Coronary Artery Disease, 2006. **17**(2): p. 181-186.

64.   Vidjak, V., et al., *Stenotic Occlusive Lesions of Internal Carotid Artery in Diabetic Patients.* Collegium Antropologicum, 2007. **31**(3): p. 775-780.

65. Topol, E.J. and S.E. Nissen, *Our Preoccupation with Coronary Luminology - the Dissociation between Clinical and Angiographic Findings in Ischemic-Heart-Disease.* Circulation, 1995. **92**(8): p. 2333-2342.
66. Alderman, E.L., et al., *5-Year Angiographic Follow-up of Factors Associated with Progression of Coronary-Artery Disease in the Coronary-Artery Surgery Study (Cass).* Journal of the American College of Cardiology, 1993. **22**(4): p. 1141-1154.
67. Hamdan, A., et al., *Imaging of Vulnerable Coronary Artery Plaques.* Catheterization and Cardiovascular Interventions, 2007. **70**(1): p. 65-74.
68. Eilertsen, K.E. and B. Osterud, *Tissue Factor: (Patho)Physiology and Cellular Biology.* Blood Coagulation & Fibrinolysis, 2004. **15**(7): p. 521-538.
69. Wilcox, J.N., et al., *Localization of Tissue Factor in the Normal Vessel Wall and in the Atherosclerotic Plaque.* Proceedings of the National Academy of Sciences of the United States of America, 1989. **86**(8): p. 2839-2843.
70. Badimon, L. *Atherosclerosis and Thrombosis: Lessons from Animal Models.* in *XVIIIth Congress of the International-Society-on-Thrombosis-and-Haemostasis.* 2001. Paris, France: F K Schattauer Verlag Gmbh.
71. Campo, G., et al., *Tissue Factor and Coagulation Factor VII Levels During Acute Myocardial Infarction - Association with Genotype and Adverse Events.* Arteriosclerosis Thrombosis and Vascular Biology, 2006. **26**(12): p. 2800-2806.
72. Morange, P.E., et al., *Prognostic Value of Plasma Tissue Factor and Tissue Factor Pathway Inhibitor for Cardiovascular Death in Patients with Coronary Artery Disease: The Atherogene Study.* Journal of Thrombosis and Haemostasis, 2007. **5**(3): p. 475-482.
73. De Stavola, B.L. and T.W. Meade, *Long-Term Effects of Hemostatic Variables on Fatal Coronary Heart Disease: 30-Year Results from the First Prospective Northwick Park Heart Study (Nphs-I).* J Thromb Haemost, 2007. **5**(3): p. 461-71.
74. Breitenstein, A., et al., *Amiodarone Inhibits Arterial Thrombus Formation and Tissue Factor Translation.* Arteriosclerosis Thrombosis and Vascular Biology, 2008. **28**(12): p. 2231-U177.
75. Chiba, N., et al., *Decreased Activated Protein C Levels as a Clinical Predictor in Patients with St-Elevation Myocardial Infarction.* American Heart Journal, 2008. **156**(5): p. 931-938.
76. Laszik, Z.G., et al., *Down-Regulation of Endothelial Expression of Endothelial Cell Protein C Receptor and Thrombomodulin in Coronary Atherosclerosis.* American Journal of Pathology, 2001. **159**(3): p. 797-802.
77. Kim, A.Y., et al., *Early Loss of Thrombomodulin Expression Impairs Vein Graft Thromboresistance - Implications for Vein Graft Failure.* Circulation Research, 2002. **90**(2): p. 205-212.
78. Mandal, S.K., U.R. Pendurthi, and L.V.M. Rao, *Cellular Localization and Trafficking of Tissue Factor.* Blood, 2006. **107**(12): p. 4746-4753.
79. Hamik, A., et al., *Down-Regulation of Monocyte Tissue Factor Mediated by Tissue Factor Pathway Inhibitor and the Low Density Lipoprotein Receptor-Related Protein.* Journal of Biological Chemistry, 1999. **274**(8): p. 4962-4969.
80. Steffel, J., et al., *Histamine Induces Tissue Factor Expression - Implications for Acute Coronary Syndromes.* Circulation, 2005. **112**(3): p. 341-349.
81. Setty, B.N.Y., et al., *Heme Induces Endothelial Tissue Factor Expression: Potential Role in Hemostatic Activation in Patients with Hemolytic Anemia.* Journal of Thrombosis and Haemostasis, 2008. **6**(12): p. 2202-2209.
82. Bevilacqua, M.P., et al., *Recombinant Tumor-Necrosis-Factor Induces Procoagulant Activity in Cultured Human Vascular Endothelium - Characterization and Comparison with the Actions of Interleukin-1.* Proceedings of the National Academy of Sciences of the United States of America, 1986. **83**(12): p. 4533-4537.
83. Egorina, E.M., et al., *Intracellular and Surface Distribution of Monocyte Tissue Factor - Application to Intersubject Variability.* Arteriosclerosis Thrombosis and Vascular Biology, 2005. **25**(7): p. 1493-1498.
84. Bach, R.R., *Tissue Factor Encryption.* Arteriosclerosis Thrombosis and Vascular Biology, 2006. **26**(3): p. 456-461.

85. Reinhardt, C., et al., *Protein Disulfide Isomerase Acts as an Injury Response Signal That Enhances Fibrin Generation Via Tissue Factor Activation.* Journal of Clinical Investigation, 2008. **118**(3): p. 1110-1122.

86. Butenas, S., T. Orfeo, and K.G. Mann, *Tissue Factor in Coagulation: Which? Where? When?* Arterioscler Thromb Vasc Biol, 2009. **29**(12): p. 1989-96.

87. Bogdanov, V.Y., et al., *Alternatively Spliced Human Tissue Factor: A Circulating, Soluble, Thrombogenic Protein.* Nature Medicine, 2003. **9**(4): p. 458-462.

88. Szotowski, B., et al., *Procoagulant Soluble Tissue Factor Is Released from Endothelial Cells in Response to Inflammatory Cytokines.* Circulation Research, 2005. **96**(12): p. 1233-1239.

89. Kushak, R.I., et al., *Detached Endothelial Cells and Microparticles as Sources of Tissue Factor Activity.* Thrombosis Research, 2005. **116**(5): p. 409-419.

90. Mallat, Z., et al., *Shed Membrane Microparticles with Procoagulant Potential in Human Atherosclerotic Plaques - a Role for Apoptosis in Plaque Thrombogenicity.* Circulation, 1999. **99**(3): p. 348-353.

91. Nieuwland, R., et al., *Cell-Derived Microparticles Generated in Patients During Cardiopulmonary Bypass Are Highly Procoagulant.* Circulation, 1997. **96**(10): p. 3534-3541.

92. Satta, N., et al., *Monocyte Vesiculation Is a Possible Mechanism for Dissemination of Membrane-Associated Procoagulant Activities and Adhesion Molecules after Stimulation by Lipopolysaccharide.* Journal of Immunology, 1994. **153**(7): p. 3245-3255.

93. Tazawa, R., et al., *Presence of Functional Cyclic-Amp Responsive Element in the 3'-Untranslated Region of the Human Thrombomodulin Gene.* Biochemical and Biophysical Research Communications, 1994. **200**(3): p. 1391-1397.

94. Dittman, W.A., et al., *Characterization of Thrombomodulin Expression in Response to Retinoic Acid and Identification of a Retinoic Acid Response Element in the Human Thrombomodulin Gene.* Journal of Biological Chemistry, 1994. **269**(24): p. 16925-16932.

95. Conway, E.M. and R.D. Rosenberg, *Tumor Necrosis Factor Suppresses Transcription of the Thrombomodulin Gene in Endothelial-Cells.* Molecular and Cellular Biology, 1988. **8**(12): p. 5588-5592.

96. Lentz, S.R., M. Tsiang, and J.E. Sadler, *Regulation of Thrombomodulin by Tumor-Necrosis-Factor-Alpha - Comparison of Transcriptional and Posttranscriptional Mechanisms.* Blood, 1991. **77**(3): p. 542-550.

97. Maruyama, I. and P.W. Majerus, *The Turnover of Thrombin-Thrombomodulin Complex in Cultured Human Umbilical Vein Endothelial-Cells and A549 Lung-Cancer Cells - Endocytosis and Degradation of Thrombin.* Journal of Biological Chemistry, 1985. **260**(29): p. 5432-5438.

98. Maruyama, I. and P.W. Majerus, *Protein-C Inhibits Endocytosis of Thrombin Thrombomodulin Complexes in A549 Lung-Cancer Cells and Human Umbilical Vein Endothelial-Cells.* Blood, 1987. **69**(5): p. 1481-1484.

99. Hayashi, T., G. Honda, and K. Suzuki, *An Atherogenic Stimulus Homocysteine Inhibits Cofactor Activity of Thrombomodulin and Enhances Thrombomodulin Expression in Human Umbilical Vein Endothelial-Cells.* Blood, 1992. **79**(11): p. 2930-2936.

100. Glaser, C.B., et al., *Oxidation of a Specific Methionine in Thrombomodulin by Activated Neutrophil Products Blocks Cofactor Activity - a Potential Rapid Mechanism for Modulation of Coagulation.* Journal of Clinical Investigation, 1992. **90**(6): p. 2565-2573.

101. Gailani, D. and G.J. Broze, *Factor-Xi Activation in a Revised Model of Blood-Coagulation.* Science, 1991. **253**(5022): p. 909-912.

102. Lammle, B., et al., *Thromboembolism and Bleeding Tendency in Congenital Factor-Xii Deficiency - a Study on 74 Subjects from 14 Swiss Families.* Thrombosis and Haemostasis, 1991. **65**(2): p. 117-121.

103. Girolami, A., et al., *The Occasional Venous Thromboses Seen in Patients with Severe (Homozygous) Fxii Deficiency Are Probably Due to Associated Risk Factors: A Study of Prevalence in 21 Patients and Review of the Literature.* Journal of Thrombosis and Thrombolysis, 2004. **17**(2): p. 139-143.

104. Jones, D.W., et al., *Reduced Factor XII Levels in Patients with the Antiphospholipid Syndrome Are Associated with Antibodies to Factor XII.* British Journal of Haematology, 2000. **110**(3): p. 721-726.

105. Koster, T., et al., *Hageman,John Factor and Deep-Vein Thrombosis - Leiden Thrombophilia Study.* British Journal of Haematology, 1994. **87**(2): p. 422-424.

106. Naito, K. and K. Fujikawa, *Activation of Human Blood-Coagulation Factor-Xi Independent of Factor-Xii - Factor-Xi Is Activated by Thrombin and Factor-Xia in the Presence of Negatively Charged Surfaces.* Journal of Biological Chemistry, 1991. **266**(12): p. 7353-7358.

107. Colman, R.W., *Biologic Activities of the Contact Factors in Vivo - Potentiation of Hypotension, Inflammation, and Fibrinolysis, and Inhibition of Cell Adhesion, Angiogenesis and Thrombosis.* Thrombosis and Haemostasis, 1999. **82**(6): p. 1568-1577.

108. Ragni, M.V., et al., *Comparison of Bleeding Tendency, Factor-Xi Coagulant Activity, and Factor-Xi Antigen in 25 Factor-Xi-Deficient Kindreds.* Blood, 1985. **65**(3): p. 719-724.

109. Meijers, J.C.M., et al., *High Levels of Coagulation Factor XI as a Risk Factor for Venous Thrombosis.* New England Journal of Medicine, 2000. **342**(10): p. 696-701.

110. Yang, D.T., et al., *Elevated Factor XI Activity Levels Are Associated with an Increased Odds Ratio for Cerebrovascular Events.* American Journal of Clinical Pathology, 2006. **126**(3): p. 411-415.

111. Berliner, J.I., et al., *Elevated Levels of Factor XI Are Associated with Cardiovascular Disease in Women.* Thrombosis Research, 2002. **107**(1-2): p. 55-60.

112. Gruber, A. and S.R. Hanson, *Factor XI-Dependence of Surface- and Tissue Factor-Initiated Thrombus Propagation in Primates.* Blood, 2003. **102**(3): p. 953-955.

113. Espana, F., et al., *Invivo and Invitro Complexes of Activated Protein-C with 2 Inhibitors in Baboons.* Blood, 1991. **77**(8): p. 1754-1760.

114. Scully, M.F., et al., *Activation of Protein-C and Its Distribution between Its Inhibitors, Protein-C Inhibitor, Alpha(1)-Antitrypsin and Alpha(2)-Macroglobulin, in Patients with Disseminated Intravascular Coagulation.* Thrombosis and Haemostasis, 1993. **69**(5): p. 448-453.

115. Liu, L.B., et al., *Inhibition of Thrombin by Antithrombin-Iii and Heparin-Cofactor-Ii in-Vivo.* Thrombosis and Haemostasis, 1995. **73**(3): p. 405-412.

116. Fay, P.J., J.V. Coumans, and F.J. Walker, *Vonwillebrand-Factor Mediates Protection of Factor-Viii from Activated Protein-C-Catalyzed Inactivation.* Journal of Biological Chemistry, 1991. **266**(4): p. 2172-2177.

117. StearnsKurosawa, D.J., et al., *The Endothelial Cell Protein C Receptor Augments Protein C Activation by the Thrombin-Thrombomodulin Complex.* Proceedings of the National Academy of Sciences of the United States of America, 1996. **93**(19): p. 10212-10216.

118. Walker, F.J., *Regulation of Activated Protein-C by Protein-S - the Role of Phospholipid in Factor-Va Inactivation.* Journal of Biological Chemistry, 1981. **256**(21): p. 1128-1131.

119. Dahlback, B. and B.O. Villoutreix, *Regulation of Blood Coagulation by the Protein C Anticoagulant Pathway - Novel Insights into Structure-Function Relationships and Molecular Recognition.* Arteriosclerosis Thrombosis and Vascular Biology, 2005. **25**(7): p. 1311-1320.

120. Rosing, J., et al., *Low-Dose Oral Contraceptives and Acquired Resistance to Activated Protein C: A Randomised Cross-over Study.* Lancet, 1999. **354**(9195): p. 2036-2040.

121. Sandset, P.M., *Tissue Factor Pathway Inhibitor (Tfpi) - an Update.* Haemostasis, 1996. **26**: p. 154-165.

122. Ameri, A., et al., *Expression of Tissue Factor Pathway Inhibitor by Cultured Endothelial-Cells in Response to Inflammatory Mediators.* Blood, 1992. **79**(12): p. 3219-3226.

123. Abildgaard, U., *Heparin Low-Molecular-Weight Heparin and Tissue Factor Pathway Inhibitor.* Haemostasis, 1993. **23**: p. 103-106.

124. Sandset, P.M., U. Abildgaard, and M.L. Larsen, *Heparin Induces Release of Extrinsic Coagulation Pathway Inhibitor (Epi).* Thrombosis Research, 1988. **50**(6): p. 803-813.

125. Lupu, C., et al., *Thrombin Induces the Redistribution and Acute Release of Tissue Factor Pathway Inhibitor from Specific Granules within Human Endothelial-Cells in Culture.* Arteriosclerosis Thrombosis and Vascular Biology, 1995. **15**(11): p. 2055-2062.
126. Anand, M., K. Rajagopal, and K.R. Rajagopal, *A Viscoelastic Fluid Model for Describing the Mechanics of a Coarse Ligated Plasma Clot.* Theoretical and Computational Fluid Dynamics, 2006. **20**(4): p. 239-250.
127. Anand, M., K. Rajagopal, and K.R. Rajagopal, *A Model for the Formation, Growth, and Lysis of Clots in Quiescent Plasma. A Comparison between the Effects of Antithrombin III Deficiency and Protein C Deficiency.* Journal of Theoretical Biology, 2008. **253**(4): p. 725-738.
128. Fogelson, A.L. and R.D. Guy, *Platelet-Wall Interactions in Continuum Models of Platelet Thrombosis: Formulation and Numerical Solution.* Mathematical Medicine and Biology-a Journal of the Ima, 2004. **21**(4): p. 293-334.
129. Filipovic, N., M. Kojic, and A. Tsuda, *Modelling Thrombosis Using Dissipative Particle Dynamics Method.* Philosophical Transactions of the Royal Society a-Mathematical Physical and Engineering Sciences, 2008. **366**(1879): p. 3265-3279.

CHAPTER 4

**SIMULATED THROMBIN GENERATION PROFILES AS A PREDICTOR OF
THROMBOTIC RISK AMONG PRE-MENOPAUSAL WOMEN**

Abstract

A large number of individuals are at risk for deep venous thrombosis (DVT) due
to alterations in multiple coagulation factors and inhibitors secondary to malignancy,
drug interactions, or other general medical conditions. We have utilized a computational
model of blood coagulation, which addresses the interplay between biochemical factors,
blood flow, and physiologic surface initiation of coagulation, to calculate an
individualized, systems-based metric of clotting potential, FSTG, for 210 pre-
menopausal women in the Leiden Thrombophilia Study (LETS). Both DVT and oral
contraceptive (OC) use were associated with higher values of FSTG. We demonstrated
a 166% increased risk of DVT for each standard deviation increase in $FSTG_{venous}$ above
the mean that remained highly predictive after adjustment for age and OC status
(adjusted OR 2.66; 95% CI 1.69-4.19; P<0.0001).

4.1.   Introduction

As early as the 19th century, certain clinical settings have been associated with
increased risk of thrombosis. These acquired thrombophilias include both rare and
common conditions such as cancer, hormone therapy, nephrotic syndrome,
antiphospholipid syndrome, and hyperhomocysteinemia. Over one hundred million
women worldwide are prescribed exogenous hormones as oral contraceptives or for
postmenopausal hormone replacement. Oral contraceptive use is associated with a 2 to
6-fold increased risk of venous thrombosis, 6-fold increased risk of cerebral vein
thrombosis [1], 5-fold increased risk of myocardial infarction, and 3-fold increased risk of

ischemic stroke [2]. The risk is particular high during the first year of use and among women with underlying coagulation abnormalities or a history of venous thromboembolic event (VTE) [3]. Several population-based studies have reported elevations in plasma levels of factors II, VII, VIII, X, and fibrinogen, lower plasma levels of factor V, ATIII, protein S, and circulating thrombomodulin, and decreased activated partial thromboplastin time (aPTT) [4-7]. Additionally, acquired APC resistance comparable to that found in heterozygous factor V Leiden has been observed in women prescribed third-generation oral contraceptives [8, 9].

Presently, thrombophilia screening is generally limited to inheritable conditions, such as protein C/S deficiencies, antithrombin III deficiency, factor V Leiden polymorphism (G1691A), or activated protein C resistance, prothrombin G20210A, or hyperprothrombinemia, and dysfibrinogenemia [10]. Additional assays include antiphosholipid antibody, lupus anticoagulant, and anticardiolipin antibody tests. While these tests are available, prohibitive costs limit their utility for widespread population screening. Thus, current guidelines by the College of American Pathologists (CAP) and the American College of Medical Genetics (ACMG) recommend that these tests be reserved for those patients who present with a venous thromboembolic event (VTE) and a high suspicion of hereditary thrombophilia, characterized by initial presentation <50 years of age, recurrent thromboembolic events, unusual site of thrombosis, such as mesenteric vein and upper extremities, or a strong family history of thrombosis [11, 12]. Additionally, testing is recommended for patients with pregnancy or OC-associated VTE. Screening is not currently performed on asymptomatic patients to assess the risk of having developed an acquired hypercoagulable state, even among high risk subgroups, such as those on oral contraceptives.

Several population-based studies, including the Leiden Thrombophilia Study (LETS), have compiled considerable data regarding thrombotic risk associated with

increases in individual plasma coagulation factor levels. Specifically, factors II, VIII, and IX had adjusted odds ratios calculated using a 90th percentile cutpoint of 2.1, 4.8, and 2.5, respectively, for first-time deep venous thrombosis (DVT) [13-15]. However, there are conflicting studies regarding the association of elevations in these factors with risk of recurrent DVT [16-18]. Notably, increased levels of factors V, VII, and X were not independently associated with venous thrombosis [19-21]. It is generally accepted that changes in individual coagulation factors are not sufficiently predictive for assessing risk in a clinical setting due to the highly dynamic and complex nature of blood coagulation, which includes numerous positive and negative feedback mechanisms [22]. It is clear that a systems-based approach, which does not rely on any one intermediary of coagulation, but rather, considers initiation, amplification, and regulation of thrombin generation as an integrative network, is required to adequately assess hemostatic status. In this study, we utilized a finite element model of surface-induced blood coagulation under flow to simulate thrombin generation based on patient coagulation factor profiles obtained from the Leiden Thrombophilia Study (LETS) and evaluated the association between simulated thrombin levels and risk of deep venous thrombosis among oral contraceptive users.

4.2.   Methods

4.2.1. Study populations

The Leiden Thrombophilia Study (LETS) [13-15] is a case-control study from the Netherlands with enrollment between 1988 and 1992 comparing participants with a first-time, objectively diagnosed DVT to sex and age-matched controls (N=474 per study arm). Original exclusion criteria included known malignancies and age greater than 70 years. Blood samples were drawn between 6 and 56 months from the date of thrombosis. We analyzed pre-menopausal females whose OC status was known and

unchanged at the time of thrombosis and blood draw. Additionally, participants on oral

anticoagulants were excluded. Our study groups were composed of 80 case individuals

and 130 control individuals. Coagulation factor levels were reported as percentages and

were converted to molar concentrations by multiplying by published physiologic values

(Table 4.1) [22-24].

Table 4.1. Reference plasma concentrations

Coagulation factor	Plasma level (nM)	Ref.
Factor II	1400	[22]
Factor V	20	[22]
Factor VII	10	[22]
Factor VIII	0.7	[22]
Factor IX	90	[22]
Factor X	170	[22]
Antithrombin III	2400	[23]
Protein C	60	[22]
Protein S	300	[22]
TFPI	2.5	[24]

4.2.2. Numerical model of thrombin generation

A finite element model has been formulated that describes thrombin generation

under defined flow conditions, initiated and modulated by spatially discrete regions of

surface-bound tissue factor and thrombomodulin, respectively (Figure 4.1). The model

incorporates fluid phase and surface-localized reactions of the extrinsic, intrinsic, and

common pathways, as well as three major inhibitory pathways. The spatially

heterogeneous model describes coagulation events that occur following tissue factor

exposure at a discrete site and incorporates mechanisms that regulate thrombin

generation, including those mediated by an intact endothelium, represented as a

thrombomodulin containing surface. Specifically, we assume that the coagulation

cascade is initiated by binding of factor VIIa to tissue factor, leading to the formation of extrinsic tenase. Activation of factor X leads to activation of factors V and VII. The resultant surface-associated complex, Xa/Va, or prothrombinase, cleaves prothrombin to thrombin, which serves as a positive feedback loop by activating factors V and VIII. Generation of activated factor VIIIa, in association with IXa, affords intrinsic tenase, or IXa/VIIIa. We assume that factor IXa is generated solely by TF/VIIa without participation of intrinsic pathway factors XI and XII. Inhibitory reactions include the inactivation of factors IXa, Xa, and thrombin, by antithrombin III. Additionally, inhibition of TF/VIIa by tissue factor pathway inhibitor (TFPI) is incorporated into the model as a two-step process, whereby TFPI binds factor Xa, followed by its reversible association with TF/VIIa. The protein C pathway serves as an additional negative feedback loop. Binding of thrombin to thrombomodulin leads to formation of activated protein C, which inactivates factors Va and VIIIa. Protein S directly modulates the kinetic efficiency of the latter inactivation reactions, but its interactions as a cofactor are not explicitly described.

The reaction area of interest is modeled as a two-dimensional flow field with upper and lower inert and reactive surfaces, respectively. Steady, one-dimensional, parabolic flow is assumed. Convective-diffusive transport is described by the conservation equation. All fluid-phase zymogen and enzyme concentrations are initially set to zero. The surface density of tissue factor and thrombomodulin remain constant, and at the outset both are free of bound cofactors. Convective flux transports 16 fluid phase species into the flow field at constant inlet concentrations derived from mean physiologic values, unless otherwise specified. Diffusion transports coagulation factors to the lower reactive surface, where reaction kinetics define flux boundary conditions. The reactive boundary is divided into localized upstream TF and downstream TM regions. The primary analysis was performed assuming a 10 mm entrance region, 2 mm TF region, and a 34 mm TM region. The length of the TF region is similar in dimension

to that of a ruptured coronary plaque or vascular graft anastomosis [25]. Simulations were performed on a high performance computing (HPC) cluster (School of Chemical and Biomolecular Engineering, Georgia Institute of Technology, Atlanta, GA). All assumptions and implementation details along with basic validation of the model have been described elsewhere [26].

An integrative parameter, flow simulated thrombin generation (FSTG), is derived from a consideration of the total thrombin generated beyond the site of TF expression at y=0 during the course of a 60-min flow period. One-hour was chosen as the default simulation time to ensure that all phases of coagulation, *e.g.* initiation and propagation, were included in the analysis for all runs. In other words, the simulation time exceeded the time course of the least thrombogenic simulation conditions. FSTG represents the average thrombin concentration over the surface of interest during the course of the simulation and acts as a global variable incorporating both spatial and temporal information. As described elsewhere, FSTG is a bimodal variable with values greater than 10 nM considered to exceed an activation threshold for a prothrombotic response. A value below 10 nM, notably the minimum thrombin concentration reported to induce platelet activation,[27] was categorized as lying either below an activation-threshold.

In order to obtain the greatest sensitivity for evaluating the effects of perturbations in hemostatic concentration profiles, conditions of the vessel wall, which normally result in FSTG concentrations just below the activation threshold (FSTG < 10nM) under venous (75 s^{-1}) and arterial flow conditions (500 s^{-1}) were utilized for all simulations. These sub-threshold settings represent a 'pivot point' between a dampened thrombin response and full activation of the coagulation cascade and have been previously determined and include a tissue factor bearing injury zone that is 2 mm in length in which the density of TF is 0.07 and 0.8 fmol/cm^2 for venous and arterial conditions, respectively, and a downstream region presenting surface bound

thrombomodulin at a concentration of 1000 fmol/cm^2. While a different choice of parameters would result in quantitatively different thrombin responses, the comparative effects would be similar.

4.2.3. Statistical analysis

Female study participants whose OC status was known at the time of phlebotomy (N=210) were analyzed. Descriptive statistics are reported as mean ± standard deviation for continuous variables and number (%) for categorical variables. Group-wise comparisons were performed using T-tests or nonparametric methods for continuous variables (based on data distributions) and X^2 tests for categorical variables.

FSTG was assessed as a continuous covariate in patients exceeding the 10 nM threshold for thrombin generation. Associations between venous (FSTG$_{venous}$) and arterial (FSTG$_{arterial}$) FSTG, coagulation factor levels, and DVT were evaluated using univariate and multivariable logistic regression.   Multivariable modeling was performed using stepwise selection with P≤0.10 required for model entry and P≤0.05 required for covariate retention in the final model.DVT models based on coagulation factors and/or FSTG as covariates were adjusted post-hoc for participant age and oral contraceptive use. For continuous covariates, odds ratios (OR) are expressed per standard deviation change. Significance was assessed at an α level of 0.05 and all statistical analyses were performed using SAS version 9.2 (SAS Institute, Cary, NC).
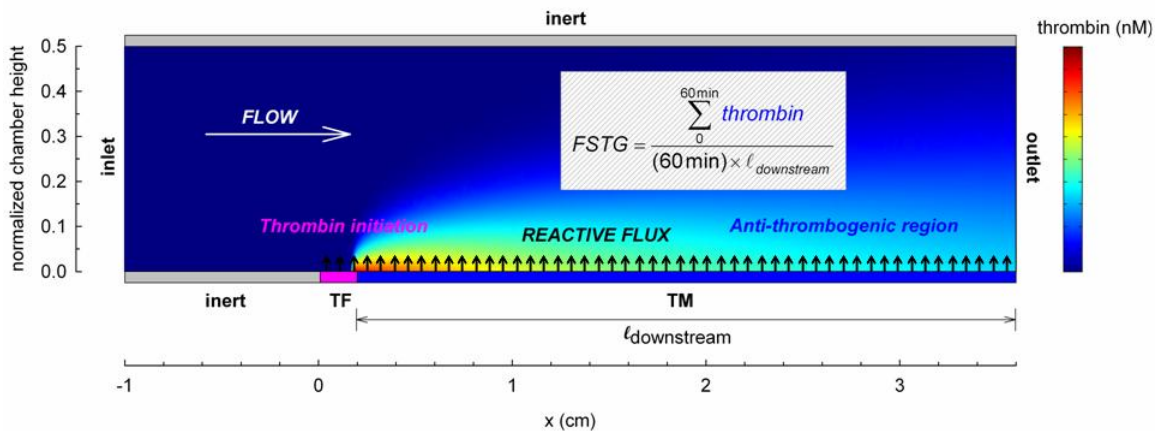
Figure 4.1. Formulation of a spatially heterogeneous model of surface-induced thrombin generation in a flow field. Blood flow carries proteins into the flow field at constant inlet concentrations. Diffusion transports coagulation factors to the lower reactive surface, where reaction kinetics define flux boundary conditions. Convective flux removes soluble species at the outlet. The upper boundary is inert. Geometric conditions include a 10 mm inert entrance region (gray), 2 mm thrombin-initiating TF region (pink), and a 34 mm anti-thrombogenic TM region (blue). Flow simulated thrombin generation (FSTG) is defined as the integral of the downstream thrombin surface concentration over the 60-min simulation time, normalized by time and length.

4.3. Results

4.3.1. Descriptive statistics

Among pre-menopausal female participants in LETS (N=210), approximately 75% of the total population exceeded the 10 nM FSTG activation threshold (N=159 and N=152 for venous and arterial FSTG, respectively), with similar rates observed between control and DVT populations (Table 4.2). OC use had no effect on threshold rates within the DVT group, but increased the proportion of participants that exceeded the activation threshold within the control group.

Table 4.2a. Number of participants with $FSTG_{venous}$ > 10 nM

Group	DVT	
	No	**Yes**
All participants	98/130 (75.3)	61/80 (76.3)
Non-OC users	53/80 (66.3)	38/50 (76.0)
OC users	45/50 (90.0)	23/30 (76.7)

Data is displayed as N/N_{total} (%).

Table 4.2b. Number of participants with $FSTG_{arterial}$ > 10 nM

Group	DVT	
	No	**Yes**
All participants	93/130 (71.5)	59/80 (73.8)
Non-OC users	49/80 (61.3)	35/50 (70.0)
OC users	44/50 (88.0)	24/30 (80.0)

Data is displayed as N/N_{total} (%).

Mean participant age was 38.2 ± 9.4 years. Mean venous and arterial FSTG were 435.0 ± 221.2 and 656.3 ± 307.5 nM, respectively. Descriptive statistics stratified by DVT status are shown in Table 4.3. Higher concentrations of factors VII, VIII, IX, and X, and protein S were observed in the DVT population. No difference was noted for the remaining plasma concentrations. Stratified analysis based on DVT status revealed higher mean venous and arterial FSTG in the DVT group ($FSTG_{venous}$ 535.8 nM versus 372.3 nM, P<0.0001; $FSTG_{arterial}$ 789.8 nM versus 571.5 nM, P<0.0001) (Figure 4.2). Stratified analysis based on OC use revealed higher venous and arterial mean FSTG in OC users ($FSTG_{venous}$ 514.5 nM versus 375.6 nM, P<0.0001; $FSTG_{arterial}$ 754.4 nM versus 576.8 nM, P=0.0003) (Figure 4.3). Patients using OC were also younger (mean age 32.5 ± 10.1 versus 41.8 ± 6.9 years; P<0.0001).

Table 4.3. Descriptive statistics for the entire study population[*]

Variable	DVT	
	No	Yes
Age (years)	38.3 ± 9.2	38.0 ± 9.7
OCP use	50 (38.5)	30 (37.5)
Factor II (%)	103.8 ± 15.2	109.2 ± 17.9
Factor V (%)	119.6 ± 28.7	122.9 ± 32.2
Factor VII (%)	110.0 ± 22.3	109.3 ± 17.9
Factor VIII (%)	119.8 ± 31.4	135.4 ± 34.2
Factor IX (%)	102.4 ± 22.6	113.6 ± 30.2
Factor X (%)	104.8 ± 21.1	114.0 ± 23.0
Antithrombin III (%)	98.6 ± 10.5	97.2 ± 12.0
Protein C (%)	101.5 ± 16.5	107.1 ± 24.2
Protein S (%)	91.8 ± 18.5	99.0 ± 19.6
TFPI (ng/mL)	59.1 ± 13.9	59.7 ± 12.0
Venous FSTG (nM)	372 ± 196	536 ± 224
Arterial FSTG (nM)	572 ± 285	790 ± 296

[*]Data are displayed as mean ± standard deviation for continuous variables and N (%) for categorical variables. Factor concentrations are reported as % of normal.

4.3.2. Associations between FSTG and thrombosis

DVT occurred in 80 participants (38.1%). Univariate models of DVT are shown in Table 4.4. Venous and arterial FSTG demonstrated highly significant univariate associations with DVT [OR 2.26, 95% CI (1.56-3.30) for $FSTG_{venous}$; OR 2.23, 95% CI (1.51-3.30) for $FSTG_{arterial}$]. Adjusted ORs incorporating participant age and OC use were generally comparable to those observed with univariate analyses (Table 4.5). Multivariable associations with DVT were observed for $FSTG_{venous}$ (OR 2.46; 95%CI (1.60-3.77); P<0.0001) and protein S (OR 1.48; 95% CI (1.03-2.14); P=0.0332) (Table 4.6). After adjusting the selected multivariable model for participant age and OC use, the association between DVT and $FSTG_{venous}$ remained highly significant (OR 2.66; 95% CI 1.69-4.19; P<0.0001), but the adjusted OR for protein S was no longer significant (OR1.24; 95% CI (0.80-1.91; P=0.3318).

Table 4.4. Univariate models with DVT as outcome

Variable	OR[*] (95% CI)	P
Venous FSTG	2.26 (1.56-3.30)	<0.0001
Arterial FSTG	2.23 (1.51-3.30)	<0.0001
Factor II	1.40 (1.05-1.87)	0.0227
Factor V	1.12 (0.85-1.45)	0.4381
Factor VII	1.39 (1.04-1.85)	0.0251
Factor VIII	6.37 (2.07-19.62)	0.0013
Factor IX	1.54 (1.15-2.05)	0.0032
Factor X	1.53 (1.14-2.05)	0.0043
ATIII	0.88 (0.66-1.16)	0.3597
Protein C	1.33 (0.99-1.76)	0.0510
Protein S	1.46 (1.10-1.95)	0.0097
TFPI	1.05 (0.80-1.38)	0.7409

[*]Odds ratios for expressed per standard deviation change.

Table 4.5. Single factor models adjusted for participant age and OC use

Variable	OR[*] (95% CI)	P
Venous FSTG	2.81 (1.81-4.36)	<0.0001
Arterial FSTG	2.56 (1.66-3.93)	<0.0001
Factor II	1.42 (1.06-1.90)	0.0187
Factor V	1.14 (0.85-1.53)	0.3725
Factor VII	1.46 (1.08-1.98)	0.0150
Factor VIII	7.48 (2.33-24.40)	0.0007
Factor IX	1.71 (1.24-2.34)	0.0009
Factor X	1.70 (1.23-2.35)	0.0015
ATIII	0.86 (0.64-1.15)	0.3054
Protein C	1.38 (1.02-1.86)	0.0348
Protein S	1.62 (1.17-2.24)	0.0040
TFPI	1.05 (0.77-1.44)	0.7497

[*]Odds ratios expressed per standard deviation change

Table 4.6. Multivariable models with DVT as outcome

Variable	Unadjusted		Adjusted[*]	
	OR(95% CI)	P	OR(95% CI)	P
Venous FSTG	2.46 (1.60-3.77)	<0.0001	2.66 (1.69-4.19)	<0.0001
Protein S	1.48 (1.03-2.14)	0.0332	1.24 (0.80-1.91)	0.3318

[*]Adjusted for participant age and oral contraceptive use at time of phlebotomy

Figure 4.2. Venous and arterial FSTG distribution stratified by DVT status. Box plots represent median, 10th, 25th, 75th, and 90th percentiles. Open circles denote 5th and 95th percentiles. Dashed lines indicate the mean. Asterisks indicate statistical significance. Flow simulated thrombin generation (FSTG) simulated over a 60-min flow period at shear rates of (**A**) 75 s^{-1} and (**B**) 500 s^{-1}.

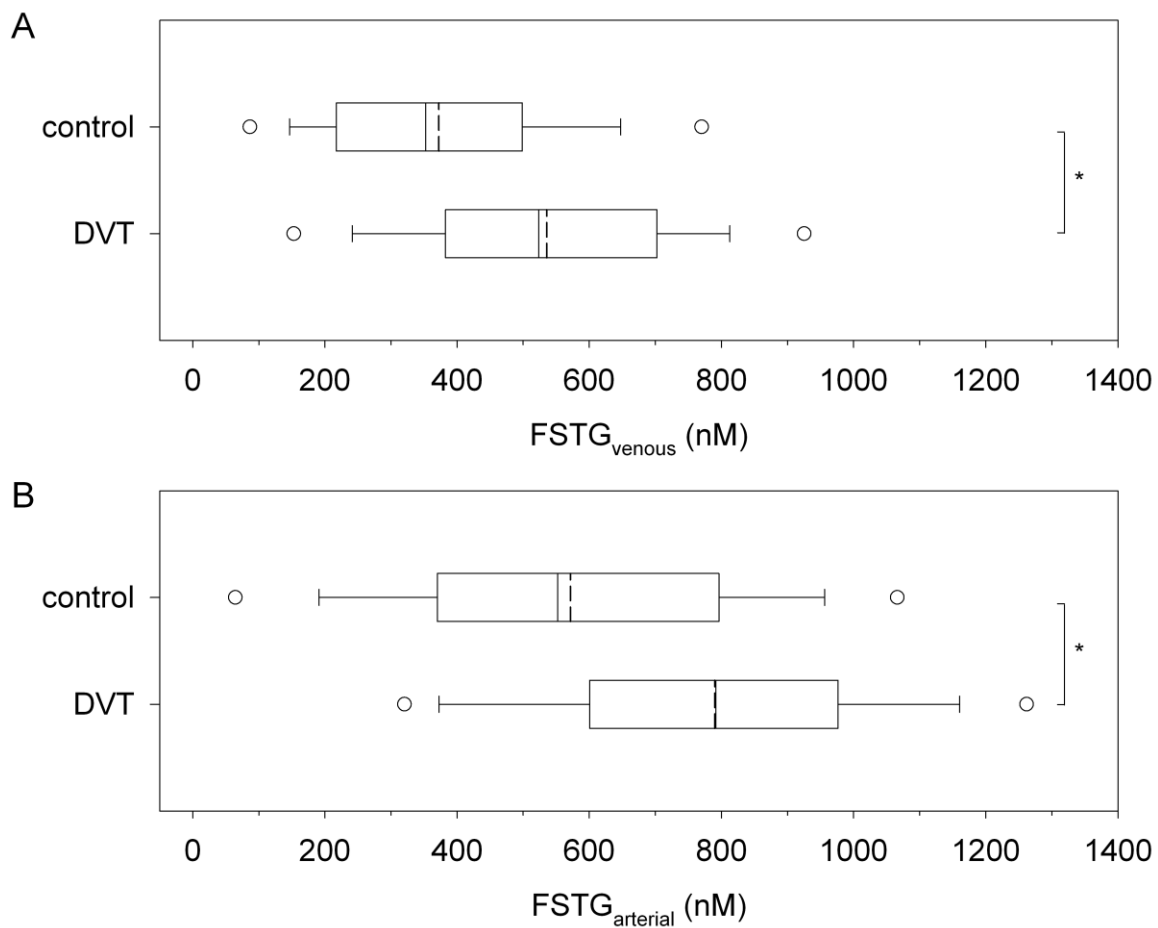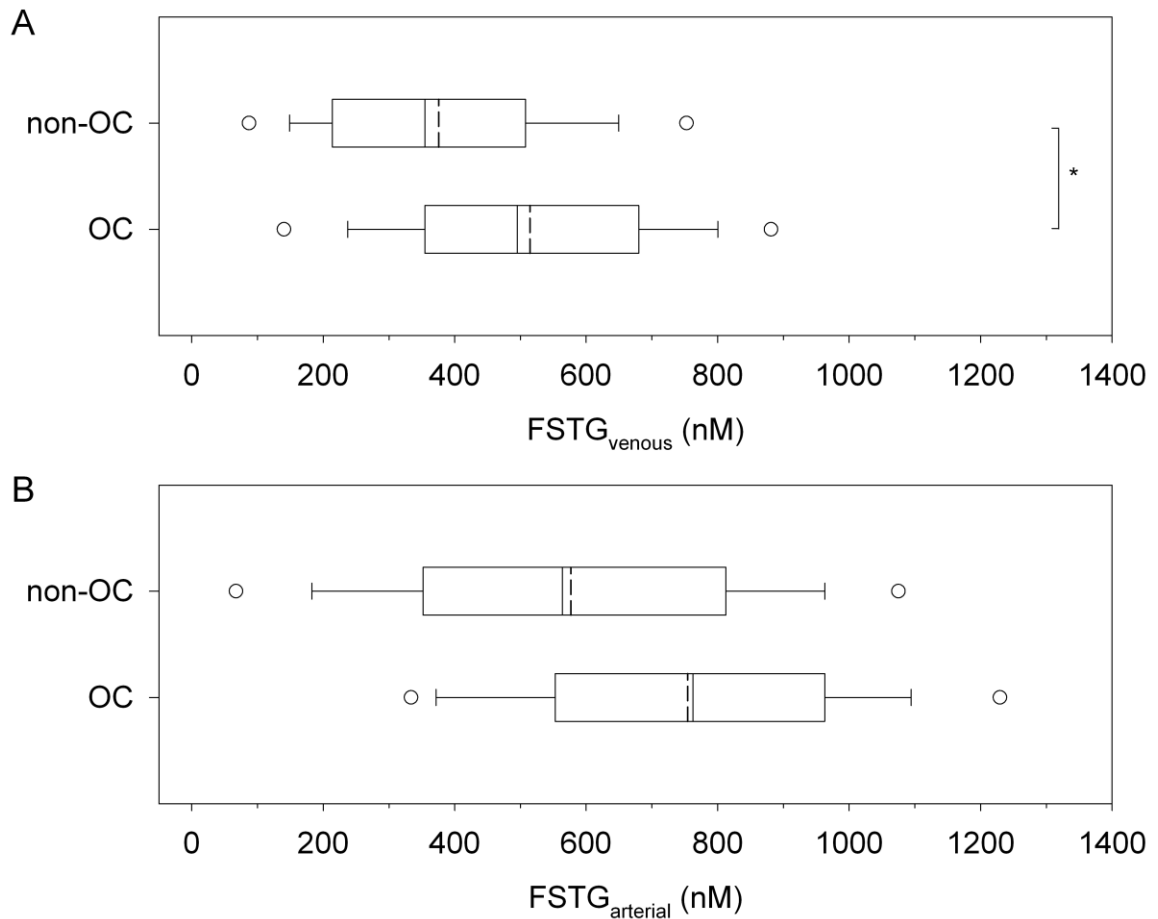**Figure 4.3. Venous and arterial FSTG distribution stratified by OC use.** Box plots represent median, 10th, 25th, 75th, and 90th percentiles. Open circles denote 5th and 95th percentiles. Dashed lines indicate the mean. Asterisks indicate statistical significance. Flow simulated thrombin generation (FSTG) simulated over a 60-min flow period at shear rates of (A) 75 s^{-1} and (B) 500 s^{-1}.

4.4. Discussion

4.4.1. Patient screening and clinical assessment

Given the large population at risk for thrombophilia, whether genetic or acquired and the complexities of integrating multiple risk factors, *e.g.* a FV Leiden carrier wishing to take oral contraceptives, there exists a need for a diagnostic screening tool to assess an individual's hemostatic state. Due to low absolute risk, the cost-effectiveness of universal screening has been disparaged, particularly for those who have been prescribed oral contraceptives [28, 29]. However, selective thrombophilia screening and subsequent optimization of prophylactic treatment is likely to improve overall clinical outcomes [28, 30]. The primary methods of hemostatic assessment remains 'prothrombin time' (PT) and 'activated partial thromboplastin time' (aPTT), both initially described over a half century ago. Prothrombin time is a measure of the integrity of the extrinsic and common pathways and is defined as the time required for citrated plasma to clot following the addition of tissue factor and calcium. Activated partial thromboplastin time, also measured using recalcified citrated plasma, is not dependent on tissue factor and therefore is a reflection of the integrity of the intrinsic pathway of coagulation. APTT is particularly useful for identifying hemophilias and monitoring anticoagulant therapy [31]. Importantly, these assays are relatively insensitive to thrombotic risk. A more global approach, the thrombin generation assay (TGA) uses a fluorogenic-based method to measure thrombin concentration over time in platelet-poor plasma, platelet-rich plasma, or whole blood. In 1993, Hemker *et al.* [32] defined the term 'endogenous thrombin potential' (ETP) as the area under the curve of the thrombin generation curve, or 'thrombogram', and proposed the ETP as a sensitive marker of the capacity of plasma to form thrombin in response to a stimulus. A number of studies have been performed to evaluate the predictive value of ETP with respect to hyper- and hypocoagulable states and hemostatic risk, recently reviewed by Van veen *et al.* [33].

However, there remains significant inter-laboratory variability, and standardization of techniques along with large prospective clinical trials are required before thrombin generation testing will be useful for routine clinical practice.

Computational methods, in conjunction with individual coagulation protein profiles, have the potential to be high throughput screening tools given recent advances in both biochemical assays and computer processing. Brummel-Ziedins *et al.* [34] input coagulation factor data from the control population of LETS into a 27-equation computational model [35] and examined the variation in simulated thrombin generation curves stratified by risk group, such as sex, increased body mass index (BMI > 26 kg/m^2), and use of oral contraceptives. Input parameters included factors II, V, VII, VIII, IX, X, and the inhibitors ATIII and TFPI. Output parameters included time to 10 nM of thrombin, time to maximum thrombin, maximum rate of thrombin generation (MaxR), maximum level of thrombin generation (MaxL), and total thrombin generated. Together these parameters described the initiation, propagation, and termination phases of thrombin generation triggered by a fixed quantity of TF in solution. Interestingly, their study identified subpopulations, termed 'fast- and slow-thrombin generators', which the authors proposed represented categories of risk. OC use was associated with increases in thrombin-related parameters in both control and DVT populations. The reported OR using the 90th percentile cutpoint for their greatest risk-associated parameter, MaxR, and OC use was 2.9 (95% CI 1.1-7.7). Brummel-Ziedens *et al.* proposed the combination of an individual's plasma coagulation profile with a computational tool for evaluation of thrombotic risk, as well as assessment of global hemostatic changes following the initiation of oral contraceptives. However, their numerical model was limited in its treatment of the protein C pathway and more critically, the absence of a well defined flow regime.

4.4.2. Assumptions and limitations

Given the known association of OC use with thrombosis, we chose to focus on a cohort of pre-menopausal females with known and consistent OC status at the time of thrombosis and blood draw. This subset of the original LETS case-control data set, matched by age and sex, may not be fully representative of the entire population. However, $FSTG_{venous}$ remained highly associated with DVT when adjusted for demographic variables such as age and OC use, while other coagulation variables did not. Prospective studies of $FSTG_{venous}$ adjusting for other known risk factors of DVT including smoking, obesity, and race are warranted and are necessary to determine a clinically relevant cutpoint for $FSTG_{venous}$.

Only those participants whose coagulation profiles yielded thrombin responses above an activation threshold (FSTG > 10) were included in the calculation of OR. Interestingly, similar rates of sub-threshold thrombin activation (~25%) were observed in control and DVT populations. These individuals were predicted to have the lowest coagulable risk based on plasma factor levels alone. While further refinements in the computational model, as previously noted, may improve its sensitivity to detect thrombotic risk, several mechanisms of thrombosis are not accounted for solely by measurable plasma factors of the coagulation cascade, including platelet activation, the fibrinolytic pathway, conditions that affect the surface expression of tissue factor or thrombomodulin, and local anatomic factors that predispose towards stasis. Drawing from Virchow's triad, *i.e.* stasis, endothelial injury, and hypercoagulability, the presented model directly addresses the latter, but in contrast to other existing assays and models, our approach is also deeply rooted in the former two mechanisms through its incorporation of flow effects and surface TF and TM expression.

It bears emphasis that the reaction pathways and related kinetic parameters are largely well-defined for the coagulation cascade, and furthermore, that no parameter

fitting was performed for our model system to calculate FSTG. Kinetic parameters were obtained from the experimental literature of isolated reaction systems with preference given to studies deemed most relevant with respect to substrate and enzyme concentrations within the physiologic range, the presence of appropriate cofactors such as phospholipid surfaces and calcium, where applicable, and method of measurement. Given a different set of physiologically relevant parameters, the qualitative trends observed in our studies would have remained the same, and thus the model would still be useful for the comparison of altered hemostatic parameters.

Furthermore, the simulations in this study assumed high levels of TM, previously shown to be within the transport-limited regime, and a fixed TF surface density which corresponded to thrombin generation just below the activation threshold for two flow conditions. Near threshold conditions represent the most sensitive cases for detecting patients at risk of thrombosis and may be set precisely in terms of both spatial dimensions, density of surface-bound TF, and flow conditions. Compared to well-mixed solution phase systems such as the thrombin generation assay, which operate well above the activation threshold, near threshold systems should be more sensitive in distinguishing between normal and susceptible population groups.

While the inclusion of surface-bound TF and TM renders the computational model more sensitive and more physiologically relevant, diagnostically, there are no direct measures of alterations in TF or TM surface expression. Circulating TF on the surface of monocytes and microparticles may be detected by flow cytometry, but their role in coagulation and the correlation to endothelial and subendothelial surface expression remain undefined at this time [36-39]. In contrast, soluble thrombomodulin has been established as a marker of early endothelial cell damage [40, 41]. Kunz *et al.* utilized monocyte expression of TM as an *in vivo* marker of endothelial cell expression in a familial study of TM deficiency. However, the ability to quantify the extent of reduced

TM expression in endothelial cells was limited by the relatively low levels of TM found on the surface of circulating monocytes [42]. As measurement methods continue to evolve, TF and TM concentrations could easily be incorporated into our existing computational model.

Protein S is a vitamin K-dependent plasma protein that acts as a necessary cofactor for the anticoagulant functions of activated protein C [43]. The cofactor activity of protein S was accounted for in the model through the choice of kinetic parameters for APC-mediated inactivation of factor Va and VIIIa, which were measured in the presence of thrombomodulin and physiologic concentrations of protein S [44]. Heterozygous protein S deficiency is associated with thrombotic risk similar to that caused by heterozygous protein C deficiency, and APC resistance caused by acquired protein S deficiency is thought to be a contributory factor in hypercoagulability associated with pregnancy and oral contraceptive use [8, 45]. Notably, in our subset population, protein S levels were actually greater in the DVT population than the control population. Future mechanistic inclusion of protein S or the incorporation of laboratory APC sensitivity measurements may be useful for the representation and study of pathologic states.

4.4.3. A systems-based method to predict thrombosis

Our univariate analysis recapitulated some of the findings previously published by the LETS group [13-15] regarding the association of elevations in certain prothrombotic factors with venous thrombosis. Adjusted for demographic variables, age and OC use, the systems-based variables, *i.e.* $FSTG_{venous}$ and $FSTG_{arterial}$, had the highest predictive value, followed by the individual factors VIII, IX, and X. When all candidate covariates were allowed to compete and adjusted for age and OC use, only $FSTG_{venous}$ remained significant. Notably, $FSTG_{venous}$ is a robust risk-associated variable

with little perturbation in the adjusted OR observed regardless of logistic model selection.

We have utilized a computational model of blood coagulation, which addresses the interplay between biochemical factors, blood flow, and physiologic surface initiation of coagulation, to calculate a systems-based metric of clotting potential, $FSTG_{venous}$. We demonstrated a 166% increased risk of DVT for each SD (221 nM) increase in $FSTG_{venous}$ above the mean (435 nM) for our study population. A large number of individuals are at risk for DVT due to alterations in multiple coagulation factors and inhibitors secondary to malignancy, drug interactions, or other general medical conditions. While no one plasma marker is sufficiently predictive of thrombotic risk, a systems-based screening approach is both logical and necessary to identify the small subgroup of patients at risk that may benefit from oral anticoagulants to improve both cost-effectiveness as well as individual patient safety and health.

4.5.   REFERENCES

1.   Dentali, F., M. Crowther, and W. Ageno, *Thrombophilic Abnormalities, Oral Contraceptives, and Risk of Cerebral Vein Thrombosis: A Meta-Analysis.* Blood, 2006. **107**(7): p. 2766-2773.
2.   Martinelli, I. *Risk Factors in Venous Thromboembolism.* in *XVIIIth Congress of the International-Society-on-Thrombosis-and-Haemostasis.* 2001. Paris, France: F K Schattauer Verlag Gmbh.
3.   Bloemenkamp, K.W.M., et al., *Higher Risk of Venous Thrombosis During Early Use of Oral Contraceptives in Women with Inherited Clotting Defects.* Archives of Internal Medicine, 2000. **160**(1): p. 49-52.
4.   Bloemenkamp, K.W.M., et al., *Venous Thrombosis, Oral Contraceptives and High Factor VIII Levels.* Thrombosis and Haemostasis, 1999. **82**(3): p. 1024-1027.
5.   Mackie, I.J., et al., *Protein S Levels Are Lower in Women Receiving Desogestrel-Containing Combined Oral Contraceptives (Cocs) Than in Women Receiving Levonorgestrel-Containing Cocs at Steady State and on Cross-Over.* British Journal of Haematology, 2001. **113**(4): p. 898-904.
6.   Quehenberger, P., et al., *Increased Levels of Activated Factor VII and Decreased Plasma Protein S Activity and Circulating Thrombomodulin During Use of Oral Contraceptives.* Thrombosis and Haemostasis, 1996. **76**(5): p. 729-734.
7.   Tans, G., et al., *A Randomized Cross-over Study on the Effects of Levonorgestrel- and Desogestrel-Containing Oral Contraceptives on the Anticoagulant Pathways.* Thrombosis and Haemostasis, 2000. **84**(1): p. 15-21.
8.   Rosing, J., et al., *Low-Dose Oral Contraceptives and Acquired Resistance to Activated Protein C: A Randomised Cross-over Study.* Lancet, 1999. **354**(9195): p. 2036-2040.
9.   Rosing, J., et al., *Oral Contraceptives and Venous Thrombosis: Different Sensitivities to Activated Protein C in Women Using Second- and Third-Generation Oral Contraceptives.* British Journal of Haematology, 1997. **97**(1): p. 233-238.
10.   Favaloro, E.J., D. McDonald, and G. Lippi, *Laboratory Investigation of Thrombophilia: The Good, the Bad, and the Ugly.* Semin Thromb Hemost, 2009. **35**(7): p. 695-710.
11.   Grody, W.W., et al., *American College of Medical Genetics Consensus Statement on Factor V Leiden Mutation Testing.* Genet Med, 2001. **3**(2): p. 139-48.
12.   Olson, J.D., *College of American Pathologists Consensus Conference Xxxvi: Diagnostic Issues in Thrombophilia - Introduction and General Considerations.* Archives of Pathology & Laboratory Medicine, 2002. **126**(11): p. 1277-1280.
13.   Poort, S.R., et al., *A Common Genetic Variation in the 3'-Untranslated Region of the Prothrombin Gene Is Associated with Elevated Plasma Prothrombin Levels and an Increase in Venous Thrombosis.* Blood, 1996. **88**(10): p. 3698-3703.
14.   Koster, T., et al., *Role of Clotting Factor-VIII in Effect of Von-Willebrand-Factor on Occurrence of Deep-Vein Thrombosis.* Lancet, 1995. **345**(8943): p. 152-155.
15.   Vlieg, A.V., et al., *High Levels of Factor IX Increase the Risk of Venous Thrombosis.* Blood, 2000. **95**(12): p. 3678-3682.
16.   Kyrle, P.A., et al., *High Plasma Levels of Factor VIII and the Risk of Recurrent Venous Thromboembolism.* New England Journal of Medicine, 2000. **343**(7): p. 457-462.
17.   Weltermann, A., et al., *The Risk of Recurrent Venous Thromboembolism among Patients with High Factor IX Levels.* Journal of Thrombosis and Haemostasis, 2003. **1**(1): p. 28-32.
18.   Christiansen, S.C., et al., *Thrombophilia, Clinical Factors, and Recurrent Venous Thrombotic Events.* Jama-Journal of the American Medical Association, 2005. **293**(19): p. 2352-2361.
19.   Kamphuisen, P.W., et al., *Factor V Antigen Levels and Venous Thrombosis - Risk Profile, Interaction with Factor V Leiden, and Relation with Factor VIII Antigen Levels.* Arteriosclerosis Thrombosis and Vascular Biology, 2000. **20**(5): p. 1382-1386.

20. Koster, T., et al., *Factor-VII and Fibrinogen Levels as Risk-Factors for Venous Thrombosis - a Case-Control Study of Plasma-Levels and DNA Polymorphisms - the Leiden Thrombophilia Study (Lets).* Thrombosis and Haemostasis, 1994. **71**(6): p. 719-722.

21. de Visser, M.C.H., et al., *Factor X Levels, Polymorphisms in the Promoter Region of Factor X, and the Risk of Venous Thrombosis.* Thrombosis and Haemostasis, 2001. **85**(6): p. 1011-1017.

22. Butenas, S., C. van't Veer, and K.G. Mann, *"Normal" Thrombin Generation.* Blood, 1999. **94**(7): p. 2169-2178.

23. Murano, G., et al., *Some Properties of Antithrombin-III and Its Concentration in Human Plasma.* Thromb Res, 1980. **18**(1-2): p. 259-62.

24. Novotny, W.F., et al., *Plasma Antigen Levels of the Lipoprotein-Associated Coagulation Inhibitor in Patient Samples.* Blood, 1991. **78**(2): p. 387-93.

25. Nakazawa, G., et al., *Delayed Arterial Healing and Increased Late Stent Thrombosis at Culprit Sites after Drug-Eluting Stent Placement for Acute Myocardial Infarction Patients - an Autopsy Study.* Circulation, 2008. **118**(11): p. 1138-1145.

26. Jordan, S.W. and E.L. Chaikof, *Simulated Surface-Induced Thrombin Generation in a Flow Field.* 201X.

27. Brummel, K.E., et al., *Thrombin Functions During Tissue Factor-Induced Blood Coagulation.* Blood, 2002. **100**(1): p. 148-152.

28. Martinelli, I., *Pros and Cons of Thrombophilia Testing: Pros.* Journal of Thrombosis and Haemostasis, 2003. **1**(3): p. 410-411.

29. Vandenbroucke, J.P., et al., *Factor V Leiden: Should We Screen Oral Contraceptive Users and Pregnant Women?* British Medical Journal, 1996. **313**(7065): p. 1127-1130.

30. Wu, O., et al., *Screening for Thrombophilia in High-Risk Situations: A Meta-Analysis and Cost-Effectiveness Analysis.* British Journal of Haematology, 2005. **131**(1): p. 80-90.

31. Kamal, A.H., A. Tefferi, and R.K. Pruthi, *How to Interpret and Pursue an Abnormal Prothrombin Time, Activated Partial Thromboplastin Time, and Bleeding Time in Adults.* Mayo Clin Proc, 2007. **82**(7): p. 864-73.

32. Hemker, H.C., et al., *Continuous Registration of Thrombin Generation in Plasma, Its Use for the Determination of the Thrombin Potential.* Thrombosis and Haemostasis, 1993. **70**(4): p. 617-624.

33. van Veen, J.J., A. Gatt, and M. Makris, *Thrombin Generation Testing in Routine Clinical Practice: Are We There Yet?* British Journal of Haematology, 2008. **142**(6): p. 889-903.

34. Brummel-Ziedins, K., et al., *The Plasma Hemostatic Proteome: Thrombin Generation in Healthy Individuals.* Journal of Thrombosis and Haemostasis, 2005. **3**(7): p. 1472-1481.

35. Hockin, M.F., et al., *A Model for the Stoichiometric Regulation of Blood Coagulation.* Journal of Biological Chemistry, 2002. **277**(21): p. 18322-18333.

36. Kushak, R.I., et al., *Detached Endothelial Cells and Microparticles as Sources of Tissue Factor Activity.* Thrombosis Research, 2005. **116**(5): p. 409-419.

37. Mallat, Z., et al., *Shed Membrane Microparticles with Procoagulant Potential in Human Atherosclerotic Plaques - a Role for Apoptosis in Plaque Thrombogenicity.* Circulation, 1999. **99**(3): p. 348-353.

38. Nieuwland, R., et al., *Cell-Derived Microparticles Generated in Patients During Cardiopulmonary Bypass Are Highly Procoagulant.* Circulation, 1997. **96**(10): p. 3534-3541.

39. Satta, N., et al., *Monocyte Vesiculation Is a Possible Mechanism for Dissemination of Membrane-Associated Procoagulant Activities and Adhesion Molecules after Stimulation by Lipopolysaccharide.* Journal of Immunology, 1994. **153**(7): p. 3245-3255.

40. Boehme, M.W.J., P. Galle, and W. Stremmel, *Kinetics of Thrombomodulin Release and Endothelial Cell Injury by Neutrophil-Derived Proteases and Oxygen Radicals.* Immunology, 2002. **107**(3): p. 340-349.

41. Ishii, H., H. Uchiyama, and M. Kazama, *Soluble Thrombomodulin Antigen in Conditioned Medium Is Increased by Damage of Endothelial-Cells.* Thrombosis and Haemostasis, 1991. **65**(5): p. 618-623.

42. Kunz, G., et al., *Identification and Characterization of a Thrombomodulin Gene Mutation Coding for an Elongated Protein with Reduced Expression in a Kindred with Myocardial Infarction.* Blood, 2000. **95**(2): p. 569-576.
43. Walker, F.J., *Regulation of Activated Protein-C by Protein-S - the Role of Phospholipid in Factor-Va Inactivation.* Journal of Biological Chemistry, 1981. **256**(21): p. 1128-1131.
44. Solymoss, S., M.M. Tucker, and P.B. Tracy, *Kinetics of Inactivation of Membrane-Bound Factor-Va by Activated Protein-C - Protein-S Modulates Factor-XA Protection.* Journal of Biological Chemistry, 1988. **263**(29): p. 14884-14890.
45. Dahlback, B. and B.O. Villoutreix, *Regulation of Blood Coagulation by the Protein C Anticoagulant Pathway - Novel Insights into Structure-Function Relationships and Molecular Recognition.* Arteriosclerosis Thrombosis and Vascular Biology, 2005. **25**(7): p. 1311-1320.

CHAPTER 5

DISCUSSION

5.1.   Summary of major findings

In Section I, we developed and characterized a mathematical model of coagulation, which integrates the effects of reaction kinetics, a simple, yet computationally expandable, flow regime, and uniquely, heterogeneous surface expression of TF and TM. The major findings of our studies include: (i) The FEM model simulated threshold effects with respect to the length of the TF site, TF and TM surface densities, and wall shear rate, and reproduced the classic time course characterized by initiation and amplification of thrombin generation. Furthermore, even without parameter fitting, our TF length and density thresholds were consistent with several experimental reports. (ii) Prothrombotic effects may extend significantly beyond the dimensions of the spatially discrete site of TF expression, a phenomenon that was quantified by the definition of an effective prothrombotic zone (EPZ). Notably, the EPZ quantifies the vital function of hemostasis to confine thrombus formation to an injury site in both axial and radial directions. (iii) In the setting of tandem TF-containing lesions, the relationship between the length of the EPZ and the interval distance between TF sites dictate the net response of the system. Additive prothrombotic effects of sub-clinical lesions and interestingly, suppressive antithrombotic effects of intervening TM-containing regions were observed.

In Section II, the computational model was applied to calculate an individualized, systems-based metric of clotting potential for 210 pre-menopausal women in the Leiden Thrombophilia Study (LETS). Flow-simulated thrombin generation (FSTG) was reflective of three key qualities of the thrombin response: 1) intensity of response, 2) relative onset of amplification, and 3) localization of the thrombin foci near to the

upstream injury area, and was found to be a highly predictive parameter for deep venous thrombosis risk. Diagnostic methods that utilize computational methods in conjunction with individualized biochemical profiles are both logical and necessary to identify the subgroup of patients at risk who may benefit from oral anticoagulants to improve cost-effectiveness as well as patient safety and health.

5.2. Future works

5.2.1. Model development

Next generations of model development should be aimed at addressing three areas: 1) addition of well-defined biochemical constituents previously omitted for computational simplicity, specifically factor XI and protein S, 2) exploration of complex flow fields and geometries, e.g., stenosis, pulsatile flow, and 3) modeling of transient TF surface presentation and additional surface-mediated pathways, e.g. heparin-like molecules.

The initial model described a steady, parabolic flow profile in a two-dimensional, rectangular flow field. Several complex flow fields may be considered subsequently, given the versatility of the FEM approach. In the context of atherosclerotic lesions, which represent sources of potential TF exposure and are often areas of stenosis, model geometry reflecting both single and tandem patterns of stenosis would be of immediate interest. It may be hypothesized that increased shear rate in stenotic regions would provide a protective effect; however, the decreased shear immediately downstream of the plaque may decrease the ability of unaffected vasculature to abrogate the thrombin load. Furthermore, the hemodynamic effects of tandem lesions and the measurement of fractional flow reserve (FFR) have generated recent interest [1, 2]. The interplay between these hemodynamic effects and the potential biochemical interactions reported in our studies, both additive and inhibitory, has direct clinical implications. Finally, other

complex flow patterns such as arterial pulsatile flow, or modeling of venous flow patterns under sequential compression device (SCD) prophylaxis, may be considered.

While our model includes regulation of thrombin formation by three physiologic biochemical pathways and blood flow, the model does not take into account physical inhibition of surface-bound TF by fibrin and platelet deposition. Proposed modeling approaches include thrombin-independent and –dependent TF mechanisms. For example, in a thrombin-independent system, TF surface concentration may be simply modeled by exponential or linear decay. In thrombin-dependent models, fibrin and platelet deposition might be assumed to be proportional to thrombin generation, and thus available TF might decrease with increasing thrombin.

5.2.2. Population-based studies

Preliminary studies using a subset of data from LETS demonstrated that a systems-based parameter of coagulation was predictive of DVT risk and may have potential application as a diagnostic screening tool. Future population-based studies may include: 1) a follow-up simulation study to examine the predictive value of FSTG for recurrent DVT using the LETS data, 2) FSTG analysis of the GATE (Genetic Attributes of Thrombosis Epidemiology, Centers for Disease Control, Atlanta, GA) study to examine the effects of age, race, smoking, obesity, and OC use, 3) prospective studies to better determine a clinical FSTG cutpoint, 4) prospective studies to examine the change in FSTG following initiation and/or discontinuation of oral contraceptives.

5.3.   REFERENCES

1.   Pijls, N.H., et al., *Measurement of Fractional Flow Reserve to Assess the Functional Severity of Coronary-Artery Stenoses.* N Engl J Med, 1996. **334**(26): p. 1703-8.
2.   Tonino, P.A., et al., *Fractional Flow Reserve Versus Angiography for Guiding Percutaneous Coronary Intervention.* N Engl J Med, 2009. **360**(3): p. 213-24.

APPENDIX A:

Model equations & boundary conditions

The non-dimensionalized, convection-diffusion equation governs the transport of all soluble species:

$$\delta_{ts}\frac{\partial c_i}{\partial t} + \frac{Pe}{\alpha}\frac{\partial c_i}{\partial x} = D_i\left(\frac{1}{\alpha^2}\frac{\partial^2 c_i}{\partial x^2} + \frac{\partial^2 c_i}{\partial y^2}\right) + \delta_{ts}R_{soln} \qquad\qquad \text{A.1}$$

Surface-associated reaction kinetics, which appear as flux boundary conditions for TF or TM-defined boundaries, are listed for each individual species below. Solution-phase reaction rates, R_{soln}, are also defined.

Factor II (prothrombin)

$$-D_2\frac{\partial c_2}{\partial y}(y=0)\Big|_{TF,TM} = \frac{-k_{cat2}\times c_{5a10as}\times c_2}{K_{m2}+c_2}$$
$$R_2 = 0 \qquad\qquad \text{BC.1}$$

Factor IIa (thrombin)

$$-D_{2a}\frac{\partial c_{2a}}{\partial y}(y=0)\Big|_{TF} = \frac{k_{cat2}\times c_{5a10as}\times c_2}{K_{m2}+c_2}$$
$$-D_{2a}\frac{\partial c_{2a}}{\partial y}(y=0)\Big|_{TM} = \frac{k_{cat2}\times c_{5a10as}\times c_2}{K_{m2}+c_2} - (k_{a3}\times c_{2a}\times(TM_{total}-c_{TTMs}) - k_{d3}\times c_{TTMs}) \qquad \text{BC.2}$$
$$R_{2a} = -k_{a5}\times c_{2a}\times c_{AT3}$$

Factor V

$$-D_5\frac{\partial c_5}{\partial y}(y=0)\Big|_{TF,TM} = \frac{-k_{cat10}\times c_{10a}\times c_5}{K_{m10}+c_5}$$
$$R_5 = \frac{-k_{cat8}\times c_{2a}\times c_5}{K_{m8}+c_5} \qquad\qquad \text{BC.3}$$

Factor Va

$$-D_{5a} \frac{\partial c_{5a}}{\partial y}(y=0)\Big|_{TF,TM} = -(k_{a2} \times c_{5a} \times c_{10a} - k_{d2} \times c_{5a10as}) - \frac{k_{cat4} \times c_{5a} \times c_{apc}}{K_{m4} + c_{5a}}$$

$$+ \frac{k_{cat10} \times c_{10a} \times c_5}{K_{m10} + c_5} \qquad \text{BC.4}$$

$$R_{5a} = \frac{k_{cat8} \times c_{2a} \times c_5}{K_{m8} + c_5}$$

Factor VII

$$-D_7 \frac{\partial c_7}{\partial y}(y=0)\Big|_{TF,TM} = 0$$

$$R_7 = \frac{-k_{cat9} \times c_{10a} \times c_7}{K_{m9} + c_7} - \frac{k_{cat11} \times c_{2a} \times c_7}{K_{m11} + c_7} \qquad \text{BC.5}$$

Factor VIIa

$$-D_{7a} \frac{\partial c_{7a}}{\partial y}(y=0)\Big|_{TF} = -k_{a1} \times c_{7a} \times TF_{free} + k_{d1} \times c_{TF7as}$$

$$-D_{7a} \frac{\partial c_{7a}}{\partial y}(y=0)\Big|_{TM} = 0 \qquad \text{BC.6}$$

$$R_{7a} = \frac{k_{cat9} \times c_{10a} \times c_7}{K_{m9} + c_7} + \frac{k_{cat11} \times c_{2a} \times c_7}{K_{m11} + c_7}$$

Factor VIII

$$-D_8 \frac{\partial c_8}{\partial y}(y=0)\Big|_{TF,TM} = 0$$

$$R_8 = \frac{-k_{cat6} \times c_{2a} \times c_8}{K_{m6} + c_8} \qquad \text{BC.7}$$

Factor VIIIa

$$-D_{8a} \frac{\partial c_{8a}}{\partial y}(y=0)\Big|_{TF,TM} = -(k_{a4} \times c_{8a} \times c_{9a} - k_{d4} \times c_{8a9as}) - \frac{k_{cat4} \times c_{8a} \times c_{apc}}{K_{m4} + c_{8a}}$$

$$R_{8a} = \frac{k_{cat6} \times c_{2a} \times c_8}{K_{m6} + c_8} \qquad \text{BC.8}$$

Factor IX

$$-D_9 \frac{\partial c_9}{\partial y}(y=0)\Big|_{TF} = \frac{-k_{cat5} \times c_{TF7as} \times c_9}{K_{m5} + c_9}$$

$$-D_9 \frac{\partial c_9}{\partial y}(y=0)\Big|_{TM} = 0 \qquad\qquad\qquad\qquad\qquad\qquad \text{BC.9}$$

$$R_9 = 0$$

Factor IXa

$$-D_{9a} \frac{\partial c_{9a}}{\partial y}(y=0)\Big|_{TF} = \frac{-k_{cat5} \times c_{TF7as} \times c_9}{K_{m5} + c_9} - (k_{a4} \times c_{8a} \times c_{9a} - k_{d4} \times c_{8a9as})$$

$$-D_{9a} \frac{\partial c_{9a}}{\partial y}(y=0)\Big|_{TM} = -(k_{a4} \times c_{8a} \times c_{9a} - k_{d4} \times c_{8a9as}) \qquad\qquad \text{BC.10}$$

$$R_{9a} = -k_{a9} \times c_{9a} \times c_{AT3}$$

Factor X

$$-D_{10} \frac{\partial c_{10}}{\partial y}(y=0)\Big|_{TF} = \frac{-k_{cat1} \times c_{TF7as} \times c_{10}}{K_{m1} + c_{10}} - \frac{k_{cat7} \times c_{8a9as} \times c_{10}}{K_{m7} + c_{10}}$$

$$-D_{10} \frac{\partial c_{10}}{\partial y}(y=0)\Big|_{TM} = \frac{-k_{cat7} \times c_{8a9as} \times c_{10}}{K_{m7} + c_{10}} \qquad\qquad\qquad \text{BC.11}$$

$$R_{10} = 0$$

Factor Xa

$$-D_{10a} \frac{\partial c_{10a}}{\partial y}(y=0)\Big|_{TF} = \frac{k_{cat1} \times c_{TF7as} \times c_{10}}{K_{m1} + c_{10}} - \frac{k_{cat7} \times c_{8a9as} \times c_{10}}{K_{m7} + c_{10}}$$

$$\qquad\qquad - (k_{a2} \times c_{5a} \times c_{10a} - k_{d2} \times c_{5a10as})$$

$$-D_{10a} \frac{\partial c_{10a}}{\partial y}(y=0)\Big|_{TM} = \frac{k_{cat7} \times c_{8a9as} \times c_{10}}{K_{m7} + c_{10}} - (k_{a2} \times c_{5a} \times c_{10a} - k_{d2} \times c_{5a10as}) \qquad \text{BC.12}$$

$$R_{10a} = -k_{a9} \times c_{10a} \times c_{AT3} - (k_{a6} \times c_{TFPI} \times c_{10a} - k_{d6} \times c_{TFPI10a})$$

Protein C

$$-D_{pc} \frac{\partial c_{pc}}{\partial y}(y=0)\big|_{TF} = 0$$

$$-D_{pc} \frac{\partial c_{pc}}{\partial y}(y=0)\big|_{TM} = \frac{-k_{cat3} \times c_{TTMs} \times c_{pc}}{K_{m3} + c_{pc}} \qquad \text{BC.13}$$

$$R_{pc} = 0$$

AT3

$$-D_{AT3} \frac{\partial c_{AT3}}{\partial y}(y=0)\big|_{TF,TM} = 0 \qquad \text{BC.14}$$

$$R_{AT3} = -k_{a9} \times c_{9a} \times c_{AT3} - k_{a9} \times c_{10a} \times c_{AT3} - k_{a5} \times c_{2a} \times c_{AT3}$$

TFPI

$$-D_7 \frac{\partial c_7}{\partial y}(y=0)\big|_{TF,TM} = 0 \qquad \text{BC.15}$$

$$R_7 = -(k_{a6} \times c_{TFPI} \times c_{10a} - k_{d6} \times c_{TFPI10a})$$

TFPI/ Xa

$$-D_{tfpi10a} \frac{\partial c_{TFPI10a}}{\partial y}(y=0)\big|_{TF} = -(k_{a7} \times c_{TFPI10a} \times c_{TF7as} - k_{d7} \times c_{TFIs})$$

$$-D_{tfpi10a} \frac{\partial c_{TFPI10a}}{\partial y}(y=0)\big|_{TM} = 0 \qquad \text{BC.16}$$

$$R_{tfpi10a} = k_{a6} \times c_{TFPI} \times c_{10a} - k_{d6} \times c_{TFPI10a}$$

Surface complexes are defined by their time derivatives.

TF/ VIIa (extrinsic Xase)

$$\frac{\partial c_{TF7as}}{\partial t}(y=0)\big|_{TF} = (k_{a1} \times c_{7a} \times TF_{free} - k_{d1} \times c_{TF7as}) - (k_{a7} \times c_{TFPI10a} \times c_{TF7as} - k_{d7} \times c_{TFIs})$$

$$\frac{\partial c_{TF7as}}{\partial t}(y=0)\big|_{TM} = 0$$

A.2

Va/ Xa (prothrombinase)

$$\frac{\partial c_{5a10as}}{\partial t}(y=0)\big|_{TF,TM} = k_{a2} \times c_{5a} \times c_{10a} - k_{d2} \times c_{5a10as}$$

A.3

Thrombin-TM

$$\frac{\partial c_{TTMs}}{\partial t}(y=0)\big|_{TF} = 0$$

$$\frac{\partial c_{TTMs}}{\partial t}(y=0)\big|_{TM} = k_{a3} \times c_{2a} \times (TM - c_{TTMs}) - k_{d3} \times c_{TTMs}$$

A.4

VIIIa/ IXa (intrinsic Xase)

$$\frac{\partial c_{8a9as}}{\partial t}(y=0)\big|_{TF,TM} = k_{a4} \times c_{8a} \times c_{9a} - k_{d4} \times c_{8a9as}$$

A.5

TFPI/ Xa/ TF/ VIIa

$$\frac{\partial c_{TFi}}{\partial t}(y=0)\big|_{TF} = k_{a7} \times c_{TFPI10a} \times c_{TF7as} - k_{d7} \times c_{TFIs}$$

$$\frac{\partial c_{TFi}}{\partial t}(y=0)\big|_{TM} = 0$$

A.6

APPENDIX B:

Dimensional analysis

The governing equations of the mathematical model were non-dimensionalized for numerical convenience. Listed below are the dimensional scales chosen. Variables are as listed in the text. Dimensionless variables are denoted with a superscript, *, while dimensional scales are denoted with a subscript, s.

$$x^* = \frac{x}{x_s}; \quad x_s = \frac{L}{3.6}$$

$$y^* = \frac{y}{y_s}; \quad y_s = \frac{2B}{1}$$

$$\alpha = \frac{x_s}{y_s}$$

$$t^* = \frac{t}{t_s}; \quad t_s = 60 \text{ s}$$

$$\delta_{ts} = \frac{z_s^2}{D_s t_s}$$

$$c_{sol'n}^* = \frac{c_{sol'n}}{c_s}$$

$$c_{surface}^* = \frac{c_{surface}}{e_s}$$

$$e_s = \theta = TM_{total}$$

$$c_s = \frac{e_s y_s}{D_s t_s}$$

$$D_i^* = \frac{D_i}{D_s}; \quad D_s = 1 \times 10^{-6} \ \frac{\text{cm}^2}{\text{s}}$$

$$Pe = \frac{u y_s}{D_s}$$

$$k_{cat}^* = k_{cat} t_s$$

$$k_1^* = k_1 c_s t_s$$

$$k_{-1}^* = k_{-1} t_s$$

$$K_m^* = \frac{K_m}{c_s}$$

$$k_{assoc}^* = k_{assoc} c_s t_s$$

$$k_{dissoc}^* = k_{dissoc} t_s$$

Substituting, the governing equations become:

$$\delta_{ts} \frac{\partial c_i^*}{\partial t^*} + \frac{Pe}{\alpha} \frac{\partial c_i^*}{\partial x^*} = D_i^* \left(\frac{1}{\alpha^2} \frac{\partial^2 c_i^*}{\partial x^{*2}} + \frac{\partial^2 c_i^*}{\partial y^{*2}} \right) + \delta_{ts} R_{soln}^*$$

Annotated MATLAB script for three spatially discrete TF regions

```
% COMSOL Multiphysics Model M-file (THmodel6_spotted)
% Generated by COMSOL 3.4 (COMSOL 3.4.0.248, $Date: 2007/10/10 16:07:51
$)
% all units umol, cm, s

flclear fem

% COMSOL version
clear vrsn
vrsn.name = 'COMSOL 3.4';
vrsn.ext = '';
vrsn.major = 0;
vrsn.build = 248;
vrsn.rcs = '$Name:  $';
vrsn.date = '$Date: 2007/10/10 16:07:51 $';
fem.version = vrsn;

% Geometry

% Define a rectangle of total length 4, height 1, anchored by the lower
% left corner at position (-1,0)

g1=rect2('4','1','base','corner','pos',{'-1','0'},'rot','0');

% Define intersection points to sub-divide lower reactive boundary
% TF length 0.02, TF interval distance 1

% start of TF1 (0,0)
parr={point2(0,0)};
g2=geomcoerce('point',parr);

% end of TF1, start of TM1
parr={point2(0.02,0)};
g3=geomcoerce('point',parr);

% start of TF2
parr={point2(1,0)};
g4=geomcoerce('point',parr);

% end of TF2, start of TM2
parr={point2(1.02,0)};
g5=geomcoerce('point',parr);

% start of TF3
parr={point2(2,0)};
g6=geomcoerce('point',parr);

% end of TF3, start of TM3
```

```
parr={point2(2.02,0)};
g7=geomcoerce('point',parr);

% Name points (p) and boundaries (s)

clear p s
p.objs={g2,g3,g4,g5,g6,g7};
p.name={'TFstart1','TFend1','TFstart2','TFend2','TFstart3','TFend3'};
p.tags={'g2','g3','g4','g5','g6','g7'};

s.objs={g1};
s.name={'parallel_plate'};
s.tags={'g1'};

% Draw geometry objects

fem.draw=struct('p',p,'s',s);
fem.geom=geomcsg(fem);
```

% Mesh

```
% Increase mesh density over intersection points (vertices 3-8) and
% over the lower surface (edges 2, 4-9)

fem.mesh=meshinit(fem, ...
                  'hauto',5, ...

'hmaxvtx',[3,0.01,4,0.02,5,0.01,6,0.02,7,0.01,8,0.02], ...

'hmaxedg',[2,0.03,4,0.02,5,0.03,6,0.02,7,0.03,8,0.02,9,0.03]);
```

% Constants

```
fem.const = {'B','0.01/2', ...              % half-height
  'L','3', ...                              % length
  'xs','L/L', ...                           % longitudinal length scale
  'ys','2*B/1', ...                         % radial length scale
  'alpha','xs/ys', ...
  ...
  'Df2','6.21e-7', ...                      % diffusion coefficients
  'Df2a','7.78e-7', ...
  'Df5','3.74e-7', ...
  'Df5a','4.69e-7', ...
  'Df7','7.02e-7', ...
  'Df7a','7.02e-7', ...
  'Df8','4.67e-7', ...
  'Df8a','4.7e-7', ...
  'Df9','6.8e-7', ...
  'Df9a','7.27e-7', ...
  'Df10','6.64e-7', ...
  'Df10a','7.22e-7', ...
  'Dpc','6.53e-7', ...
  'Dapc','6.75e-7', ...
  'DLpc','(Dpc+Dapc)/2', ...  % averaged diffusivity for PC and APC
  'DAT3','6.68e-7', ...
  'Dtfpi','7.98e-7', ...
  'Dtfpi10a','6e-7', ...
```

```
  'Ds','1e-6', ...                        % diffusion scale
  ...
  'Dqf2','Df2/Ds', ...                     % normalized diffusion
coefficients
  'Dqf2a','Df2a/Ds', ...
  'Dqf5','Df5/Ds', ...
  'Dqf5a','Df5a/Ds', ...
  'Dqf7','Df7/Ds', ...
  'Dqf7a','Df7a/Ds', ...
  'Dqf8','Df8/Ds', ...
  'Dqf8a','Df8a/Ds', ...
  'Dqf9','Df9/Ds', ...
  'Dqf9a','Df9a/Ds', ...
  'Dqf10','Df10/Ds', ...
  'Dqf10a','Df10a/Ds', ...
  'DqLpc','DLpc/Ds', ...
  'DqAT3','DAT3/Ds', ...
  'Dqtfpi','Dtfpi/Ds', ...
  'Dqtfpi10a','Dtfpi10a/Ds', ...
  ...
  'c2in','1.4e-3', ...                     % inlet concentrations
  'c2ain','0', ...
  'c5in','20e-6', ...
  'c5ain','0', ...
  'c7in','10e-6', ...
  'c7ain','0.01*c7in', ...                 % inlet VIIa is 1% of inlet
VII
  'c8in','0.7e-6', ...
  'c8ain','0', ...
  'c9in','90e-6', ...
  'c9ain','0', ...
  'c10in','160e-6', ...
  'c10ain','0', ...
  'cpcin','0.1e-3', ...
  'capcin','0', ...
  'ctfpiin','2.5e-6', ...
  'cAT3in','1e-3', ...

  'ts','60'};                              % time scale
```

% Application modes

% Application mode 1 (factor X)
% Convection and diffusion application mode

```
clear appl
appl.mode.class = 'FlConvDiff';
appl.dim = {'c10'};
appl.name = 'f10';
appl.assignsuffix = '_f10';
```

% Boundary settings

```
clear bnd
```

% Concentration
```
bnd.c0 = {0,0,'c10in/cs',0,0};
```

```
% Inward flux
bnd.N = {0,'-kcat1q*ctf7as*c10/(Km10q+c10)-
kcat7q*c8a9as*c10/(Km7q+c10)', ...
  0,0,'-kcat7q*c8a9as*c10/(Km7q+c10)'};

% Boundary type ('N0' is insulation; 'N' is flux, 'C' is concentration,
'Nc' is
% convective flux)

bnd.type = {'N0','N','C','Nc','N'};

% c0, N, and type array indices.  bnd.ind[1] = 3, thus boundary 1
% (inlet) is described by bnd.c0[3]='c10in/cs', bnd.N[3]=0, bnd.type
% [3]='C', or in words, boundary 1 is defined by a Dirichlet boundary
% condition with a constant concentration equal to c10in/cs.  Boundary
% number labels are shown in
Figure .

bnd.ind = [3,1,1,2,5,2,5,2,5,4];
appl.bnd = bnd;

% Subdomain settings

clear equ

% Anisotropic diffusivity tensor
equ.dtype = 'aniso';
equ.dtensor = {{{'Dqf10/alpha^2';'Dqf10'}}};

% Flow velocity
equ.u = 'Pey*un/alpha';
equ.v = 'Pey*0';

% Time-scaling coefficient
equ.Dts = 'dts';

equ.ind = [1];
appl.equ = equ;
fem.appl{1} = appl;

% Application mode 2 (factor Xa)
% Convection and diffusion application mode

clear appl
appl.mode.class = 'FlConvDiff';
appl.dim = {'c10a'};
appl.name = 'f10a';
appl.assignsuffix = '_f10a';
clear prop
clear weakconstr
weakconstr.value = 'off';
weakconstr.dim = {'lm2'};
prop.weakconstr = weakconstr;
appl.prop = prop;

clear bnd
```

```
bnd.c0 = {0,0,'c10ain/cs',0,0};
bnd.N = {0,'kcat1q*ctf7as*c10/(Km1q+c10)+kcat7q*c8a9as*c10/(Km7q+c10)-
(ka2q*c5a*c10a-kd2q*c5a10as)', ...
  0,0,'kcat7q*c8a9as*c10/(Km7q+c10)-(ka2q*c5a*c10a-kd2q*c5a10as)'};
bnd.type = {'N0','N','C','Nc','N'};
bnd.ind = [3,1,1,2,5,2,5,2,5,4];
appl.bnd = bnd;

clear equ
equ.dtensor = {{{'Dqf10a/alpha^2';'Dqf10a'}}};
equ.v = 'Pey*0';
equ.u = 'Pey*un/alpha';
equ.Dts = 'dts';

% Fluid-phase reaction rate
equ.R = 'dts*(-ka9q*c10a*cAT3-(ka6q*ctfpi*c10a-kd6q*ctfpi10a))';
equ.dtype = 'aniso';
equ.ind = [1];
appl.equ = equ;
fem.appl{2} = appl;

% Application mode 3 (factor VIIa)
% Convection and diffusion application mode

clear appl
appl.mode.class = 'FlConvDiff';
appl.dim = {'c7a'};
appl.name = 'f7a';
appl.assignsuffix = '_f7a';
clear prop
clear weakconstr
weakconstr.value = 'off';
weakconstr.dim = {'lm3'};
prop.weakconstr = weakconstr;
appl.prop = prop;

clear bnd
bnd.c0 = {0,0,'c7ain/cs',0};
bnd.N = {0,'-ka1q*c7a*TFfreeq+kd1q*ctf7as',0,0};
bnd.type = {'N0','N','C','Nc'};
bnd.ind = [3,1,1,2,1,2,1,2,1,4];
appl.bnd = bnd;

clear equ
equ.dtensor = {{{'Dqf7a/alpha^2';'Dqf7a'}}};
equ.v = 'Pey*0';
equ.u = 'Pey*un/alpha';
equ.Dts = 'dts';
equ.R = 'dts*(kcat9q*c10a*c7/(Km9q+c7)+kcat11q*c2a*c7/(Km11q+c7))';
equ.dtype = 'aniso';
equ.ind = [1];
appl.equ = equ;
fem.appl{3} = appl;

% Application mode 4 (TF/VIIa)
% Weak form, boundary application mode
```

```
clear appl
appl.mode.class = 'FlPDEWBoundary';
appl.dim = {'ctf7as','ctf7as_t'};
appl.name = 'tf7a';
appl.assignsuffix = '_tf7a';
clear prop
clear weakconstr
weakconstr.value = 'off';
weakconstr.dim = {'lm4','lm5'};
prop.weakconstr = weakconstr;
appl.prop = prop;

% Boundary Settings

clear bnd

% Time-dependent weak term
bnd.dweak = {0,'ctf7as_test*ctf7as_time'};
bnd.usage = {0,1};

% Weak term
bnd.weak = {0,'ctf7as_test*((ka1q*c7a*TFfreeq-kd1q*ctf7as)-
(ka7q*ctfpi10a*ctf7as-kd7q*ctfis))'};

% Weak term array indices. Boundary number labels shown in Figure.
bnd.ind = [1,1,1,2,1,2,1,2,1,1];
appl.bnd = bnd;
fem.appl{4} = appl;

% Application mode 5 (prothrombin)
% Convection and diffusion application mode

clear appl
appl.mode.class = 'FlConvDiff';
appl.dim = {'c2'};
appl.name = 'f2';
appl.assignsuffix = '_f2';

clear bnd
bnd.c0 = {0,0,'c2in/cs',0};
bnd.N = {0,'-kcat2q*c5a10as*c2/(Km2q+c2)',0,0};
bnd.type = {'N0','N','C','Nc'};
bnd.ind = [3,1,1,2,2,2,2,2,2,4];
appl.bnd = bnd;

clear equ
equ.dtensor = {{{'Dqf2/alpha^2';'Dqf2'}}};
equ.v = 'Pey*0';
equ.u = 'Pey*un/alpha';
equ.Dts = 'dts';
equ.dtype = 'aniso';
equ.ind = [1];
appl.equ = equ;
fem.appl{5} = appl;

% Application mode 6 (thrombin)
% Convection and diffusion application mode
```

```
clear appl
appl.mode.class = 'FlConvDiff';
appl.dim = {'c2a'};
appl.name = 'f2a';
appl.assignsuffix = '_f2a';
clear prop
clear weakconstr
weakconstr.value = 'off';
weakconstr.dim = {'lm7'};
prop.weakconstr = weakconstr;
appl.prop = prop;

clear bnd
bnd.c0 = {0,0,'c2ain/cs',0,0};
bnd.N =
{0,'kcat2q*c5a10as*c2/(Km2q+c2)',0,0,'kcat2q*c5a10as*c2/(Km2q+c2)-
(ka3q*c2a*(TMq-cttms)-kd3q*cttms)'};
bnd.type = {'N0','N','C','Nc','N'};
bnd.ind = [3,1,1,2,5,2,5,2,5,4];
appl.bnd = bnd;

clear equ
equ.dtensor = {{{'Dqf2a/alpha^2';'Dqf2a'}}};
equ.v = 'Pey*0';
equ.u = 'Pey*un/alpha';
equ.Dts = 'dts';
equ.R = 'dts*(-ka5q*c2a*cAT3)';
equ.dtype = 'aniso';
equ.ind = [1];
appl.equ = equ;
fem.appl{6} = appl;

% Application mode 7 (factor Va)
% Convection and diffusion application mode

clear appl
appl.mode.class = 'FlConvDiff';
appl.dim = {'c5a'};
appl.name = 'f5a';
appl.assignsuffix = '_f5a';
clear prop
clear weakconstr
weakconstr.value = 'off';
weakconstr.dim = {'lm8'};
prop.weakconstr = weakconstr;
appl.prop = prop;

clear bnd
bnd.c0 = {0,0,'c5ain/cs',0};
bnd.N = {0,'-(ka2q*c5a*c10a-kd2q*c5a10as) -kcat4q*c5a*capc/(Km4q+c5a)
+kcat10q*c10a*c5/(Km10q+c5)', ...
  0,0};
bnd.type = {'N0','N','C','Nc'};
bnd.ind = [3,1,1,2,2,2,2,2,2,4];
appl.bnd = bnd;
```

```
clear equ
equ.dtensor = {{{'Dqf5a/alpha^2';'Dqf5a'}}};
equ.v = 'Pey*0';
equ.u = 'Pey*un/alpha';
equ.Dts = 'dts';
equ.R = 'dts*(kcat8q*c2a*c5/(Km8q+c5))';
equ.dtype = 'aniso';
equ.ind = [1];
appl.equ = equ;
fem.appl{7} = appl;

% Application mode 8 (Va/Xa)
% Weak form, boundary application mode

clear appl
appl.mode.class = 'FlPDEWBoundary';
appl.dim = {'c5a10as','c5a10as_t'};
appl.name = 'f5af10a';
appl.assignsuffix = '_f5af10a';
clear prop
clear weakconstr
weakconstr.value = 'off';
weakconstr.dim = {'lm9','lmq10'};
prop.weakconstr = weakconstr;
appl.prop = prop;

clear bnd
bnd.dweak = {0,'c5a10as_test*c5a10as_time'};
bnd.usage = {0,1};
bnd.weak = {0,'c5a10as_test*(ka2q*c5a*c10a-kd2q*c5a10as)'};
bnd.ind = [1,1,1,2,2,2,2,2,2,1];
appl.bnd = bnd;
fem.appl{8} = appl;

% Application mode 9 (protein C)
% Convection and diffusion application mode

clear appl
appl.mode.class = 'FlConvDiff';
appl.dim = {'cpc'};
appl.name = 'pc';
appl.assignsuffix = '_pc';

clear bnd
bnd.c0 = {0,0,'cpcin/cs',0};
bnd.N = {0,'-kcat3q*cttms*cpc/(Km3q+cpc)',0,0};
bnd.type = {'N0','N','C','Nc'};
bnd.ind = [3,1,1,1,2,1,2,1,2,4];
appl.bnd = bnd;

clear equ
equ.dtensor = {{{'DqLpc/alpha^2';'DqLpc'}}};
equ.v = 'Pey*0';
equ.u = 'Pey*un/alpha';
equ.Dts = 'dts';
equ.dtype = 'aniso';
equ.ind = [1];
```

```matlab
appl.equ = equ;
fem.appl{9} = appl;

% Application mode 10 (thrombin-TM)
% Weak form, boundary application mode

clear appl
appl.mode.class = 'FlPDEWBoundary';
appl.dim = {'cttms','cttms_t'};
appl.name = 'ttm';
appl.assignsuffix = '_ttm';
clear prop
clear weakconstr
weakconstr.value = 'off';
weakconstr.dim = {'lm12','lm13'};
prop.weakconstr = weakconstr;
appl.prop = prop;

clear bnd
bnd.dweak = {0,'cttms_test*cttms_time'};
bnd.usage = {0,1};
bnd.weak = {0,'cttms_test*(ka3q*c2a*(TMq-cttms)-kd3q*cttms)'};
bnd.ind = [1,1,1,1,2,1,2,1,2,1];
appl.bnd = bnd;
fem.appl{10} = appl;

% Application mode 11 (factor IX)
% Convection and diffusion application mode

clear appl
appl.mode.class = 'FlConvDiff';
appl.dim = {'c9'};
appl.name = 'f9';
appl.assignsuffix = '_f9';

clear bnd
bnd.c0 = {0,0,'c9in/cs',0};
bnd.N = {0,'-kcat5q*ctf7as*c9/(Km5q+c9)',0,0};
bnd.type = {'N0','N','C','Nc'};
bnd.ind = [3,1,1,2,1,2,1,2,1,4];
appl.bnd = bnd;

clear equ
equ.dtensor = {{{'Dqf9/alpha^2';'Dqf9'}}};
equ.v = 'Pey*0';
equ.u = 'Pey*un/alpha';
equ.Dts = 'dts';
equ.dtype = 'aniso';
equ.ind = [1];
appl.equ = equ;
fem.appl{11} = appl;

% Application mode 12 (factor IXa)
% Convection and diffusion application mode

clear appl
appl.mode.class = 'FlConvDiff';
```

```
appl.dim = {'c9a'};
appl.name = 'f9a';
appl.assignsuffix = '_f9a';
clear prop
clear weakconstr
weakconstr.value = 'off';
weakconstr.dim = {'lm15'};
prop.weakconstr = weakconstr;
appl.prop = prop;

clear bnd
bnd.c0 = {0,0,'c9ain/cs',0,0};
bnd.N = {0,'kcat5q*ctf7as*c9/(Km5q+c9)-(ka4q*c8a*c9a-kd4q*c8a9as)',...
   0, 0,'-(ka4q*c8a*c9a-kd4q*c8a9as)'};
bnd.type = {'N0','N','C','Nc','N'};
bnd.ind = [3,1,1,2,5,2,5,2,5,4];
appl.bnd = bnd;

clear equ
equ.dtensor = {{{'Dqf9a/alpha^2';'Dqf9a'}}};
equ.v = 'Pey*0';
equ.u = 'Pey*un/alpha';
equ.Dts = 'dts';
equ.R = 'dts*(-ka9q*c9a*cAT3)';
equ.dtype = 'aniso';
equ.ind = [1];
appl.equ = equ;
fem.appl{12} = appl;

% Application mode 13 (factor VIII)
% Convection and diffusion application mode

clear appl
appl.mode.class = 'FlConvDiff';
appl.dim = {'c8'};
appl.name = 'f8';
appl.assignsuffix = '_f8';

clear bnd
bnd.c0 = {0,'c8in/cs',0};
bnd.type = {'N0','C','Nc'};
bnd.ind = [2,1,1,1,1,1,1,1,1,3];
appl.bnd = bnd;

clear equ
equ.dtensor = {{{'Dqf8/alpha^2';'Dqf8'}}};
equ.v = 'Pey*0';
equ.u = 'Pey*un/alpha';
equ.Dts = 'dts';
equ.R = 'dts*(-kcat6q*c2a*c8/(Km6q+c8))';
equ.dtype = 'aniso';
equ.ind = [1];
appl.equ = equ;
fem.appl{13} = appl;

% Application mode 14 (factor VIIIa)
% Convection and diffusion application mode
```

```
clear appl
appl.mode.class = 'FlConvDiff';
appl.dim = {'c8a'};
appl.name = 'f8a';
appl.assignsuffix = '_f8a';
clear prop
clear weakconstr
weakconstr.value = 'off';
weakconstr.dim = {'lm17'};
prop.weakconstr = weakconstr;
appl.prop = prop;

clear bnd
bnd.c0 = {0,'c8ain/cs',0,0};
bnd.N = {0,0,0,'-(ka4q*c8a*c9a-kd4q*c8a9as)-
kcat4q*c8a*capc/(Km4q+c8a)'};
bnd.type = {'N0','C','Nc','N'};
bnd.ind = [2,1,1,4,4,4,4,4,4,3];
appl.bnd = bnd;

clear equ
equ.dtensor = {{{'Dqf8a/alpha^2';'Dqf8a'}}};
equ.v = 'Pey*0';
equ.u = 'Pey*un/alpha';
equ.Dts = 'dts';
equ.R = 'dts*(kcat6q*c2a*c8/(Km6q+c8))';
equ.dtype = 'aniso';
equ.ind = [1];
appl.equ = equ;
fem.appl{14} = appl;

% Application mode 15 (VIIIa/ IXa)
% Weak form, boundary application mode

clear appl
appl.mode.class = 'FlPDEWBoundary';
appl.dim = {'c8a9as','c8a9as_t'};
appl.name = 'f8af9a';
appl.assignsuffix = '_f8af9a';
clear prop
clear weakconstr
weakconstr.value = 'off';
weakconstr.dim = {'lm18','lmq19'};
prop.weakconstr = weakconstr;
appl.prop = prop;

clear bnd
bnd.dweak = {0,'c8a9as_test*c8a9as_time'};
bnd.usage = {0,1};
bnd.weak = {0,'c8a9as_test*(ka4q*c8a*c9a-kd4q*c8a9as)'};
bnd.ind = [1,1,1,2,2,2,2,2,2,1];
appl.bnd = bnd;
fem.appl{15} = appl;

% Application mode 16 (factor V)
% Convection and diffusion application mode
```

```
clear appl
appl.mode.class = 'FlConvDiff';
appl.dim = {'c5'};
appl.name = 'f5';
appl.assignsuffix = '_f5';

clear bnd
bnd.c0 = {0,'c5in/cs',0,0};
bnd.N = {0,0,0,'-kcat10q*c10a*c5/(Km10q+c5)'};
bnd.type = {'N0','C','Nc','N'};
bnd.ind = [2,1,1,4,4,4,4,4,4,3];
appl.bnd = bnd;

clear equ
equ.dtensor = {{{'Dqf5/alpha^2';'Dqf5'}}};
equ.v = 'Pey*0';
equ.u = 'Pey*un/alpha';
equ.Dts = 'dts';
equ.R = 'dts*(-kcat8q*c2a*c5/(Km8q+c5))';
equ.dtype = 'aniso';
equ.ind = [1];
appl.equ = equ;
fem.appl{16} = appl;

% Application mode 17 (factor VII)
% Convection and diffusion application mode

clear appl
appl.mode.class = 'FlConvDiff';
appl.dim = {'c7'};
appl.name = 'f7';
appl.assignsuffix = '_f7';

clear bnd
bnd.c0 = {0,'c7in/cs',0};
bnd.type = {'N0','C','Nc'};
bnd.ind = [2,1,1,1,1,1,1,1,1,3];
appl.bnd = bnd;

clear equ
equ.dtensor = {{{'Dqf7/alpha^2';'Dqf7'}}};
equ.v = 'Pey*0';
equ.u = 'Pey*un/alpha';
equ.Dts = 'dts';
equ.R = 'dts*(-kcat9q*c10a*c7/(Km9q+c7) -kcat11q*c2a*c7/(Km11q+c7))';
equ.dtype = 'aniso';
equ.ind = [1];
appl.equ = equ;
fem.appl{17} = appl;

% Application mode 18 (TFPI)
% Convection and diffusion application mode

clear appl
appl.mode.class = 'FlConvDiff';
appl.dim = {'ctfpi'};
```

```
appl.name = 'tfpi';
appl.assignsuffix = '_tfpi';

clear bnd
bnd.c0 = {0,'ctfpiin/cs',0};
bnd.type = {'N0','C','Nc'};
bnd.ind = [2,1,1,1,1,1,1,1,1,3];
appl.bnd = bnd;

clear equ
equ.dtensor = {{{'Dqtfpi/alpha^2';'Dqtfpi'}}};
equ.v = 'Pey*0';
equ.u = 'Pey*un/alpha';
equ.Dts = 'dts';
equ.R = 'dts*(-(ka6q*ctfpi*c10a-kd6q*ctfpi10a))';
equ.dtype = 'aniso';
equ.ind = [1];
appl.equ = equ;
fem.appl{18} = appl;

% Application mode 19 (TFPI/ Xa)
% Convection and diffusion application mode

clear appl
appl.mode.class = 'FlConvDiff';
appl.dim = {'ctfpi10a'};
appl.name = 'tfpi10a';
appl.assignsuffix = '_tfpi10a';

clear bnd
bnd.N = {0,0,0,'-(ka7q*ctfpi10a*ctf7as-kd7q*ctfis)'};
bnd.type = {'N0','C','Nc','N'};
bnd.ind = [2,1,1,4,1,4,1,4,1,3];
appl.bnd = bnd;

clear equ
equ.dtensor = {{{'Dqtfpi10a/alpha^2';'Dqtfpi10a'}}};
equ.v = 'Pey*0';
equ.u = 'Pey*un/alpha';
equ.Dts = 'dts';
equ.R = 'dts*(ka6q*ctfpi*c10a-kd6q*ctfpi10a)';
equ.dtype = 'aniso';
equ.ind = [1];
appl.equ = equ;
fem.appl{19} = appl;

% Application mode 20 (TFPI/ Xa/ TF/ VIIa)
% Weak form, boundary application mode

clear appl
appl.mode.class = 'FlPDEWBoundary';
appl.dim = {'ctfis','ctfis_t'};
appl.name = 'tfi';
appl.assignsuffix = '_tfi';
clear prop
clear weakconstr
weakconstr.value = 'off';
```

```matlab
weakconstr.dim = {'lm24','lmq25'};
prop.weakconstr = weakconstr;
appl.prop = prop;

clear bnd
bnd.dweak = {0,'ctfis_test*ctfis_time'};
bnd.usage = {0,1};
bnd.weak = {0,'ctfis_test*((ka7q*ctfpi10a*ctf7as-kd7q*ctfis))'};
bnd.ind = [1,1,1,2,1,2,1,2,1,1];
appl.bnd = bnd;
fem.appl{20} = appl;

% Application mode 21 (antithrombin III)
% Convection and diffusion application mode

clear appl
appl.mode.class = 'FlConvDiff';
appl.dim = {'cAT3'};
appl.name = 'AT3';
appl.assignsuffix = '_AT3';
clear prop
clear weakconstr
weakconstr.value = 'off';
weakconstr.dim = {'lm6'};
prop.weakconstr = weakconstr;
appl.prop = prop;

clear bnd
bnd.c0 = {0,0,'cAT3in/cs'};
bnd.N = {0,0,0};
bnd.type = {'N0','Nc','C'};
bnd.ind = [3,1,1,1,1,1,1,1,1,2];
appl.bnd = bnd;

clear equ
equ.D = 'dts';
equ.dtensor = {{{'DqAT3/alpha^2';'DqAT3'}}};
equ.v = 'Pey*0';
equ.u = 'Pey*un/alpha';
equ.Dts = 'dts';
equ.R = 'dts*(-ka9q*c9a*cAT3-ka9q*c10a*cAT3-ka5q*c2a*cAT3)';
equ.dtype = 'aniso';
equ.ind = [1];
appl.equ = equ;
fem.appl{21} = appl;

fem.border = 1;
fem.outform = 'general';

% Subdomain settings

clear equ
equ.ind = [1];
equ.dim = {'c10','c10a','c7a','c2','c2a','c5a','cpc','c9','c9a', ...
  'c8','c8a','c5','c7','ctfpi','ctfpi10a','cAT3'};

% Subdomain expressions
```

```
equ.expr = {'f10a','1000000*c10a*cs', ...
  'thrombin','1000000*c2a*cs', ...
  'apc','1000000*capc*cs', ...
  'f5a','1000000*c5a*cs', ...
  'un','1-(-2*(0.5-y))^2', ...        % normalized velocity profile, u(y)
  'capc','cpcin/cs-cpc'};             % [APC]=[PC]in-[PC]
fem.equ = equ;
```

% Boundary settings

```
clear bnd
bnd.ind = [1,1,1,2,2,2,2,2,2,1];
bnd.dim =
{'c10','c10a','c7a','ctf7as','c2','c2a','c5a','c5a10as','cpc', ...
  'cttms','c9','c9a','c8','c8a','c8a9as','c5','c7','ctfpi','ctfpi10a',
...
  'ctfis','cAT3'};
```

% Boundary expressions

```
bnd.expr = {'pro',{'','1000000000*c5a10as*es'}, ...   % prothrombinase
  'xxase',{'','1000000000*ctf7as*es'}, ...           % extrinsic Xase
  'ixase',{'','1000000000*c8a9as*es'}, ...           % intrinsic Xase
  'ttm',{'','1000000000*cttms*es'}, ...              % thrombin-TM
  'TFfreeq',{'','TFq-ctf7as-ctfis'}, ...  % free TF (dimensionless)
  'freeTF',{'','1000000000*TFfreeq*es'}};            % free TF
fem.bnd = bnd;
```

% Scalar expressions

```
fem.expr = {'gamma','500', ...% wall shear rate
  'es','1e-9', ...            % surface concentration scale
  'TFsurf','9*1e-9', ...      % TF surface concentration
  'TFq','TFsurf/es', ...
  'TMsurf','100*1e-9', ...    % TM surface concentration
  'TMq','TMsurf/es', ...
  ...
  'kcat1','1.2', ...          % activation of X by TF/VIIa
  'Km1','4.5*1e-4', ...
  'kcat2','33', ...           % conversion of II by Va/Xa
  'Km2','2.1*1e-4', ...
  'kcat3','5.58', ...         % activation of PC by thrombin-TM
  'Km3','0.7*1e-3', ...
  'kcat4','0.4', ...          % inactivation of Va and VIIIa by APC
  'Km4','2*1e-5', ...
  'kcat5','0.34', ...         % activation of IX by TF/VIIa
  'Km5','1.7e-4', ...
  'kcat6','0.9', ...          % activation of VIII by thrombin
  'Km6','2e-4', ...
  'kcat7','20', ...           % activation of X by VIIIa/IXa
  'Km7','1.6e-4', ...
  'kcat8','0.23', ...         % activation of V by thrombin
  'Km8','7.2e-5', ...
  'kcat9','5.0', ...          % activation of VII by Xa
  'Km9','1.2*1e-3', ...
  'kcat10','0.046', ...       % activation of V by Xa
```

```
'Km10','1.04e-5', ...
'kcat11','0.061', ...          % activation of VII by thrombin
'Km11','2.7e-3', ...
'Keq1','6e-4*1e-3', ...        % TF/VIIa association/dissociation
'kd1','Keq1*ka1', ...
'ka1','1e5', ...
'Keq2','1e-7', ...             % Xa/Va association/dissociation
'kd2','Keq2*ka2', ...
'ka2','1e5', ...
'Keq3','1e-4*1e-3', ...        % thrombin-TM association/dissociation
'kd3','Keq3*ka3', ...
'ka3','1e5', ...
'Keq4','1e-7', ...             % IXa/VIIIa association/dissociation
'kd4','Keq4*ka4', ...
'ka4','1e5', ...
'ka5','6.8', ...               % thrombin-ATIII inactivation
'ka9','2.6', ...               % IXa-ATIII inactivation
'kd6','3.3e-4', ...            % TFPI/Xa association/dissociation
'ka6','1.6e4', ...
'kd7','11e-4', ...             % TFPI/Xa-TF/VIIa assoc./dissoc.
'ka7','1e4', ...
...
'cs','es/Ds/ts*ys', ...        % concentration scale
'kcat1q','kcat1*ts', ...       % dimensionless reaction parameters
'Km1q','Km1/cs', ...
'kcat2q','kcat2*ts', ...
'Km2q','Km2/cs', ...
'kcat3q','kcat3*ts', ...
'Km3q','Km3/cs', ...
'kcat4q','kcat4*ts', ...
'Km4q','Km4/cs', ...
'kcat5q','kcat5*ts', ...
'Km5q','Km5/cs', ...
'kcat6q','kcat6*ts', ...
'Km6q','Km6/cs', ...
'kcat7q','kcat7*ts', ...
'Km7q','Km7/cs', ...
'kcat8q','kcat8*ts', ...
'Km8q','Km8/cs', ...
'kcat9q','kcat9*ts', ...
'Km9q','Km9/cs', ...
'kcat10q','kcat10*ts', ...
'Km10q','Km10/cs', ...
'kcat11q','kcat11*ts', ...
'Km11q','Km11/cs', ...
'kd1q','kd1*ts', ...
'ka1q','ka1*cs*ts', ...
'kd2q','kd2*ts', ...
'ka2q','ka2*cs*ts', ...
'kd3q','kd3*ts', ...
'ka3q','ka3*cs*ts', ...
'kd4q','kd4*ts', ...
'ka4q','ka4*cs*ts', ...
'ka5q','ka5*cs*ts', ...
'ka9q','ka9*cs*ts', ...
'kd6q','kd6*ts', ...
'ka6q','ka6*cs*ts', ...
```

```
      'kd7q','kd7*ts', ...
      'ka7q','ka7*cs*ts', ...
      ...
      'umax','B/2*gamma', ...                 % maximum velocity
      'Pey','umax*ys/Ds', ...                 % modified Peclet term
      'dts','ys^2/Ds/ts'};                    % time-scaling coefficient
```

% Coupling variable elements

```
clear elemcpl

% Integration coupling variables

clear elem
elem.elem = 'elcplscalar';
elem.g = {'1'};
src = cell(1,1);

clear bnd

% Outlet concentrations based on flux integral, total surface complex
integrals

bnd.expr =
{{{},{},{},'(ntflux_c10a_f10a)*(cs*1e6)*alpha*Ds/(2/3*umax)'},{ ...

{},{},{},'(ntflux_c2a_f2a)*(cs*1e6)*alpha*Ds/(2/3*umax*2*B)'},{{{},{},{}
, ...
  '(ntflux_c7a_f7a)*(cs*1e6)*alpha*Ds/(2/3*umax*2*B)'},{{{},{},{}, ...
  '(ntflux_c5a_f5a)*(cs*1e6)*alpha*Ds/(2/3*umax*2*B)'},{{{},{},{}, ...
  'cpcin/cs-
(ntflux_cpc_pc)*(cs*1e6)*alpha*Ds/(2/3*umax*2*B)'},{{{},{},{}, ...
  '(ntflux_c9a_f9a)*(cs*1e6)*alpha*Ds/(2/3*umax*2*B)'},{{{},{},{}, ...

'(ntflux_c8a_f8a)*(cs*1e6)*alpha*Ds/(2/3*umax*2*B)'},{{{},'pro',{},{}},{
...

{},'xxase',{},{}}},{{{},'ixase',{},{}}},{{{},{},'ttm',{}}},{{{},{},'pro',{}},
{{}, ...
  {},'xxase',{}}},{{{},{},'ixase',{}}}};
bnd.ipoints =
{{{},{},{},'4'},{{{},{},{},'4'},{{{},{},{},'4'},{{{},{},{},'4'},{{{}, ...

{},{},'4'},{{{},{},{},'4'},{{{},{},{},'4'},{{{},'4','4',{}}},{{{},'4','4',{}
},{ ...

{},'4','4',{}}},{{{},'4','4',{}}},{{{},'4','4',{}}},{{{},'4','4',{}}},{{{},'4',
'4', ...
  {}}}};
bnd.frame =
{{'xy','xy','xy','xy'},{'xy','xy','xy','xy'},{'xy','xy','xy', ...

'xy'},{'xy','xy','xy','xy'},{'xy','xy','xy','xy'},{'xy','xy','xy','xy'}
,{ ...

'xy','xy','xy','xy'},{'xy','xy','xy','xy'},{'xy','xy','xy','xy'},{'xy',
...
```

```
'xy','xy','xy'},{'xy','xy','xy','xy'},{{},'xy','xy',{}},{{},'xy','xy',{
}},{ ...
  {},'xy','xy',{}}};
bnd.ind = {{'1','2','3'},{'4','6','8'},{'5','7','9'},{'10'}};
src{1} = {{},bnd,{}};
elem.src = src;
geomdim = cell(1,1);
geomdim{1} = {};
elem.geomdim = geomdim;
elem.var =
{'f10a_out','th_out','f7a_out','f5a_out','apc_out','f9a_out', ...
  'f8a_out','total_pro_tf','total_xxase_tf','total_ixase_tf', ...
  'total_ttm_tm','total_pro_tm','total_xxase_tm','total_ixase_tm'};
elem.global =
{'1','2','3','4','5','6','7','8','9','10','11','12','13','14'};
elem.maxvars = {};
elemcpl{1} = elem;
fem.elemcpl = elemcpl;

% Multiphysics
fem=multiphysics(fem);

% Extend mesh
fem.xmesh=meshextend(fem, ...
                     'linshape',[]);

% Solve problem
% Solver parameters: Output times 0 to 60, stepping by 0.05; Time
dependent PARDISO linear system solver; Manual tuning of step size

fem.sol=femtime(fem, ...
               'u',0, ...

'solcomp',{'c8a','c7a','cttms','c9a','cAT3','ctfpi','c5','c5a','c9','ct
fis','c8','c7','c2a','ctf7as','ctfpi10a','c2','cpc','c8a9as','c10','c5a
10as','c10a'}, ...

'outcomp',{'c8a','c7a','cttms','c9a','cAT3','ctfpi','c5','c5a','c9','ct
fis','c8','c7','c2a','ctf7as','ctfpi10a','cpc','c2','c8a9as','c5a10as',
'c10','c10a','c8at','c7at','cttmst','c9at','cAT3t','ctfpit','c5t','c5at
','c9t','ctfist','c8t','c7t','c2at','ctf7ast','ctfpi10at','cpct','c2t',
'c8a9ast','c5a10ast','c10t','c10at'}, ...
               'tlist',[0:0.05:60], ...
               'tout','tlist', ...
               'tsteps','intermediate', ...
               'initialstep',1e-7, ...
               'maxstep',1e-4, ...
               'linsolver','pardiso', ...
               'itol',2.0E-6, ...
               'errorchk','auto');

% Save current fem structure for restart purposes
fem0=fem;
```
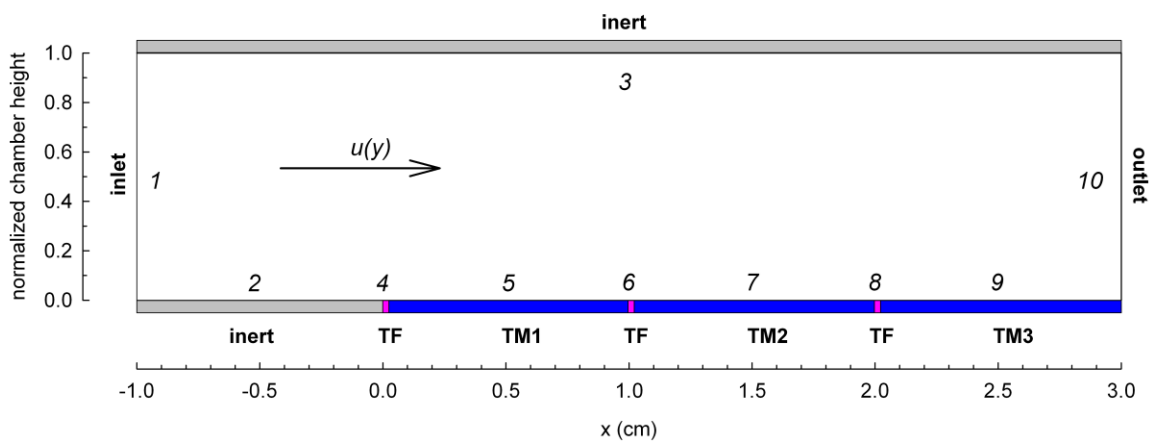
Figure C.1. Boundary number labels. (1) Inlet, (2) inert entrance region, (3) inert upper surface, (4,6,8) TF-expressing regions, (5,7,9) TM-expressing regions, (10) outlet. The arrow indicates the direction of flow with velocity, *u*.